DISSERTATION

A Temporal, Spatial and Quantitative Study on the Influenza A Virus Transcription, Translation and Virus-Host Interaction

Zur Erlangung des akademischen Grades
DOCTOR RERUM NATURALIUM
(Dr. rer. nat.)
im Fach Biologie

Eingereicht an der
Mathematisch-Naturwissenschaftlichen Fakultät I
der Humboldt-Universität zu Berlin

von
Diplom-Biologin (Univ.)
Susann Kummer

Präsident der Humboldt Universität zu Berlin
Prof. Dr. Jan-Hendrik Olbertz

Dekan der Mathemathisch-Naturwissenschaftlichen Fakultät I
Prof. Dr. Andreas Herrmann

Gutachter/in: 1. Prof. Dr. Andreas Herrmann
2. PD Dr. Michael Veit
3. Prof. Dr. Dr. hc. Edda Klipp

Datum der Einreichung: 20.05.2011
Datum der Promotion: 29.07.2011

ICH BIN IMMER NOCH VERWIRRT –

ABER AUF EINEM HÖHEREN NIVEAU.

Nobelpreis für Physik 1938,
1923 mehrmonatiger Aufenthalt in Göttingen
– dem zu dieser Zeit führenden Zentrum für theoretische Physik

ENRICO FERMI

ZUSAMMENFASSUNG

Die Vermehrung des Influenza A Virus umfasst, neben anderen wichtigen Schritten, die Transkrption der viralen mRNA und die ribosomale Translation der viralen Proteine.

Mit großem Aufwand wurde bereits an der Entwicklung von Methoden zur Untersuchung des zeitlichen Verlaufs der Synthese viraler mRNA während des Vermehrungszyklusses in der Wirtszelle geforscht. In der vorliegenden Arbeit wurden sequenzspezifische FIT-PNA-Sonden, welche einen einzelnen, als künstliche fluoreszente Nukleobase dienenden Interkalator tragen, auf die quantitative RT-PCR sowie die Lebendzellmikroskopie angewandt. Die FIT-PNA-Sonden bieten dabei eine hohe Sensitivität und eine enorme Zielspezifität unter nicht-stringenten Hybridisierungsbedingungen.

Im Speziellen wurden FIT-PNA Sonden mit Sequenzspezifität zur mRNA der Neuraminidase und des Matrixproteins 1 entworfen und untersucht. Die somit erhaltenen Ergebnisse besitzen eine hohe biologische Relevanz und weisen diese Sonden als vielversprechende Methodik in der Virologie und der Zellbiologie aus. Ihre Anwendung konnte bereits auf das Vesikular Stomatitis Virus ausgeweitet werden.

Die Kombination aus biologischer Expertise mit modernen Proteomstudien und detaillierten statistischen Analysen ermöglichte einen systemumfassenden Blick auf die durch eine Infektion bedingten Auswirkungen auf die Wirtszelle. Die Markierung von Aminosäuren mit stabilen Isotopen in Zellkultur wurde hierfür benutzt. Es wurden Proben zu verschiedene Zeitpunkten im Infektionszyklus in die Untersuchungen einbezogen, um zeitaufgelöste Detailstudien der zellulären Proteinbiosynthese und Degradation durchzuführen.

Schlagworte: Influenza A Vermehrung, FIT-PNA, Lebendzellmikroskopie, SILAC

ABSTRACT

Replication of the influenza A virus involves, amongst other critical steps, the transcription of viral mRNA and ribosomal translation of viral proteins.

Significant efforts have been devoted to the development of methods that allow the investigation of viral mRNA progression during the replication cycle inside the host cell. In the present thesis sequence specific FIT-PNA probes which contain a single intercalator serving as artificial fluorescent nucleobase were introduced for quantitative RT-PCR and live cell imaging. FIT-PNAs provide for both high sensitivity and high target specificity at non-stringent hybridisation conditions (where both matched and mismatched probe-target complexes coexist). In particular, FIT-PNAs specific to the neuraminidase and matrix protein 1 were successfully designed and examined. The obtained results are of high biological importance and suggest the FIT-PNA technique as promising tool in the field of virology and cell biology as this approach was readily applied to Vesicular Stomatitis Virus as well.

By combining biological expertise with modern high throughput quantitative proteomics and detailed statistical analysis a system wide view of the effects and dynamics of the early H1N1 infection on the cell proteome was generated. Stable isotope labelling of amino acids in cell culture (SILAC) was employed to globally track changes in gene expression at the protein level. Furthermore, samples at various time points post infection enabling a more detailed time-resolved analysis of host cell protein biosynthesis and degradation during the infection cycle were included. As a result the specific expression characteristics of single genes and functional gene subsets in response to viral infection were bioinformatically analysed.

Keywords: influenza A replication, FIT-PNA, mRNA imaging, SILAC

ABBREVIATIONS

Ac	acetyl	Mg^{+}	magnesium
Aeg	aminoethylglycine	mg, ng	micro gram(s), nano gram
BO	pyridinium benzothiazole	min	minute(s)
BSA	bovine serum album	ml, µl	milli litre, micro litre
°C	degree Celsius	M1	matrix protein 1
Ca^{2+}	calcium	NA	neuraminidase
Dabcyl	4(dimethylaminoazo)benzene-4-carboxylic acid	NaCl	natrium chloride
DAPI	4',6-diamidino-2-phenylindole	NP	nucleoprotein
dd H_2O	double destilled water	PCR	polymerase chain reaction
DMEM	Dulbecco`s modified eagle medium	PEG	polyethylenglycol
DMSO	dimethylsulphoxide	pH	*potentia hydrogenii*
DNA	deoxyribonucleic acid	p.i.	post infection
DPBS	Dulbecco`s phosphate buffered salt solution	PNA	Peptide Nucleic Acid
DTT	dithiothreitol	rev	reverse
fwd	forward	SFV	Semliki Forest Virus
h	hour(s)	SLO	streptolysin O
Hepes	4-(2-hydroxyethyl)-1-piperazineethanesulfonic acid	TMR	tetramethylrhodamine
HCl	hydrochlorid acid	TO	thiazole orange
mM, nM	milli molar, nano molar	U	unit
MB	Molecular Beacon	VSV	Vesicular Stomatitis Virus

INDEX

1. INTRODUCTION

The free online database PubMed administrated by the U.S. National Library of Medicine (NLM) as part of the National Institute of Health (NIH, U.S.A.) hosts the worldwide largest comprehension of abstracts in life sciences and biomedical research. The entry term "influenza" gives more than 61,400 results demonstrating the high significance of influenza virus research.

In addition, other numbers connected to this viral genus, like 3 to 5 million cases of disease in the two annual flu seasons (each per hemisphere) with more than 500,000 deaths or pandemic outbreaks with up to 80 million fatalities (1918), render any further explanation for the importance and urgency of intensive investigation on influenza virus.

Influenza virus belongs to the virus family of *Orthomyxoviridae.* This Greek term describes the main characteristic phenotype of influenza caused illnesses by combining standard (= *ortho*) and mucus (*myxo*) [1]. In general, influenza viruses affect the upper and lower respiratory tract. Traditionally, viruses have been classified by the implemented disease due to the lack of knowledge about viruses themselves. The aforementioned virus family is consisted of influenza A, B and C virus, the Togotovirus and recently suggested the infectious salmon anaemia virus [2].

This introductory part will focus on influenza A virus first by a short portrait of the genetic and structural properties. In the following, the impact of the virus on the host cell as well as the pandemic risk classification will be discussed.

Particular attention will be paid on the replication cycle of influenza A virus with respect to the topic examined by the present thesis.

1.1 BIOLOGY OF INFLUENZA A VIRUS

The genome of influenza A virus consists of 8 segments composed of single-stranded RNA in negative sense orientation [1]. The viral RNAs (vRNAs) are packed in ribonucleoprotein (RNP) complexes and function as templates for the messenger RNA (mRNA) and the complementary RNA (cRNA) synthesis.

Antigenic variations in the sequence of the 2 major surface proteins, hemagglutinin (HA) and neuraminidase (NA), are the reason for the influenza A virus standard nomenclature. There are 16 HA variants and 9 NA variants known [3, 4]. Due to host restrictions only 6 subtypes (H1N1, H2N2, H3N2, H5N1, H7N7 and H9N2) have been isolated from humans [1].

The virions exhibit a pleiomorphic shape built up by a lipid envelope which is derived from the host`s membrane as a result of the budding process. Virus morphology can range from spherical shape with a diameter of 100 nm to filament with a length in excess of 300 nm. There are indications, that the viral proteins [5-8] and conversely the host cell type [9] influence the physiological appearance of the virion morphology. A common feature are the embedded proteins, the HA, NA and the matrix protein 2 (M2), which are anchored by short hydrophobic amino acid sequences. Beneath the lipid envelope the viral matrix protein 1 (M1) forms a protein layer [10], the virion core. Apart from M1, the nucleoprotein (NP) is the most abundant protein in the virion and interacts with the sugar-backbone of the vRNA molecules in a 1 monomer to 20 nucleotides ratio [11]. It is assumed that the polymerase complex (subunits PB1, PB2 and PA) is linked to the higher ordered structure (e.g. supercoils) formed by the vRNAs [12, 13]. The non-structure protein (NS2, also NEP) plays a minor role inside the virion but is responsible for the nuclear export of the viral genome segments [14]. The last out of ten viral proteins is a non-structural protein (NS1) which has major influence on the regulation of influenza A replication and the cellular biosynthesis machinery.

1.2 GENOME AND PROTEOME OF INFLUENZA A VIRUS

Except the segments 2, 7 and 8 all of the influenza A virus genes are in monocistronic organisation. The segments are ordered by their sequence length.

Segment 1: 2341 nucleotides (Basic Polymerase Protein 2 – PB2)

The polymerase subunit PB2 exhibits a nuclear localisation signal in order to fulfil its function related to the viral transcription and replication inside of the cellular nucleus [15]. The characteristic cap-snatching mechanism is mediated by the PB2 [16, 17]. In particular, the cap-binding site is localised at the carboxyl terminal end. In concert with its endonuclease activity it uses cellular cap-structures to provide primers for the viral transcription [18]. Furthermore, the PB2 contains binding sites for the PB1 subunit at its amino terminus. Additional binding sequences for the NP are supposed to function for regulatory purposes [19].

Segment 2: 2341 nucleotides (Basic Polymerase Protein 1 – PB1)

PB1 contains the 4 conserved amino acid motifs of RNA-dependent RNA polymerases and thus represents the functional protein for RNA polymerization [20]. The binding sites for PA and PB2 are located at the amino- and the carboxyl terminal end, respectively [21], indicating that PB1 exhibits a central role for the assembly of the polymerase complex and its function. Interestingly, in some influenza A strains an alternative open reading frame encoding for the accessory protein PB1-F2 can be found. This exhibits pro-apoptotic activity in host immune cells [22].

Segment 3: 2233 nucleotides (Acidic Polymerase Protein – PA)

The smallest subunit PA is a phosphorylated protein [23] which function is restricted to the nucleus and the presence of the whole polymerase complex. It is suggested that PA has helicase and ATP-binding activity and is required for PB1 accumulation in the nucleus [24, 25]. Inside of the nucleus the PA subunit induces proteolysis resulting in an aberrant nuclear morphology and chromatin condensation [26].

Segment 4: 1778 nucleotides (Hemagglutinin – HA)

HA is the most prominent and best studied influenza A protein. It mediates the binding of the virus to sialic acid residues on the cell surface and the fusion of the viral with the endosomal membrane. Segment 4 encodes for a precursor polypeptide HA_0 which is cleaved by serine proteases into the HA_1 and the HA_2 subunits which remain linked by a disulfide bound. This posttranslational process is essential for the conformational change of the HA. This is triggered by low-pH conditions inside the late endosome and leads to exposition of the fusion peptide which is situated at the amino terminal end of HA_2 [27]. Attachment to the host is mediated by the pocket region localised at the globular head of the HA_1 subunit which therefore alters the host specificity [28]: a discrimination between *α*-2,3- (avian) and *α*-2,6- (human and avian) linkages of the sialic acid and galactose is caused by one amino acid residue (glutamine or leucine at position 226, respectively). On the contrary, the HA_2 portion exhibits the fusion activity [29]. HA is organized in the viral lipid-envelope as a homotrimeric transmembrane protein.

The attention for HA is also contributed to the susceptibility for neutralizing antibodies and the effect on the pathogenicity of the virus subtype [30].

Segment 5: 1565 nucleotides (Nucleoprotein – NP)

As an essential component of the ribonucleoprotein complex the NP binds via an RNA-binding domain in a non-sequence dependent manner to the vRNAs [31]. This binding is assumed to regulate the switch from the transcription to the replication mode as NP may act as an anti-termination control factor [32]. Nuclear localisation signals within the NP amino acid sequence indicate that this shuttle protein is involved in the transport of viral RNP complexes into the cellular nucleus and the export of novel vRNAs in association with M1 and NS2 [33-35].

Segment 6: 1413 nucleotides (Neuraminidase – NA)

The glycosylated homotetrameric [36] NA is not required for virus entry, replication and assembly [37] but plays an important role in the very late stage of the infection cycle which is the detachment of novel synthesized virus particles from the host cell membrane [38]. The cleavage of an *α*-ketosidic linkage between a terminal sialic acid and a neighbouring D-galactose or D-galactoseamine residue of cell-surface glycoproteins or gangliosides, respectively, prevents virions from aggregation on the cell surface [38]. Likewise the NA removes sialic-acid residues from the viral envelope in order to prevent self-accumulation and thus enhances infectivity [38]. Host anti-NA antibodies or NA inhibitors (e.g. oseltamivir carboxylate) prevent viral replication. Each NA monomer is composed of 4 structural domains: a globular head, a stalk, a transmembrane domain and a cytoplasmic domain [36]. The latter is thought to influence the (neuro-) virulence (glycosylation site at position 130 [39]) and virion morphology [7]. Matrosovich *et al.* 2004 experimentally evidenced the essential role of NA also for virus invasion of the ciliated human airway epithelium. Removal of decoy receptors prevents strong binding of the virion to non-target cells which would impede virus access to target cells [40].

Segment 7: 1027 nucleotides (Matrix proteins – M1 and M2)

The mRNA of segment 7 is bicistronic: while M1 is a direct transcript, M2 is produced by using an alternative splicing site [10, 41].

Several functions of M1 are described: inhibition of viral transcription [42], assistance of vRNP nuclear export [33, 43], support of the NP self-assembly into the helical structure of the vRNP [44], and involvement in virus assembly and budding process [6, 8]. It is assumed that the amino-terminus where the nuclear localisation signal is encoded is responsible for self-polymerization and membrane binding, in concert with the NS2 protein [45].

In contrast to M1, M2 appears as a homotetrameric transmembrane protein [46] embedded in the viral envelope. M2 functions as an ion channel [47] and regulats the pH inside the virus particle when incorporated in endosomes. Internal acidification causes the dissociation of the vRNPs from the M1 [33], a process termed uncoating, that allows the viral genome to enter the host nucleus. This step in the viral infection cycle is a target for antiviral therapies blocking further replication [48-50]. The impact of the transmembrane domain of M2 for an efficient replication is still under discussion [51, 52].

Segment 8: 890 nucleotides (Nonstructural proteins – NS1 and NS2)

Analogue to segment 7 the mRNA transcribed from segment 8 is as well biscistronic. Therefore, the NS2 protein is an alternative splicing variant of the NS1 mRNA [53].

The only absolute non-structural viral protein NS1 binds to a wide range of RNA molecules [54] indicating its functional influence on splicing of mRNAs, cellular and viral transcription [55], cellular mRNA export [54] and adenylation [56] as well as viral mRNA translation [57, 58]. NS1 activity might result in decreased susceptibility to cellular antiviral defence mechanisms [59].

The description "non-structural protein NS2" is misleading because it exhibits a binding domain specific to M1 at its carboxyl-terminal end and is incorporated at low amounts into the virion [60]. O´Neill *et al.* 1998 [14] suggested to rename it in "nuclear export protein (NEP)" with reference to the presence of a nuclear export signal and the indispensability for vRNA nuclear export [61].

1.3 REPLICATION OF INFLUENZA A VIRUS

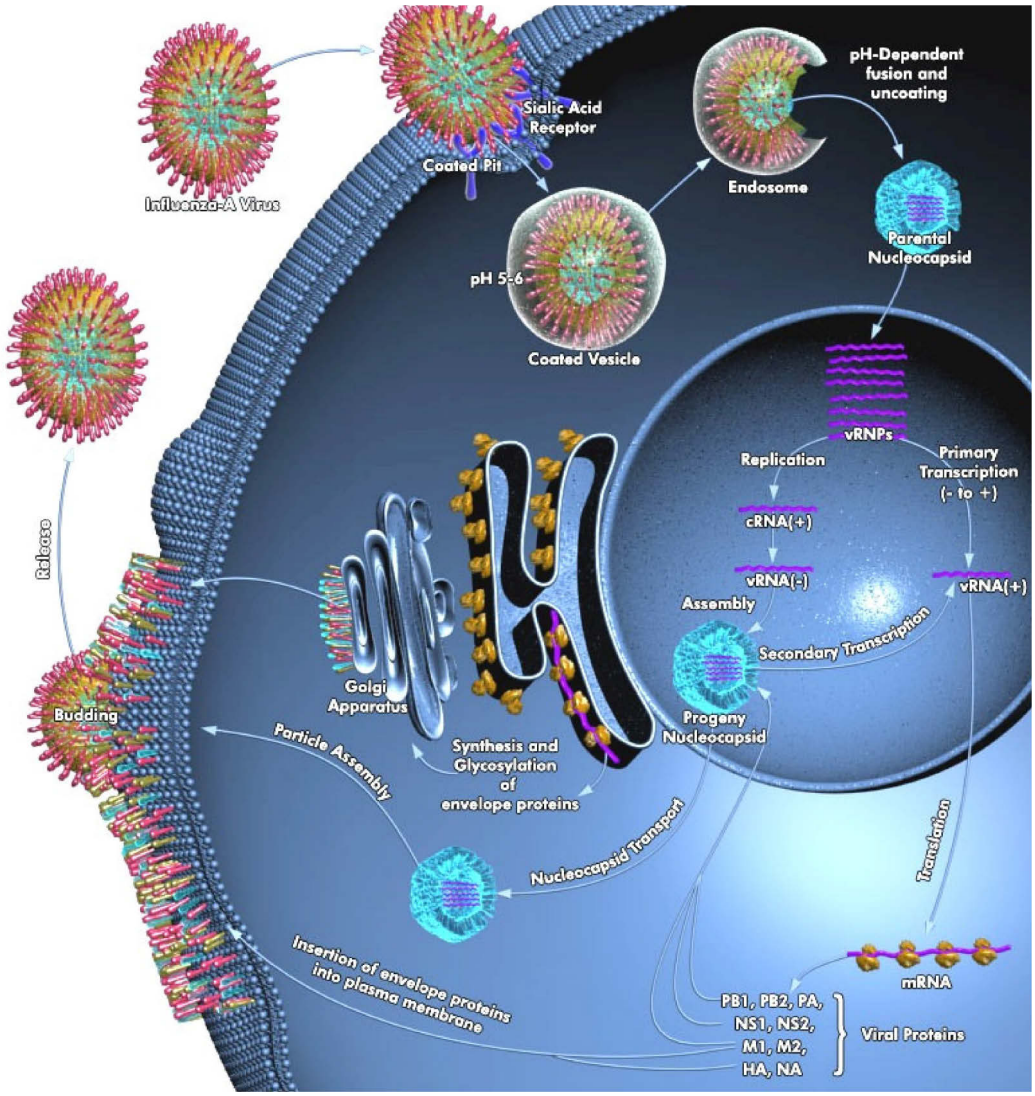

Figure 1: Replication cycle of influenza A virus (taken from www.qiagen.de). Recognition of ubiquitous exposed sialic acid residues on the cell surface by the viral HA allows attachment of the virus particle to the host cell surface. This is followed by the uptake of the virus into the endosome. After uncoating, the viral ribonucleoparticles are delivered into the host cytoplasm and subsequently into the nucleus where transcription and replication take place. Translation occurs on free and membrane-associated ribosomes. Self-assembly of viral proteins leads to the budding of progeny influenza A virus particles from distinct regions of the host plasma membrane.

Due to the requirement of cellular resources, the vRNPs are trafficked to the nucleus hijacking the cellular import machinery. For this purpose, the viral proteins carry nuclear localisation signals, as aforementioned.

The nucleus represents the place of action for both, the transcription of capped and polyadenylated viral mRNA and the replication producing antigenomic viral cRNA molecules and progeny vRNP complexes [62]. The templates are still the negative-stranded vRNAs. They all exhibit conserved motifs at their endings: 12 bases at the 3´end and 13 bases at the 5´end showing partly inverted complementation. These sequences are thought to interact with each other forming hairpin shaped structures [63]. Whereas cRNA molecules are exact and full length copies of the complementary vRNAs [64], the viral mRNA lacks circa 17 nucleotides at the 3´end (complementary to 5´end of the corresponding vRNA) [65]. The afore described nuclear export mechanisms involving the NP, M1 and NS2 [35, 45, 61] are restricted to mRNA and vRNA whereas the cRNA stays in the nucleus for the entire replication process [66].

Transcription of influenza A virus

One fundamental aspect of influenza A virus transcription initiation is the cap-snatching from cellular mRNA molecules by the endonuclease activity of the PB2 polymerase [18]. These 10 to 15 nucleotides are used as primers for the complementary strand synthesis [67] and protect the viral mRNA from endonucleolytic degradation [68]. In addition, a successful initiation of transcription also requires a specific secondary structure of the promoter sequence [11, 69] indicating that sequences at both ends of the cRNA molecule are necessary.

Simultaneously to the cellular termination an uracil rich sequence in close proximity to the template`s 5´ end produces the synthesis of a poly(A) tail finishing transcription [65]. Plotch *et al.* 1977 demonstrated the host-independency of viral mRNA polyadenylation by in vitro experiments [70]. The poly(A) tail and the cap structure are essential features of mRNA molecules with respect to nuclear export and biostability [71].

As transcription is a selective process, the appearance of individual viral mRNA species varies during the time course of infection. An early and a late transcription can be distinguished. While in the first step the synthesis of all 8 mRNA species occurs equally, preferentially the NS1 and NP mRNAs are transcribed at the beginning of the late transcription. Shapiro *et al.* 1988 evidenced the early synthesis of NS1 mRNA with respect to the delayed presence of M1 mRNA [66].

Replication of influenza A virus

The formation of copy RNA in full length requires neither primer sequences nor polyadenylation [64]. Generally, the key question how the virus facilitates the regulation of transcription versus replication was under strong discussion suggesting viral as well as cellular factors [66, 72]. Even the degradation of novel synthesized cRNA molecules without bound viral RNA polymerase or the viral NP [73] might result in the switch to the replication mode.

Recently, Olson *et al.* 2010 presented a comprehensive description of the underlying regulative interactions. The process involves the polymerase, the three viral RNA species, and the cap structure, consequently ending up in a complex interaction cycle [74].

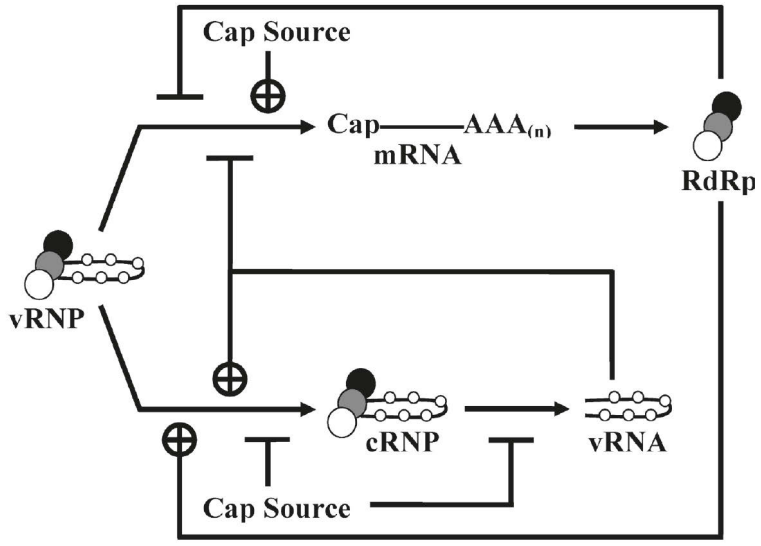

Figure 2: How influenza A virus controls the switch from transcription to replication mode. (taken from Olson et al. 2010) The transcriptional mode is maintained by increased concentrations of cap source, whereas increased concentrations of vRNA and viral polymerase will lead to a switch toward replication. Encircled plus signs indicate stimulation while T bars indicate repression. RdRp = RNA-dependent RNA polymerase

Translation of influenza A virus

The hypothesis that the amount of translated viral proteins is mostly influenced by the amount of the corresponding mRNA species is widely accepted. As a consequence of the unevenly synthesis of the different mRNA species, the NS1 and the NP are over-represented in the early phase of influenza A protein translation. With progression NS1 production is reduced and HA, NA and M1 are predominantly translated [66]. Transmembrane proteins (HA, NA and M2) are translated by membrane-bound ribosomes into the endoplasmic reticulum (where folding takes place) and maturate in the secretory pathway of the trans-Golgi network. An apical sorting signal ensures the trafficking to the plasma membrane and incorporation into the budding site [75].

The replication cycle is finished by the self-assembly of the newly synthesised viral proteins followed by the budding and release from the host plasma membrane.

1.4 PANDEMIC DANGER CAUSED BY INFLUENZA A VIRUS

Epidemics among the human population, in terms of sustained, widespread, person-to-person transmission, are caused only by three HA (H1, H2 and H3) and two NA (N1 und N2) subtypes.

The generation of influenza A virus subtypes that have pandemic potency is contributed to an *antigenic shift*. This term describes the reassortment of genome segments as a result of double infection. Consequently, these reassortants may encode for novel antigenic proteins with new immunogenic properties [75]. The most prominent case of such an antigenic shift produced the influenza A (H1N1) virus, called "Spanish flu" of 1918-1919, with a high rate of mortality [76]. Low infectivity combined with high pathogenicity of avian derived influenza A subtypes is caused by the host receptor discrimination. Sialylated proteins containing a terminal *α*-2,3-linkage are localised in the lower regions of the human respiratory tract. Therefore, infections with avian viruses are relatively rare and the human immune system is not adapted. That is why human infections with avian influenza A subtypes cause fatal progressive pneumonia [77].

Additionally, a mechanism named *antigenic drift*, describes the accumulation of multiple mutations in antigenic sites (for instance around the receptor binding region at the globular head of HA) and may lead to the formation of a drifting strain which is not longer inhibited by neutralizing antibodies against the parental virus. The host might be infected and produces clinical signs of disease [75].

1.5 HOST INTERACTION AND INFECTION HETEROGENEITY

Variation among individuals is a common concept in population biology. Recently this idea of heterogeneity became more and more prominent for cell biologists and virologists. In a given cell population the environment of individual cells and the specific intracellular conditions lead to heterogeneities in their status. Virus infection strongly depends on the biochemical, physiological and physical status of the host cell as several distinct cellular processes and resources are involved. Consequently, the individual cell status is critical for influenza A virus infection and for its efficient replication and reassortment [1, 9, 78].

Influenza A virus infection can be seen as a concert of viral protein activity and cellular protein interaction which is an evolving process. Pathogen sensors (like RIG-I) of the host cell detect viral RNA and induce antiviral defence (e.g. type I interferons). On the other hand, viral proteins (like NS1) suppress antiviral actions [79] or hijack cellular mechanisms and resources [80]. There is strong evidence that viruses mimic cellular motifs, named SLiMs (short linear motifs), to regulate and control cellular proteins. For instance, the influenza A protein PB2 mimics the nuclear localisation signal of the cellular importin *α* [80].

The underlying cellular networks have been reviewed by Watanabe T., Watanabe S. and Kawaoka in 2010 demonstrating the wide spectrum of applied approaches and the inconsistency of the findings in different labs [81].

Systematic and genome-wide RNA interference screens [82-85] are contributed to great efforts in the identification of virus-host interaction partners. These studies revealed hundreds of factors involved in all steps of the replication cycle. They have to be interpreted with care for experimental (e.g. efficiency of knockdown, influence on general cell viability) and analytical reasons (e.g. false negative/positive results).

Employing yeast-two-hybrid assays and computational approaches several human interaction partners were identified. These data include RNA-binding proteins,

transport proteins, transcription factors, and proteins of the intra-cellular signalling pathways (NFκB, apoptosis, MAPK, and WNT) [79].

However, all these *in vitro* or *in silico* analysis of host-virus interaction partners do not display the dynamic process of individual interactions and/or the impact on the viral replication. Validation and detailed information on the dynamics of the existing network are required. Moreover, investigation of different virus strains and/or cell types will expand the knowledge about general mechanisms and thus, uncover novel antiviral compounds.

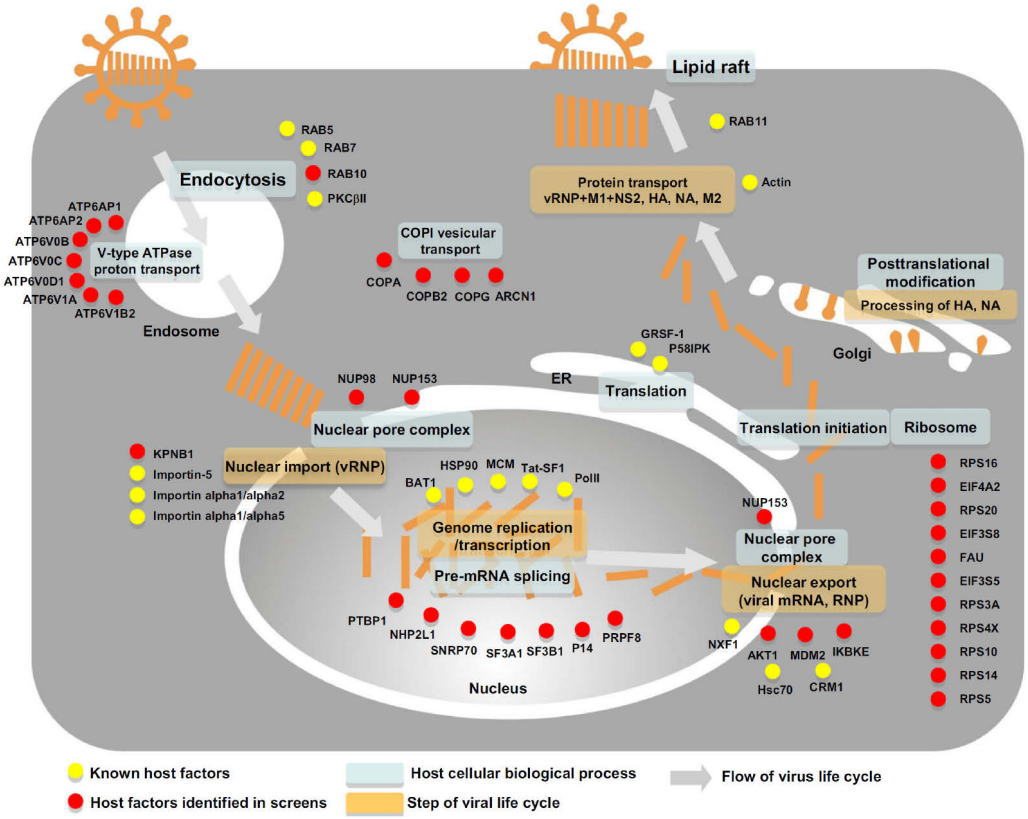

Figure 3: Influenza Virus Life Cycle and Host Factors (taken from Watanabe et al. 2010). The light-orange rectangles indicate individual steps of the influenza virus life cycle. The light-blue rectangles indicate host cellular processes that may be involved in the virus life cycle. Red circles indicate host factors identified in the screens discussed in the named publication and yellow circles indicate host factors identified in other previous studies. For details please review Watanabe et al. 2010.

1.6 Detection and Imaging of Nucleic Acids

The ability to study nucleic acids during their biosynthesis, intracellular transport, subcellular localisation, and degradation is of great interest in various fields of research like cell biology, medicine, pharmacology or virology. In basic and diagnostic sciences specific detection methods are required.

Indeed the underlying molecular mechanism of certain cancer subtypes [86-90] and several human diseases, like asthma [91], cutaneous, gastrointestinal and liver disease [92-94], is thought to be connected to dysfunction of microRNAs which act as posttranscriptional modulators of gene expression [88]. Furthermore, the identification of single nucleotide polymorphisms [95] or the specific identification of infection are just three out of many examples of nucleic acid research in clinical diagnostics [96-102].

Studies on endogenous as well as viral nucleic acid variants in the cellular context via microscopy imaging are one of the most relevant issues in nucleic acid research [103-105]. Particularly, virology studies on the replication cycle require specific detection methods to analyse the different steps of viral replication.

There is already a great spectrum of techniques available dealing with the visualisation of nucleic acids in fixed [106, 107] and in living [105, 108, 109] cell systems. However, most of these strategies are limited to special applications or exhibit various disadvantages making imaging of nucleic acids in living systems still a challenging task.

This introductory part gives an overview of the three exemplary techniques in nucleic acid research namely Fluorescent Proteins (FPs), Molecular Beacons (MBs) and finally Peptide Nucleic Acids (PNAs) which are applicable to living cells.

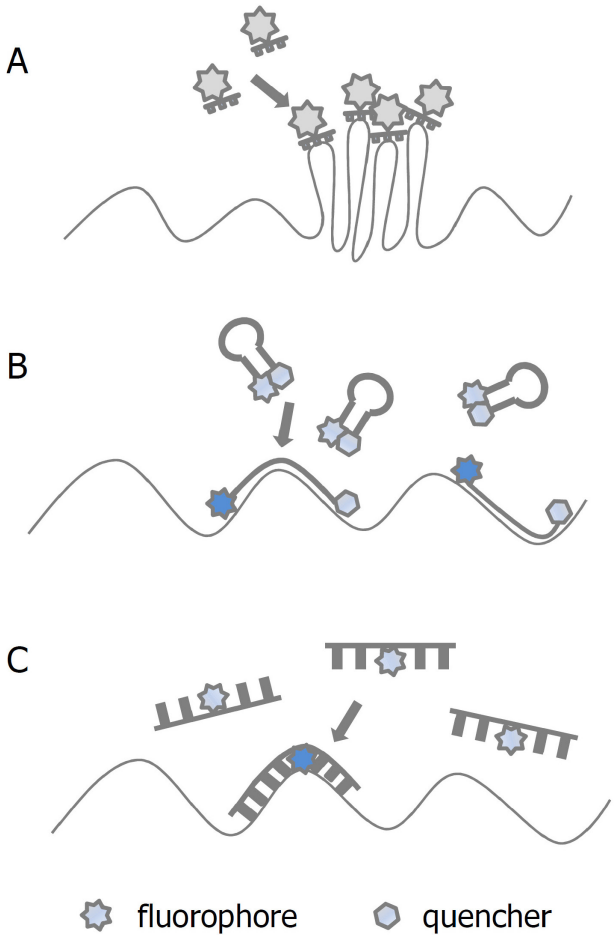

Figure 4: Schematic depiction of the functional mechanism of (A) Fluorescent Proteins, (B) Molecular Beacons and (C) Peptide Nucleic Acids in nucleic acid detection.

(A) Fluorescent Proteins like the green fluorescent protein (GFP) are used in the MS2 protein system which employs introduced hairpin structures for a sequence specific detection of mRNA molecules in living cells.
(B) Molecular Beacons are hairpin shaped structures carrying a fluorescent moiety and an equivalent quencher which keeps the probe in the non-fluorescent ground state. Spatial separation leads to enhancement of fluorescence.
(C) Peptide Nucleic Acids are nucleic acid analogues in which the backbone is a pseudopeptide rather than a sugar. Sequence specific fluorescent signals are produced with the help of an intercalating dye upon target hybridisation.

1.6.1 FLUORESCENT PROTEINS

All insights in molecular biology and cell biology based on the usage of fluorescent proteins have to be contributed to the efforts of Roger Tsien, Martin Chalfie, and Osamu Shimomura [110]. In 2008 they were honoured with the Nobel Prize in Chemistry for their work on the green fluorescent protein (GFP) and the gathered technical achievements. This fluorescent protein, isolated and cloned from the jellyfish (*Aequorea victoria*) belongs to the standard methods in nearly all fields of biology and medicine with thousands of applications [111].

Besides the versatile utilization in protein studies, recent developments made FPs suitable for the visualisation of gene expression, nuclear transport and mRNA dynamics in living cells [112]. One of the key benefits of the FP technique compared to *in situ* hybridisation or oligonucleotide labelling is that the probes are directly expressed as fusion proteins in genetically manipulated organisms. This allows imaging in real time.

Sensitivity is the biggest limitation of GFP as a detection reagent of small molecules and motivated researchers to make remarkable progress towards new strategies for single-molecule detection [113]. Recently, the MS2 protein technique for mRNA imaging in yeast was established simultaneously in the Singer lab [114] and by Bloom and colleagues [115]. The principle of this method lies in two components: (i) expression of the bacteriophage MS2 RNA coat protein (MCP) fused to the FP and (ii) expression of the mRNA of interest (including the MS2 hairpin motifs). Due to genetic modifications the expression can occur globally or in a particular tissue depending on the chosen promoter [116].

Golding *et al.* 2005 applied the MS2 technique to *Escherichia coli* with an influential supplementation: The authors introduced 96 copies of a specific RNA hairpin into the untranslated region of the mRNA of interest enabling the binding of 96 MS2-GFP fusion proteins. With this the fluorescent signal of single molecules was enhanced dramatically [117]. This had a crucial effect on the ability of counting mRNA molecules using conventional fluorescence microscopy.

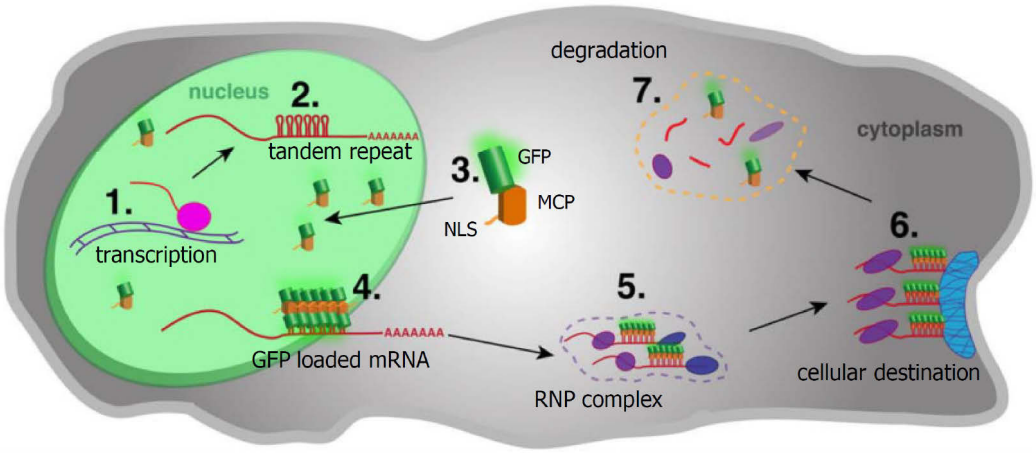

Figure 5: Depiction of MS2-MCP labelling of endogenous mRNA in living cells. (adapted from Weil et al. 2010) GFP = green fluorescent protein, MCP = MS2 coat protein, NLS = nuclear localisation signal, RNP = ribonuleoparticle

Apart from the impressive achievements in transcription research [118, 119] the MS2 method exhibits several drawbacks: (i) the lack of knowledge concerning the best position of the hairpin insertion and the difficulties to clone the hairpin repeats, (ii) the requirement of transgenic expression of the selected gene leading to a non-physiological over-expression and (iii) the tendency of the fusion proteins to form aggregates without binding the target sequence leading to false-positive cytosolic signals [116].

The most critical aspect in tagging mRNA with GFP molecules is the risk to modify their native behaviour and dynamics.

1.6.2 MOLECULAR BEACONS

Molecular Beacons have been invented as alternative RNA labelling technique to FISH (fluorescent *in situ* hybridisation) [116] as they provide the possibility to detect individual RNA molecules in living cells [105, 120-124].

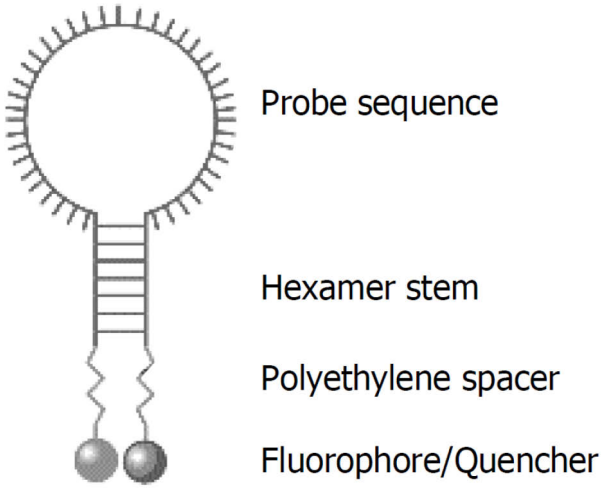

Figure 6: Depiction of the structural properties of Molecular Beacons. (modified from www.eurogentec.com)

In 1996 Tyagi [125] established the Molecular Beacon technique for RNA imaging. The hairpin structured MBs are constructed of 3 main components: (i) the 15-30 nucleotides spanning loop region, (ii) the 5-8 base pairs in length stem portion and (iii) the fluorophore-quencher pair. The fluorescent moiety is typically connected to the 5´end and the quenching group is linked to the 3´end of the molecule.

The double-stranded stem enables the looped conformation of the MB and thus the non-fluorescent ground state while the quencher is in close proximity (7-10 nm) to the fluorophore. The loop region is responsible for the sequence specific target binding and confers on the MBs target sensitivity. Upon hybridisation with the target sequence the binding energy leads to an opening of the hairpin structure and subsequent dissociation of the stem region. Hence, the thermodynamic equilibrium between the hybridisation energy of the loop sequence and the melting temperature of the stem region is enormously important for the functionality of MBs. This relation is very sensitive and requires a precise adjustment. Low melting temperatures of the MB can already provide for a hairpin structure and hybridisation to the target. However, temperatures over the threshold-set point destroy the hairpin structure and turn it into a linear oligomer. In this situation the distance between fluorophore and quencher is too long for quenching and fluorescence is emitted giving a false-positive signal [124, 126]. In contrast, if the melting temperature is too high the stem region is too stable to allow specific hybridisation of the loop sequence leading to false-negative results. In addition, the stem should be designed in order to prevent unfavourable secondary structure formation [125].

The prevention of fluorescence emission in the unbound state represents the most notable advantage as it allows the discrimination between bound and unbound probe [127]. Moreover, the MB technique profits from the possibility to use a wide range of fluorophore-quencher pairs [127]. All this contributed to the various application of MBs in (quantitative) real time polymerase chain reaction approaches [128-132], the detection of gene mutations or single nucleotide polymorphisms [133-136], and even DNA/RNA binding protein detection [137].

The combination with microscopy techniques enlarges the application spectrum of MBs by (live) cell imaging of nucleic acids, particularly RNA molecules.

Initially, the use of MBs for investigating mRNA in cells was limited to fixed conditions due to the vulnerability of MBs towards nuclease cleavage and the false-

positive signals produced by binding of RNA/DNA-binding proteins [138]. For this purpose, MBs have been modified variously to enhance the sensitivity. For example, additional FRET systems or wavelength shifts of the fluorophore were inserted and the native ribonucleotides were replaced by 2-O-methylribonucleotides to achieve nuclease resistance [125, 139-142].

Bratu *et al.* 2003 [123] demonstrated the use of such an modified MB to visualize the distribution and localisation of an endogenous mRNA (oskar mRNA) which plays an important role in *Drosophila melanogaster* development. Oocytes were microinjected with up to 10^6 MB molecules followed by immediate imaging. This method implies an invasive disruption of the plasma membrane which is apparently working with oocytes but causes cell damage or death to most cell types leading to an inefficient delivery of the probe.

A second example of an mRNA study in living cells using MBs was provided by Lennon *et al.* 2010 [120]. Here the influence of beta 1 integrin on the proliferation and differentiation of osteoblasts was investigated. The MB molecules were delivered into the living cells using the reversible permeabilisation of the plasma membrane with activated streptolysin O. The drawback of this technique is the lack of knowledge about the exact concentration of loaded probe per cell.

Furthermore, MBs have been used for imaging viral mRNA in living host cells [143]. Wang *et al.* 2008 [121] presented the sequence specific detection of the neuraminidase and the matrix protein 1 and 2 mRNA molecules inside living influenza A infected MDCK cells. Employing FRAP (fluorescence recovery after photobleaching [144]) they investigated the viral mRNA nuclear export.

The MBs used by Wang *et al.* were designed carrying at their 5´ends TAMRA (tetramethyl-6-carboxyrhodamine) which belongs to the group of heterocyclic dyes. TAMRA is quenched by DABCYL ((4-(4-dimethylaminophenyl) diazenylbenzoic acid) linked to the 3´ends of the oligomers. Fluorescence of TAMRA in the closed state of the MBs is hindered by non-radiative energy transfer (FRET, Förster resonance energy transfer [145, 146]) to the quencher. DABCYL can be

used as a universal quencher for a wide range of fluorophores. The underlying mechanism is a dipole-dipole interaction which is strongly influenced by the donor-acceptor distance and the transition dipole moments. Thus, minimal changes in the MB structure may cause false-positive or false-negative results by the aforementioned problems concerning the MB design [147, 148].

1.6.3 Peptide Nucleic Acids

In 1991 Nielsen and colleagues [149] synthesised a completely artificial analogue to nucleic acids in which the backbone was a pseudopeptide rather than monosaccharide rings and phosphodiester linkages. The structural properties gained the designation of this new molecule: peptide nucleic acid (PNA).

The nucleic bases (purine and pyrimidine) in a PNA molecule are directly attached to the glycine units by methylene carbonyl bounds, exhibiting stronger binding and more specific hybridisation properties than DNA/DNA or DNA/RNA hybrids or other common DNA derivates due to the lack of charge repulsion [150]. Moreover, they lack off-target effects due to non-specific binding to proteins or degradation by RNase H cleavage of the bound mRNA [151, 152]. PNAs are not vulnerable to nucleases or proteases [153].

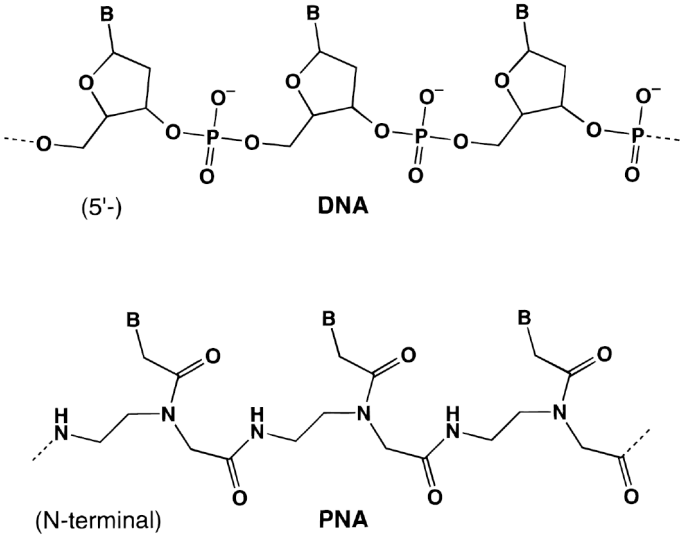

Figure 7: Depiction of the molecular structure of DNA and PNA molecules. (modified from Ratilainen et al. 1998)

The next section will present examples to emphasize the large variety of the application spectrum and practical flexibility of PNAs.

PNAs have been widely used as antisense agents in nuclear medicine [152, 154-157]. In Bonham *et al.* 1995 the described microinjection of a 15mer PNA targeted towards the untranslated region of the SV40 T antigen mRNA inhibited the expression of the T antigen in CV-1 cells with an efficiency of 99% [158]. Unwanted impact on the phenotype of cells treated with antisense oligomers may not occur while working with antisense PNAs due to the lack of a negative charge and thus excluded protein binding inside and outside of cells. Furthermore the stability of PNA/RNA hybrids is higher than PNA bound to DNA [159]. Hence, PNAs were thought to expand the potential of antisense research although predicting the susceptible mRNA target sequence has proven to be an elusive goal [160].

Recently, in the Wickstrom lab the usage of PNAs as radiohybridisation probes gave new impacts in cancer diagnostic medicine [161-164]. Chakrabarti and colleagues 2007 [165] demonstrated the detection of pancreas cancer before its physical, chemical or anatomical appearance applying PNAs to non-invasive PET

(positron emission tomography) imaging in mice of the *KRAS* mRNA carrying a disease specific (95 % of all ductal pancreas cancer patients) single nucleotide polymorphism (point mutation in codon 12). This enables an early intervention and promising treatment of cancer patients.

In addition, PNAs in complex with the contrast agent gadolinium (Gd^{3+}) enable intravital magnetic resonance imaging [166, 167]. The proof of principle was realized by Heckl *et al.* 2003 in the form of the identification of tumour cells with the help of PNA- Gd^{3+} labelling of c-myc over-expression [168].

An innovative step forward in PNA applications was realised by the chemical introduction of an intercalating fluorophore into a PNA molecule as an artificial base-surrogate [169, 170]. Thiazole orange which is commonly used in reticulocyte flow cytometry analysis to stain residual RNA in immature blood cells [171] exhibits favourable (fluorescence) properties in order to advance this technology.

Thiazole orange (TO) belongs to the group of asymmetric cyanine dyes and is essentially non-fluorescent in solution. The cationic chromophore intercalates with high affinity to polynucleic acids resulting in enhancement of quantum yield (0.1-0.4) which is a temperature dependent process [172, 173].

Initially, Privat *et al.* 2001 microinjected modified DNA oligomers with an alkyl linkage chain to thiazole orange into fixed human osteosarcoma (HOS) cells to localise mRNA molecules in the cytoplasm and nucleus [174].

The applicability of PNAs to RNA imaging in CHO cells was already demonstrated by Berndl *et al.* in 2010 using confocal laser scanning microscopy for visualizing RNA delivery. In this work the splicing and thus shortening in length of mRNA molecules is imaged with the help of the FRET pair TO- Alexa-594 [175].

The intercalation of TO as a base substitute within a PNA molecule was a further improvement. This method was developed in the sense of FIT (forced intercalation of thiazole orange)- PNAs by Seitz, Bergmann and Heindl [170] and tested

with respect to hybridisation, fluorescence, sensitivity and stability properties [176-179].

The increase of fluorescence is reported to occur in combination with each of the nucleic bases with a preference for thymine [180] and is able to reach a 20-fold enhancement with discrimination to the neighbouring base pairs [177]. The mechanism of the interaction with the bases in close proximity is generated by the structural architecture of two heterocyclic moieties linked by a (poly-) methine bridge. In the electronic ground state (S_0) these two aromatic ring systems are in peripendicular position to each other. Twisting of the moieties around the bond avoids fluorescence even when the molecule is optically excited. Monointercalation (one dye per two base pairs at saturation) leads to a forced torsional motion of the two rings into a coplanar position. This mechanism enables the formation of a π-electron system and thus the increase in fluorescence [181, 182].

Socher *et al*. 2008 described a DNA–PNA hybridisation assay based on real-time PCR that allows sensitive quantification of specific nucleic acids in solution and simultaneous detection of single base mutations. This approach demonstrates the biological applicability of FIT-PNA probes.

To the best of the author`s knowledge, this work was the first application of FIT-PNAs to detect (viral) mRNA molecules in the living cell [183].

Although originally designed to function as antisense and antigene reagent, PNAs, in particular FIT-PNAs, hold great potential for the investigation of dynamic processes in real time.

1.7 QUANTITATIVE PROTEOMICS: SILAC (STABLE ISOTOPE LABELLING OF AMINO ACIDS IN CELL CULTURE)

During viral infection, interactions between viral and host cell proteins are major checkpoints for en efficient replication of the virus or respectively survival strategies of the host cell. Thus, these interaction pathways and the involved components offer strong potential for new antiviral drug development and deeper understanding of the entire infection mechanism.

Traditionally, for qualitative and quantitative proteomics two-dimensional (2D) gel electrophoresis has been employed. In (2D) gel electrophoresis proteins are separated in the first dimension according to their isoelectric point and in the second dimension by their molecular weight [184]. The underlying mechanism of a semi-quantitative protein analysis using 2D gel electrophoresis is the comparison of protein staining intensities with respect to a protein standard of known protein concentration [185].

The simultaneous identification and quantification of proteins was realized by introducing mass spectrometry (MS) into the field of proteomics [186]. This generic term implies a description of the complete protein set expressed by the whole genome in the lifetime of a cell including posttranscriptional and posttranslational modifications [187]. Mass spectrometry is *per se* not quantitative due to variations in the detector response or differential ionization yields for different substances. Accuracy in peak ratios can be realized by using isotopic analogues caused of their chemical uniformity [186].

Initially, isotopic labelling was performed by incorporating ^{18}O (oxygen) atoms at the C-terminus of a peptide [188] in protein chemistry or by ^{15}N (nitrogen) substitution of all N atoms for quantifying variations of microorganisms [189, 190]. These methods have crucial drawbacks as the limitation of the ^{15}N substitution to bacteria, incomplete labelling efficiency or difficulties in data interpretation caused by varying numbers of N atoms in peptides. Further attempts to improve the sensitivity including the ICAT (isotope-coded affinity tag) method [191] re-

quired the necessity of chemical modifications of the proteins making the whole process even more complicated.

A more sensitive method which guarantied an easy labelling strategy was urgently requested. For this purpose, Ong *et al.* 2002 presented an inexpensive, robust and convenient technique which was termed SILAC (stable isotope labelling of amino acids in cell culture). Precisely, cells are propagated in cell culture media supplemented with isotopic variants of essential amino acids. All newly synthesized proteins contain the labelled amino acids without performing chemical modifications or affinity purification procedures [186]. By altering the incorporated nonradioactive isotopes several protein species are distinguishable allowing determination of protein abundance based on relative MS signal intensities [192, 193].

SILAC was already used in comparative proteomic phenotyping to compare cell lines to their primary counter-parts [194], in specific investigations of histone posttranslational modification patterns and their correlation to particular tumor features [195], and for the identification of Tyr kinase substrates [196].

One of the first large-scale proteomic studies was performed in the lab of Macek [197]: two physiologically different cultures of *Bacillus subtilis* have been investigated covering 75 % of the expressed genes in the log growth phase (1928 identified proteins). Besides studies on cellular and microbial level, SILAC is also applicable to *in vivo* approaches as shown by the Selbach group (SILAC fly) [198] and by Walther and Mann (SILAC mouse) [199].

In addition, the SILAC technique is useful in virology in order to investigate virus-host interaction during the replication. Studies on the coronavirus infectious bronchial virus [200, 201] and on the respiratory syncytial virus (RSV) [202] demonstrate the importance and high information output gained from SILAC based approaches.

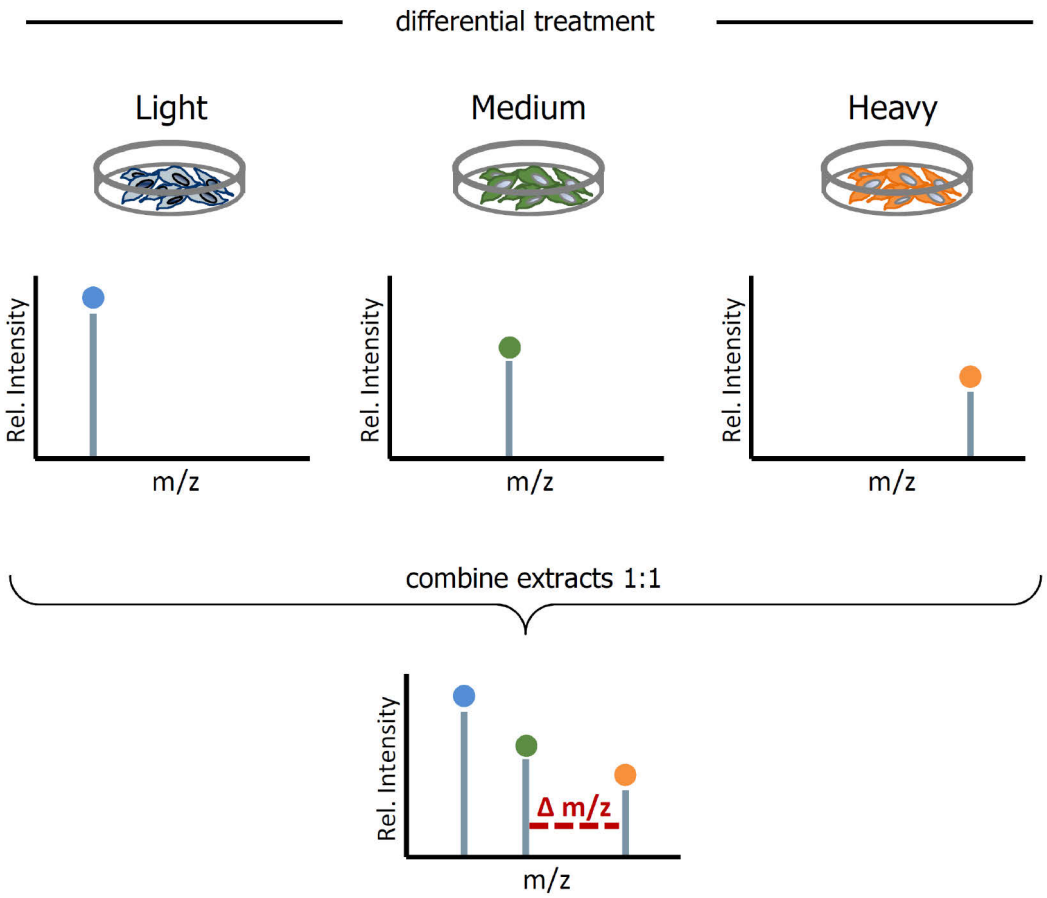

Figure 8: Depiction of the schematic procedure of a typical SILAC experiment and the mass spectrometry output. (adapted from the pSILAC scheme of Schwanhäußer et al. 2009)

2. AIM OF THE THESIS

In anticipation of a pandemic outbreak of influenza A virus with respect to the persistent threat of evolving human and avian variants with highly pathogenic potential detailed knowledge about the viral replication cycle and impact on the host cell are urgently ask for. Influenza A virus hijacks cellular biosynthetic pathways, intracellular transport mechanisms and biomolecular resources while interacting with host proteins for an efficient replication and production of progeny virus particles. Every single step of the replication cycle from entry to budding needs to be investigated to allow the development of preventive and therapeutic antiviral strategies.

Therefore this work focuses on the viral transcription and translation as well as the involvement and response of the host cell.

Due to essential drawbacks of existing nucleic acid detection techniques in the cellular context the development of a widely applicable, highly specific and sensitive method to study viral mRNA is one of the most relevant issues. The present thesis was undertaken to explore the suitability of FIT-PNA molecules to investigate the viral transcription in the early phase of influenza A virus infection in living host cells. To assess the spatial, temporal and quantitative progression of viral mRNA molecules a specific RT-qPCR shall be combined with a study in living infected cells using CLSM.

Previous studies already assessed the alterations of the cellular proteome after infection to identify viral host-interaction partners. With the help of quantitative proteomics based on mass spectrometry the early phase of an influenza A virus infection shall be characterized to reveal host factors involved in viral replication and analyse the temporal progression of viral protein synthesis.

3. MATERIAL AND METHODS

3.1 MATERIAL

3.1.1 EQUIPMENT

Designation	Provider
Centrifuge Biofuge stratos	Heraeus, Berlin, Germany
Centrifuge Fresco 17	Heraeus, Berlin, Germany
Confocal Microscope Fluo View™ 1000	Olympus, Hamburg, Germany
Fluorescence spectrometer (VC Eclipse)	Agilent Inc., Santa Clara, U.S.A.
Fridge (4 °C and -20 °C)	Bosch, Gerlingen, Germany
Fridge Hera freeze (-80 °C)	Thermo scientific, Berlin, Germany
Incubator	Heraeus, Berlin, Germany
Microliter Cell	IMPLEN GmbH, Munic, Germany
Milli-Q Ultra Pure Water Purification System	Millipore Corp., Bellerica, U.S.A.
Laminar hood	Heraeus, Berlin, Germany
Pipette, electrical (pipetus)	Hirschmann Laborgeräte, Herrenberg, Germany
Photometer (Biophotometer plus)	Eppendorf, Hamburg, Germany
iQ5 Real-Time PCR Detection System	Bio-Rad Laboratories Inc., Hercules, U.S.A.
Varioklav	Thermo Scientific, Berlin, Germany
Vortex-genie 2	Scientific industries, New York, U.S.A.
Water bath DC10	Haake, Victoria, Australia

3.1.2 Consumable Material

Designation	Provider
Cryo tubes (1.5 ml)	Sarstedt, Nümbrecht, Germany
5 ml round-bottom tubes (FACS)	Sarstedt, Nümbrecht, Germany
Glass ware	Carl Roth, Karlsruhe, Germany
Pipettes	Eppendorf, Hamburg, Germany
Pipette tips (1 - 1000 µl)	Sarstedt, Nümbrecht, Germany
Reaction tubes (1.5 ml, 15 ml, 50 ml)	Sarstedt, Nümbrecht, Germany
Cell culture flasks (T25, T75)	Nunc, Langenselbold, Germany
Cell culture plates (6 well, 12 well)	Nunc, Langenselbold, Germany
35 mm glass bottom dishes	MatTek, Ashland, U.S.A.
Fluorescence quartz cuvettes (3x3 mm)	Hellma Analystics, Müllheim, Germany

3.1.3 Biological Material

3.1.3.1 Eucaryotic Cell Lines

Cell line	Description
BHK-21 cells (baby hamster kidney)	adherent, fibroblasts
MDCK cells (madin darbin canin kidney)	adherent, epithelial cells

3.1.3.2 VIRUSES

Influenza A /Puerto Rico/34/8 and influenza A/X-31 (Institute of Biology, Humboldt University, Berlin) were grown in 10-day-old chicken embryos and purified as described previously [203].

Semliki Forest Virus and Vesicular Stomatitis Virus (kindly provided by PD Dr. M. Veit, Institute of Immunology and Molecular Biology, Free University, Berlin) were obtained in BHK-21 cells.

3.1.4 CHEMICALS

Designation	Provider
Complete, Mini Protease Inhibitor Cocktail	Roche, Mannheim, Germany
DTT	Fluka Analytical, St. Louis, U.S.A.
HCl	Sigma Aldrich, St. Louis, U.S.A.
Meliseptol	Th. Geyer, Renningen, Germany
Natrium chloride	Sigma Aldrich, St. Louis, U.S.A.
Nonidet P40 Substitute >99% (NP 40)	Fluka BioChemika, St. Louis, U.S.A.
Paraformaldehyde	Sigma Aldrich, St. Louis, U.S.A.
Propidium iodide	Sigma Aldrich, St. Louis, U.S.A.
RNasin Ribonuclease Inhibitor	Promega Corp., Madison, U.S.A.
Saponin	Fluka, St. Louis, U.S.A.
Streptolysin O	Sigma Aldrich, St. Louis, U.S.A.
TRISMA Base >99.9% Tris[hydroxymethyl]aminomethane	Sigma Aldrich, St. Louis, U.S.A.

3.1.5 Media and Solutions

Designation	Provider
DMEM (without Phenol red)	PAA GmbH, Wien, Austria
DPBS (with Calcium and Magnesium)	PAA GmbH, Wien, Austria
DPBS (Without Calcium and Magnesium)	PAA GmbH, Wien, Austria
Foetal Bovine Serum (FBS)	PAA GmbH, Wien, Austria
HEPES (25 mM) in DPBS	PAA GmbH, Wien, Austria
L-Glutamat (200 mM)	PAA GmbH, Wien, Austria
Penicillin/Streptomycin (100x)	PAA GmbH, Wien, Austria
Trypsin/EDTA (0.025 %)	PAA GmbH, Wien, Austria

3.1.6 Kits

Designation	Provider
RNeasy Mini Kit (RNA purification)	Quiagen, Hilden, Germany
SuperScript™ II (cDNA synthesis)	Invitrogen, San Diego, U.S.A.

3.1.7 Antibodies

Designation	Provider
mouse anti-NP (Influenza A), monoclonal	Chemicon, Billerica, U.S.A.
goat anti-mouse IgG, conjugated with Alexa 568	Mol. Probes, Karlsruhe, Germany
rabbit anti-VSV glycoprotein, polyclonal, serum	PD Dr. M. Veit, Free University, Berlin, Germany
goat anti-rabbit IgG, conjugated with Cy3	Mol. Probes, Karlsruhe, Germany

3.1.8 FIT-PNAs and Molecular Beacon

Name	Description	Sequence
FIT PNA 1a	neuraminidase, H1N1	H-Lys-cagtta-Aeg(TO)-tatgccgttg-Lys-NH_2
FIT-PNA 1b	neuraminidase, H1N1	Ac-Lys(PEG)-cagtta-Aeg(TO)-tatgccgttg-NH_2
FIT-PNA 1c	matrix protein, H1N1	H-Lys(PEG)-catgtctg-Aeg(BO)-ttagtg-NH_2
FIT-PNA 1d	L protein, VSV	H-Lys(PEG)-cgttt-Aeg(TO)-taattcgtctc-Lys(PEG)-NH_2
MB 2	neuraminidase, H1N1	TMR-gcgactttcagttattatgccgttgtatttgtcgc-Dabcyl

FIT-PNAs were synthesized by Dr. A. Knoll (Institute of Chemistry, Humboldt University, Berlin, Germany) and the Molecular Beacon was received from BioTez GmbH (Berlin, Germany).

3.1.9 Oligomers and Primers

Name	Description	Sequence
RNA target 3a	nt 599-615, A/PR/8, NA	5`CAACGGCAUAAUAACUG 3`
RNA target 3b	nt 594-618, A/PR/8, NA	5`AAAUACACCGGCAUAAUAACUGAAA 3`
RNA target 3c	nt 525-539, A/PR/8, M1	5`CACUAAUCUGACAUG 3`
RNA target 4	nt 16-32, H3N2, DQ874878	5`UCAAAAGAUAAUAACAA 3`
DNA target 5	nt 599-615, A/PR/8	5`CAACGGCATAATAACTG 3`
RNA target 7	nt 9108-9124, VSV, 001560	5`GAGACGAAUUAGAAACG 3`
primer fwd NA	nt 570-595	5`GATAATGGAGCAGTGGCTGTATTAA 3`
primer rev NA	nt 643-661	5`GCACATTCAGACTCTTGTGTCCTC 3`
primer fwd M1	nt 461-482	5`CTGGTATGTGCAACCTGTGAA 3`
primer rev M1	nt -595-615	5`TCACTCGATCCAGCCATTTG 3`

Nucleotides are indicated referring to the accession number NC_002018 (A/PR/8, H1N1), if not stated otherwise.

3.1.10 Software and Web Pages

Designation	Provider
Adobe Photoshop 7.0	Adobe Systems Inc., San Jose, U.S.A.
Ape- A Plasmid Editor	M. Wayne Davis
Entrez PubMed	http://www.ncbi.nlm.nih.gov/entrez/
FlowJo	Tree Star, Ashland, U.S.A.
FluoView 1000	Olympus, Tokyo, Japan
GraphPad Prism	GraphPad Software, La Jolla, U.S.A.
mfold	Zuker et al. 1991 [204]
Microsoft Office 2007	Microsoft, Washington, U.S.A.
NCBI-Blast	http://www.ncbi. nlm.nih.gov/blast/mmtrace.html
Gene Ontology Project	http://www.geneontology.org/GO.doc.shtml#ontologies

3.2 Methods

3.2.1 Working under Sterile Conditions

Preventing contamination by bacteria, yeast or fungi is one of the important aspects one has to consider while working with mammalian cell culture. Infections influence cellular processes and states and thus the behaviour within experimental treatments. All used glass and plastic ware was sterilised employing a steam autoclave. The laminar hood was cleaned by UV light for 1 h weekly. Prior to every working procedure the bench was treated with Meliseptol.

3.2.2 Cell Culture

3.2.2.1 General Handling

MDCK and BHK-21 cells were obtained in DMEM (without phenol red) supplemented with 10% FBS, 1 mM L-glutamine and 1% penicillin /streptomycin in a humid incubator at 37 °C and 5% CO_2.

For long-term storage cells were harvested using 2 ml trypsin/EDTA and transferred into freezing medium (DMEM without supplements, 20% DMSO, 80% FBS). To obtain a decrease in temperature by one degree per hour the cryo tubes have been incubated overnight at -80 °C using an isopropanole freezing box prior to storage in the liquid nitrogen tank.

Thawing was performed in a 37 °C pre-warmed water bath. Immediately after thawing the cells were transferred into 12 ml of fresh DMEM and centrifuged at 300 x g for 5 min. The cell pellet was resuspended in 5 ml pre-warmed DMEM and the cells were maintained in T25 cell culture flasks.

In a period of 3 to 4 days BHK and MDCK cells were splitted in a 1:10 ratio. Adherent growing cell lines establish connections with the plastic layer of the culture flasks since they are organised in association to their neighbouring cells in nature. Therefore a trypsin mediated peptide cleavage was necessary prior cell passaging.

Cells subjected to virus infection were seeded in 35 mm glass bottom dishes at 80% confluency in DMEM lacking phenol red. Usually, this indicator is used to assess the pH of the media. In fluorescence microscopy this red dye may disturb the fluorescence of interest or interfere in the emission range.

3.2.2.2 Cell Viability Test

Due to virus infection or SLO mediated transient cell perturbation (see chapter 3.2.2.3) the cell viability may be negatively influenced. Proofing cell viability cells

were treated with 5 µg of propidium iodide in 1 ml DPBS (Ca^{2+} / Mg^{2+}) for 5 min at room temperature and washed once with fresh DPBS (Ca^{2+} / Mg^{2+}) prior imaging. Propidium iodide is a DNA intercalating fluorophore which is commonly used for identifying dead or apoptotic cells as it is excluded from viable cells. For a positive control 10 µl of 1 N HCl was added over the cells for 20 min resulting in cell apoptosis.

3.2.2.3 DELIVERY OF PNAS INTO LIVING CELLS

Caused by their structural characteristics (e.g. uncharged peptide backbone) PNAs do not interact with Lipofectamine 2000 (Invitrogen) or related transfection reagents. Therefore the delivery of PNAs into living MDCK cells requires the help of streptolysin O, a streptococcal haemolytic exotoxin, which mediates reversible plasma membrane penetration as described previously [121]. In brief, 5 U streptolysin O in DPBS supplemented with 25 mM Hepes and 10 mM DTT were activated for 90 min at 37 °C. For staining, 250 nM PNA in 500 µl activated SLO containing solution were added to the cells for 30 min at 37 °C. Resealing was performed by adding 2 ml of fresh DMEM and incubating for additional 30 min at 37 °C. Before starting fluorescence microscopy imaging the medium was changed to 1 ml DMEM without supplements.

3.2.2.4 DELIVERY OF PNAS INTO FIXED CELLS

MDCK cells are of epithelial origin and thus exhibit a strong cell-cell-adhesion. In contrast, the fibroblast cell line BHK-21 lacks such extensive adhesion and is therefore unsuitable for SLO treatment. For FIT-PNA delivery BHK-21 cells were fixed with the help of 1 ml 4% paraformaldehyde in DPBS. After 20 min incubation at room temperature, cells were rinsed with 1 ml DPBS before adding 1 ml 0.1% Triton X-100 for 10 min at room temperature. Two washing steps with 1 ml DPBS were required to stop further permeabilisation. PNAs were delivered at a concentration of 250 nM in DPBS to achieve an efficient staining of viral mRNA. In preparation of fluorescence microscopy imaging the staining solution was replaced with 1 ml fresh DPBS.

Fixed BHK cells in 35 mm cell culture dishes can be stored at 4 °C for several weeks with negligible decrease in fluorescence signal if protected from light.

3.2.2.5 DELIVERY OF PNAS INTO FIXED CELLS IN SOLUTION

For intracellular FACS staining cells have to be in suspension. Therefore adherent growing MDCK cells were treated with trypsin and for further staining sedimented at 300 x g for 3 min. All following steps were performed on ice to maintain 4 °C during the staining procedure. The cell pellet was resuspended in 1 ml 4% para-formaldehyde. Cells were fixed for 20 min, sedimented (300 x g, 3 min) and washed with 1 ml DPBS. Permeabilisation was performed in 500 µl 0.5% saponin in DPBS. The cells were centrifuged as described above to reduce the volume by decanting the supernatant. 250 pM of FIT-PNAs were added into the remaining cell solution (circa 50 µl) and incubated for 15 min. After staining, the cells were rinsed with DPBS and stored at 4 °C until FACS analysis.

3.2.2.6 CELL LYSATE

In preparation of experiments in living cells FIT-PNAs were hold in cell lysate in order to assess their nuclease resistance. Cells seeded in 6-well plates were infected as indicated. After rinsing with 1 ml DPBS cells were lysed using 1 ml lysate buffer (50 mM Tris (pH 7.4), 150 mM NaCl, 0.8% NP-40 in dd H_2O) for 5 min at room temperature. Carefully the cell lysate was transferred into 1.5 ml reaction tubes and stored on ice until fluorescence spectrometer measurement.

Data acquisition was performed in fluorescence cuvettes filled with 100 µl cell lysate from non-infected MDCK cells. Fluorescence was measured at 530 nm after excitation at 485 nm. For hybridisation 0.1 nmol FIT-PNA probe 1a and 1 nmol target 3a were incubated in water for 10 min. 5 µl of this solution as well as a control solution lacking the target were added to the lysate containing cuvettes. The fluorescence was measured at 37 °C. Data points were collected every minute for 30 min followed by a 5 min interval for additional 30 min.

For the Molecular Beacon MB2 the excitation wavelength was 559 nm and emission was recorded at 593 nm. The measurement was performed simultaneously to the described procedure of the FIT-PNA 1a.

The relative fluorescence (=responsiveness) was determined at various time points and calculated according to the following equation:

$$relative\ fluorescence = \frac{\left[F(t)/F_0(t) \right]}{\left[F(t=0)/F_0(t=0) \right]}$$

, where F and F_0 are the fluorescence intensity of target-containing or control lysates, respectively, and $F\,(t=0)$ is the background fluorescence.

3.2.3 Infection Protocol

BHK-21 cells were infected with Vesicular Stomatitis Virus (subtype Indiana) and Semliki Forest Virus. MDCK cells were infected with influenza A/PR/8 virus. Cells were seeded 1 day prior to infection in 35 mm glass bottom dishes for microscopy imaging or in 6-well plates for e.g. FACS analysis at 80% confluence. In all indicated experiments infection with virus was performed at a multiplicity of infection (M.O.I.) of 100. To this end, the virus solution was added directly into 1 ml DMEM and added to the cells. To allow the virus to attach to the cell surface after one hour incubation at 37 °C, the supernatant was replaced by 1 ml fresh DMEM and incubation was continued.

3.2.4 Molecular Biology

To assess the viral mRNA production during the infection life cycle and to identify optimal time points for fluorescence microscopy imaging quantitative RT-PCR with influenza A specific primers was employed.

3.2.4.1 RNA PURIFICATION

Total RNA from influenza A/PR/8 (infection protocol see chapter 3.2.3) at various time points p.i. and non-infected MDCK cells was purified using the RNeasy Mini Kit following the manufactures instruction. In preparation for the purification 10^6 cells per sample were harvested by trypsinisation and sedimented at 300 x g for 5 min. Cell pellets were stored on ice until the experimental protocol was continued. RNA concentration was determined by an optical density (OD) measurement.

3.2.4.2 *IN VITRO* CDNA SYNTHESIS

As starting material for the *in vitro* reverse transcription 3 µg of total RNA was applied. The SuperScript™ II and oligo(dT) primer were employed as recommended by the manufactures protocol. It is recommended to perform the cDNA synthesis immediately after the RNA extraction in order to prevent damage to the RNA by freezing and thawing processes. The synthesised cDNA was quantified by OD measurement.

3.2.4.3 REAL-TIME QUANTITATIVE-PCR – MEASUREMENT

Measurement of the RT-qPCR was performed by Dr. Andrea Knoll (Institute of Chemistry, Humboldt University Berlin).

The reaction was carried out by using 100 ng cDNA of each sample as template employing 400 nM influenza A specific primers (see 3.1.9). This resulted in the amplification of a short sequence in the NA or M1 gene, respectively. FIT-PNA 1a or 1c was used at 500 nM (see 3.1.8) were utilized as detection fluorophore instead of the standard intercalator SYBR-Green enhancing the specificity of the data analysis. The reaction was realised in a volume of 20 µl in 96-well plates as described in table 1.

Table 1: RT-qPCR programme for cDNA amplification using the iQ5 Real-Time PCR Detection System.

Step	Temperature	Time	
initial denaturation	95 °C	3 min	
denaturation	95 °C	10 s	40 cycles
annealing	60 °C	20 s	
elongation	72 °C	20 s	

Fluorescence of the FIT-PNAs was measured during the annealing step every 3 s. As control cDNA was replaced by dd H_2O.

3.2.4.4 REAL-TIME QUANTITATIVE-PCR – DATA ANALYSIS

The calculation of specific viral mRNA copies per infected cell was based on the quantitative RT-PCR results. As mentioned above specific FIT-PNAs have been employed for signal detection.

The fluorescence intensity of TO or BO, respectively, correlates with the amplification of the template during the specific reaction in samples of infected MDCK cells. For quantification of specific target sequence (= copies of specific viral mRNA), a calibration curve was generated based on the related cycle of threshold (CT) values. The threshold fluorescence intensity was set threefold above the average no-template control fluorescence emission. The number of copies of specific viral mRNA present in 1 ng cDNA of starting material (100 ng cDNA for RT-qPCR) can be estimated according to the following equation:

$$No.\ of\ copies = \frac{mass\ of\ viral\ specific\ cDNA * N_A * 10^{-2}}{Molecular\ Weight\ of\ Amplicon}$$

, where N_A is Avogrado`s number (6.022 x 10^{23} molecules /mole) and the molecular weight of the amplicon is 61652.4 g/mol.

Considering the total amount of synthesised cDNA the copy number of specific viral sequence per total cDNA was calculated. With the help of the total amount of purified RNA with regard to the starting material for the in vitro reverse transcription, the copy number per total RNA was determined. Assuming that 10^6 cells have been used one can roughly estimate the specific viral mRNA concentration per infected cell.

3.2.5 IMMUNOCYTOCHEMISTRY (ICC)

Infected MDCK cells were stained 18 h p.i. with an anti-nucleoprotein (NP) antibody of influenza A virus to verify infection efficiency. For this purpose the intracellular labelling protocol using saponin as detergent was adapted. Cells were fixed and permeabilised as described (see chapter 3.2.2.5) but stayed attached in the cell culture dish. The fixed and permeabilised cells were rinsed twice with 1 ml DPBS for 1 min before blocking with 1 ml 3% BSA in DPBS for 1 h at 4 °C. The anti-NP antibody was diluted 1:1000 in 3% BSA in DPBS. There was no washing step required prior to incubation with the anti-NP antibody. The blocking buffer was replaced by 100 µl of the antibody solution and incubated for 1 h at room temperature. For visualisation of the antibody binding and thus indirect NP presence verification a secondary anti-mouse IgG antibody conjugated with Alexa 568 was added over the cells after rinsing the cells twice with 3% BSA in DPBS. For an efficient staining, 100 µl of the secondary antibody diluted 1:1000 in 3% BSA in DPBS was sufficient. After 1 h incubation at room temperature cells were washed twice with DPBS without supplements to prevent any interference or detaining background signals during microscopy imaging.

Verification of an efficient VSV infection in BHK-21 cells was performed following the same protocol. Specifically, the rabbit anti-VSV glycoprotein antibody was diluted 1:100 in 3% BSA in DPBS. The ICC was started 3 h p.i. to visualize VSV glycoprotein expression.

3.2.6 Fluorescence Activated Cell Sorting (FACS)

Cells can be categorised and identified based on cellular characteristics such as gene expression or status of differentiation (cluster of differentiation) using extracellular FACS analysis. FACS is a standard tool in clinical diagnostics for several applications. The applicability of the FIT-PNA technique to FACS analysis was investigated. For this purpose, influenza A infection was determined employing viral mRNA specific FIT-PNAs which were delivered into fixed MDCK cells as described in chapter 3.2.2.5.

The cell solution was transferred into FACS tubes and analysed using a BD FACS Aria™ II. TO fluorescence was recorded using the FITC channel with an excitation of 494 nm and an emission maximum of 519 nm. Each measurement was performed with 10,000 counting events. The system was calibrated with non-infected and unstained control MDCK cells to define the gate of intact cells in regard to the FCS (forward scatter, cell size) and SSC (sideward scatter, granular appearance) values. The settings were constant. FACS data were analysed using the provided software FlowJo.

3.2.7 Confocal Laser Scanning Microscopy (CLSM)

Fluorescence image acquisition was performed by a FluoView TM 1000 scanning unit using an IX 81 inverted confocal microscope and a 60x oil-immersion objective or a 60x water-immersion objective as indicated. The resolution was set to 512 x 512 pixel and sampling speed to 40 µs per pixel. Fixed cells were imaged at room temperature while for living cells a climate chamber to maintain 37 °C was required. Excitation and emission was performed as listed in table 2.

Table 2: Excitation and emission range of fluorophores used in FIT-PNAs or immunocytochemistry applications.

Fluorophore	Excitation	Emission range
TO	448 nm	510 nm - 540 nm
BO	440 nm	470 nm - 500 nm
TO and BO (sequential)	TO: 448 nm, BO: 440 nm	TO: 530 nm - 600 nm, BO: 460 nm - 490 nm
Alexa 568	559 nm	570 - 670 nm
TMR	559 nm	565 - 655 nm

3.2.8 Stable Isotope Labelling of Amino Acids in Cell Culture (SILAC) – Measurement

The following experimental part of the SILAC approach was realized in collaboration with Dr. Björn Schwanhäußer (MDC, Berlin) who kindly provided the SILAC-media and performed the liquid chromatography mass spectrometry (LC-MS) including required material preparation.

In global proteomic analysis on a systems level, recently SILAC attracted attention as a widely applicable and practical technique in combination with LC-MS.

The strategy of a typical SILAC experiment is premised on the metabolic incorporation of stable isotopic variants of amino acids. On this account, the applied FBS had to be dialysed to eliminate the natural amino acids which shall be replaced by their labelled counterpart. Here, a medium heavy and a heavy SILAC cell culture medium were prepared containing 84 mg/l ^{13}C6-L-argine in combination with 146 mg/l N4-L-lysine or 84 mg/l ^{13}C6^{15}N4-L-arginine in combination with 146 mg/l ^{13}C6^{15}N4-L-lysine, respectively. The light version of SILAC medium was supplemented with the non-labelled amino acids.

Upon cultivation in the specific SILAC medium over a period of eight passages MDCK cells incorporated uniformly the isotopic amino acids in their proteome. There was no influence on growth rate or cell viability provoked by the treatment of MDCK cells with the SILAC media.

MDCK cells were seeded in 6 well plates, infected as described (see chapter 3.2.3) with influenza A/PR/8 and harvested by trypsinisation according table 3 creating a time range 0 to 8 h p.i.

Table 3: Scheme of the experimental procedure of influenza A/PR/8 infected MDCK cell preparation within the SILAC approach.

Variant	Harvesting time point
MDCK cells in light SILAC medium	0 h post infection
MDCK cells in medium heavy SILAC medium	1 h, 2 h post infection
MDCK cells in heavy SILAC medium	4 h, 8 h post infection

After centrifugation at 300 x g for 3 min cell pellets were stored at -20 °C and mixed according to the following scheme:

Sample I: 0 h p.i. (light) + 1 h p.i. (medium heavy) + 4 h p.i. (heavy)
Sample II: 0 h p.i. (light) + 2 h p.i. (medium heavy) + 8 h p.i. (heavy)

After urea/thiourea mediated cell lyses an in-solution digest with trypsin and lysine-C protease which preferentially cleaves after lysine and/or arginine residues was performed. Peptides were desalted and concentrated with the help of self-prepared C18-columns. These elution columns operate on the principle of hydrophobic forces resulting from the binding of the peptide molecule to the C18-chain (stationary phase) upon association with the ligand in the aqueous eluent (mobile phase). Reduction of the water surface tension by adding less polar solvents (like methanol) leads to a decrease in retention of the bound peptide molecule.

Accordingly, the peptides are separated by their hydrophobic character using high performance liquid chromatography (HPLC) which automatically reduces the polarity of the mobile phase during the course of analysis producing a length gradient elution of the peptides. Immediately, the solute peptides were electrostatically ionized by electrospray ionization (ESI) and analysed by applied electrical fields inside the mass spectrometer. The peptide sequence was assessed by data analysis obtained from peptide collision with gas molecules.

3.2.9 Stable Isotope Labelling of Amino Acids in Cell Culture (SILAC) – Data Analysis

Data analysis of the LC-MS measurement was realized in collaboration with Dr. Björn Schwanhäußer (MDC, Berlin) and Max Flöttmann (Humboldt University, Berlin).

Light, medium heavy and heavy variants of a peptide were represented as clusters in an MS-output plot and discriminated due to their mass difference generated by the isotopic atoms. Quantification analysis was performed using the MaxQuant software [205] based on the formation of ratios within each isotope cluster. The measured peptides were aligned with dog protein databases (Mascot, Uniprot) which were *in silico* digested with the aforementioned proteases. Identified peptides were assigned to their biological process using gene ontology (GO) enrichment analysis via a hypergeometric test [206] package in Bioconductor for individual clusters with the complete set of measured genes as a background distribution.

The Gene Ontology Consortium provides an appropriate source of annotations for gene products and their properties. These include a cellular component, the molecular function and the biological process relevant in living systems like cells, tissues or organs. To exemplary elucidate this annotation the GO terms of cytochrom c are the following: mitochondrial matrix and mitochondrial inner membrane (= cellular component terms), oxidoreductase activity (=molecular function

term) and oxidative phosphorylation and induction of cell death (=biological process terms).

The requirement of a hypergeometric test results from the structure of the given data set: the MS analysis offers a peptide list which is connected to the corresponding GO term list.

The amount of genes in a given list (cluster) determines the value of expected frequency how often a certain GO term was assigned to this cluster. The probability that the expected value matches with the real one is expressed as p-values ranging from 0 to 1. In the hypergeometric test a GO term receives a low p-value if the real value exceeds the expected one.

Proteomic phenotyping for GO terms of the time point 8 h p.i. was performed as described in Pan *et al*. 2009 [194]. The distribution of measured log2 fold changes was divided into 4 quantiles. For each quantile a GO term enrichment test was repeated with all measured genes as background.

If a GO term reached a p-value > 0.5 for one of the quantiles it was transformed by -log10(p-value) and standardized using the following equation:

$$z = \frac{[x - mean\,(x)]}{sd\,(x)}$$

, where z is the standard score (dimensionless), x is the raw score (= p-value), mean(x) is the mean of all GO terms, sd (x) is the standard deviation.

The result of this conversion process were basically used to compute a 2D display of all values of the given data matrix. In a so called heat map the z-transformed p-values are hierarchically presented in a colour-coded diagram.

Clustering of GO terms was realized by standardizing the log2 fold-changes for the whole recorded infection time course of 8 h running a soft clustering algorithm, the fuzzy-c-means from the Mfuzz package [207] in Bioconductor [208].

This method provides on the one hand a very noise robust performance and on the other hand simplification of further filtering of relevant genes for each cluster. Accordingly, the membership value (0 – 1) is designated for each protein to the corresponding cluster and also subject to the fuzziness value c each appoint can be assigned to more than one cluster. The membership value defines the distance of a gene from the cluster centre. The number of clusters (c = 6) was defined by an iterative approach.

4. RESULTS

4.1 STUDIES ON THE NEURAMINIDASE TRANSCRIPT OF INFLUENZA A VIRUS

In fields of virology and medicine it is of great interest to investigate the virus replication in detail. Designing new and efficient antiviral drugs relies on the complete knowledge of the whole infection cycle. After attachment and fusion the production of viral mRNA is the first critical step for infection establishment.

In the following paragraphs of this chapter a novel strategy to investigate the time-resolved progression of viral mRNA synthesis *in vitro* and its cellular localisation in living infected MDCK cells using sequence specific FIT-PNAs is described. For initial experiments the neuraminidase transcript of influenza A virus was chosen as target due to its high relevance for the viral replication (please review Introduction chapters 1.2 to 1.4) and the possibility to use an accessible target sequence described in a previous imaging study [121]. All presented results in chapters 4.1.1 to 4.1.6 were published in Kummer *et al.* 2011 [183].

4.1.1 IDENTIFICATION OF A SUITABLE FIT-PNA

The solid phase synthesis [178] and fluorescence spectroscopy was performed by Dr. A. Knoll (Institute of Chemistry, Humboldt University Berlin) for all used PNA molecules.

The suitable FIT-PNA 1a was chosen out of the PNA oligomers listed in table 4. Keeping the length of the PNA oligomers constant, the TO-containing PNA-monomer was shifted through the sequence.

Table 4: PNA oligomers used to identify suitable FIT-PNA 1a with corresponding enhancement factors upon hybridisation with complementary target at 37 °C. Lys = Lysine

Sequence	Enhancement factor
H-Lys-cagtt-Aeg(TO)-ttatgccgttg-Lys-NH_2	3.5
H-Lys-cagtta-Aeg(TO)-tatgccgttg-Lys-NH_2	5.4
H-Lys-cagttat-Aeg(TO)-tatgccgttg-Lys-NH_2	3.9
H-Lys-cagttatt-Aeg(TO)-tgccgttg-Lys-NH_2	2.6
H-Lys-cagttatta-Aeg(TO)-gccgttg-Lys-NH_2	1.5
H-Lys-cagttattat-Aeg(TO)-ccgttg-Lys-NH_2	0.8
H-Lys-cagttattatg-Aeg(TO)-cgttg-Lys-NH_2	1.2
H-Lys-cagttattatgc-Aeg(TO)-gttg-Lys-NH_2	1.1

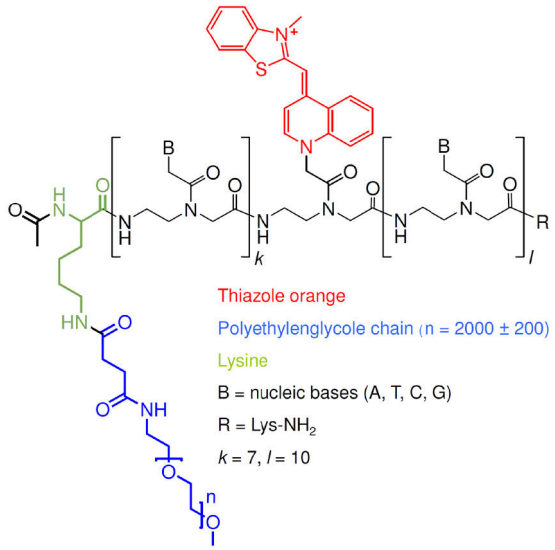

Figure 9: Chemical structure of FIT-PNA 1a.

Aiming on the development of a probe applicable for mRNA imaging in living cells and for quantification of mRNA expression levels by real-time PCR analysis the probe was tested at both conditions. Accordingly, fluorescence spectra of FIT-PNA 1a in absence of the complementary target and in the hybridised status

were recorded. To emulate the physiological condition in living cells RNA 3a (see 3.1.9) was used as target at 37 °C and to maintain RT-PCR conditions DNA 5 was employed as target at 60 °C. FIT-probe 1a provided an 11-fold increase of the TO emission upon hybridisation with complementary RNA target 3a and a 12-fold increase upon hybridisation with DNA 5 at 60 °C (see figure 10).

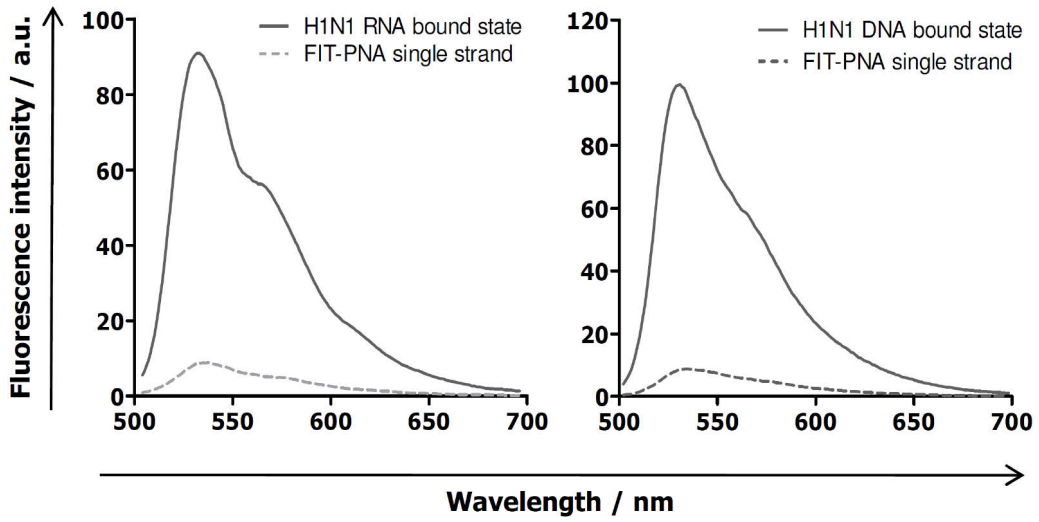

Figure 10: Fluorescence spectroscopic measurements of FIT-PNA 1a. Excitation wavelength was set to 485 nm. FIT-PNA 1a in presence (solid) and absence (dotted) of matched H1N1 RNA 3a (left panel) and H1N1 DNA target 5 (right panel) at 37 °C and 60 °C, respectively. Conditions: 1 µM probe and 10 µM target in 100 mM NaCl, 10 mM NaH_2PO_4, pH 7.0.

The N1 specificity of FIT-PNA 1a was confirmed by employing the sequence of the influenza A swine H1N1/Mexico/2009 variant which is shortened in length but the remaining sequence is identical to the A/PR/8 strain (see figure 11).

Additionally, the sub-type specificity was assessed employing the analogous sequence of the X-31 influenza A strain (NA mRNA, H3N2, nt 16–32). The X-31 sequence exhibits seven continuous matched base pairs situated in proximity to the TO base surrogate. Nevertheless, the fluorescence intensity of FIT-PNA 1a remained virtually unchanged upon supplementation of RNA 4 (see figure 11) at 37 °C.

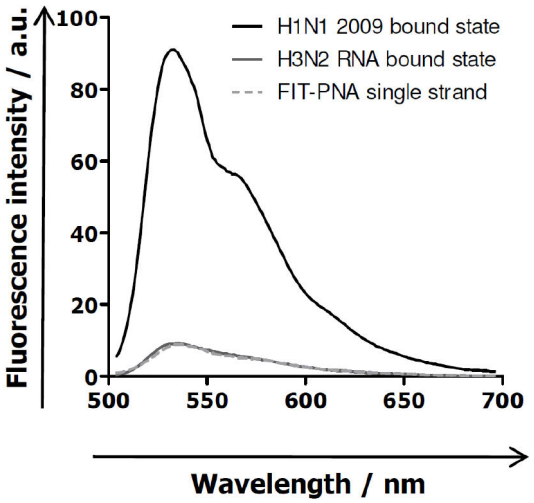

Figure 11: Fluorescence spectroscopic measurement of FIT-PNA 1a. Excitation wavelength was set to 485 nm. Emission spectra of FIT-PNA 1a in presence (solid, grey) and absence (dotted) of semi-matched H3N2 RNA 4 as well as in presence of the H1N1 2009 RNA (solid, black) was recorded from 500 nm to 700 nm at 37 °C. Conditions: 1 µM probe and 10 µM target in 100 mM NaCl, 10 mM NaH_2PO_4, pH 7.0.

4.1.2 Measurement of FIT-PNA Biostability in Cell Lysate

One of the main issues in nucleic acid research is the biostability of the detection probes. For instance fluorescent RNA or DNA oligomers for FISH (fluorescence *in-situ* hybridisation) applications lack nuclease-resistance and therefore their usage is essentially limited to fixed cells.

The enhanced biostability of FIT-PNAs relies on the peptide backbone (see Introduction chapter 1.6.3). This was demonstrated by comparing the fluorescence intensity of the FIT-PNA 1a with a DNA-Molecular Beacon (MB 2) both bound to the complementary RNA target over a time-scale of 60 min in MDCK cell lysate (see chapter 3.2.2.6).

The fluorescence intensity of MB 2 increased and consequently the sensitivity decreased by more than 40% as a result of just 60 min exposure to the cell lysate. This phenomenon can be caused by nuclease-mediated degradation and/or unselective binding of DNA binding proteins. This separates the chromophores spatially and leads to an increase of F0 in the absence of target. In contrast, the

increase of fluorescence F/F0 provided by FIT-probe 1a remained high, regardless of the duration of exposure as shown in figure 12.

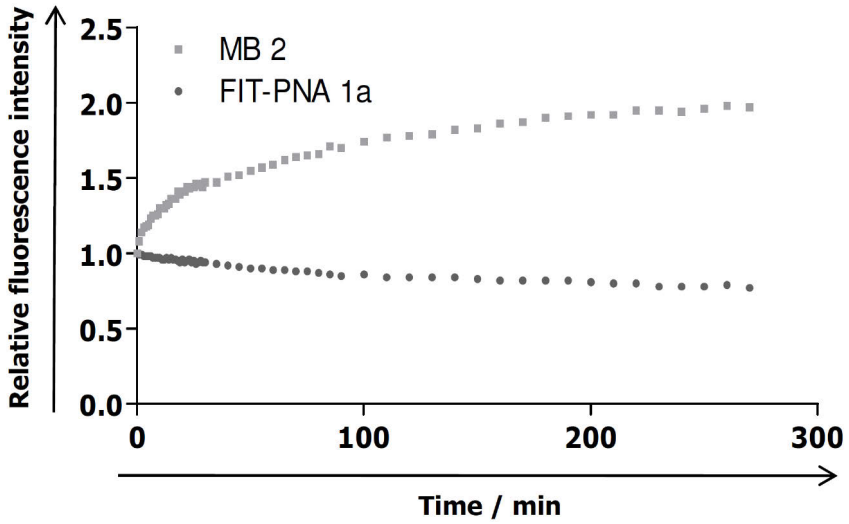

Figure 12: Relative fluorescent intensities of FIT-PNA 1a and MB 2 in cell lysate upon addition of complementary target. Probes were excited at 485 nm and 559 nm and emission was recorded at 530 nm and 593 nm for FIT-PNA 1a and MB 2, respectively. Conditions: 1 µM probe, 10 µM RNA target in 100 µl cell lysate, 37 °C.

We concluded that FIT-probe 1a is stable in cell lysates and thus, very likely also in living cells.

4.1.3 Real-Time Quantitative PCR

Real-time qPCR is frequently employed in the field of gene expression research. With the help of this sensitive method even very small changes in the expression level are detected. In this work RT-qPCR was used to assess the viral mRNA production during the infection cycle of influenza A/PR/8 in MDCK cells. The applied infection protocol, total RNA purification from MDCK cells, *in vitro* cDNA synthesis and RT-qPCR were carried out as described (see chapters 3.2.4.1 to 3.2.4.4).

In contrast to standard RT-PCR the detection fluorophore SYBR-Green (Invitrogen) was replaced by the NA specific FIT-PNA 1a. The increase in TO fluorescence during the amplification revealed the synthesis of an influenza A/PR/8 NA specific sequence in infected samples, which was not observed for the non-

template control (absence of cDNA) and for non-infected MDCK cells (see figure 13, left panel).

For quantitative analysis, a 10-fold dilution series of the amplicon was performed (see figure 13, right panel) and from this data a calibration curve was calculated (see figure 14). The cycle numbers needed to furnish threshold fluorescence (threefold above the average of non-template control fluorescence emission at cycles 3 – 12) were plotted against the template concentration. The CT value is linear, inversely proportional to the corresponding logarithmic template concentration: if the concentration of template decreases, the CT value increases, because there is less specific product synthesised. Therefore the coefficient of determination R^2 is used to estimate the proportion of variability in a data set. R^2 (given in figure 14) showed a high correlation and revealed high amplification efficiency and specificity. Over at least seven orders of magnitude the FIT-probe 1a provided a linear measuring range.

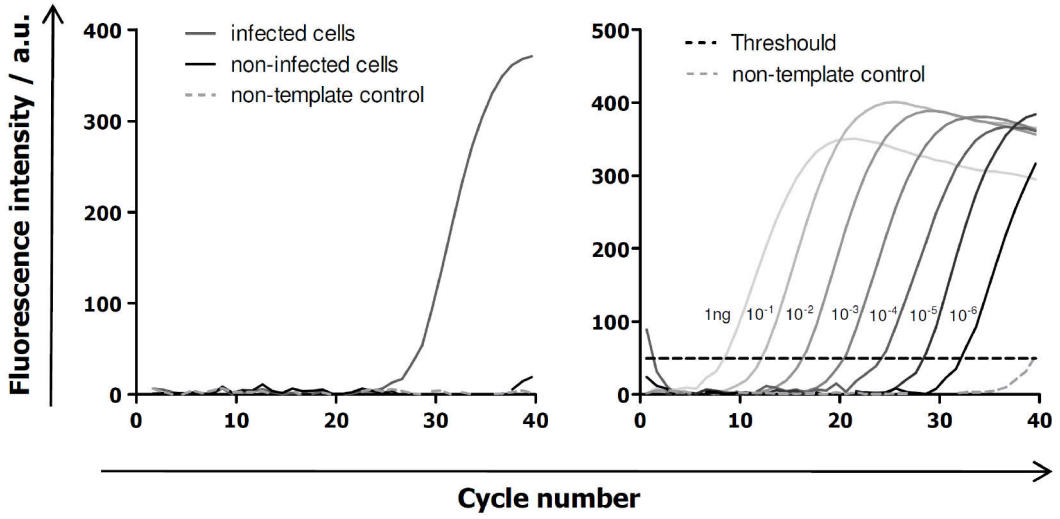

Figure 13: Quantitative Real-time PCR analysis. Left: Amplification curve on measuring fluorescence of FIT-PNA 1a in response to 1 ng cDNA obtained from influenza A/PR/8 infected MDCK cells 4.5 h p.i. (solid, grey), non-infected control cells (solid, black) and the non-template control (dotted). Right: Amplification curve of a short sequence encoding for the NA (H1N1) in a 10-fold dilution series. For conditions please review chapter 3.2.4.3. The mean of three independent experiments is plotted.

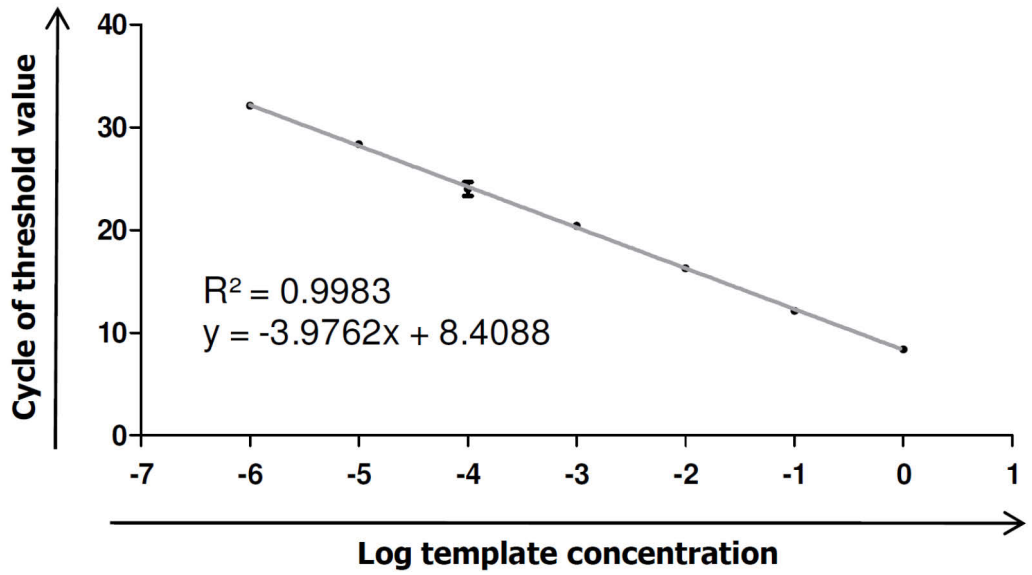

Figure 14: Logarithmic presentation of the calibration curve. Cycle of threshold values plotted against the logarithm of the template concentration in ng/µl to estimate the specificity of the RT-qPCR (R^2).

The results of the qPCR analysis revealed the time-dependency of the expression levels of viral mRNA. In figure 15 the NA copy number per 1 ng cDNA at 1 - 9 h p.i. is given. The graphed results revealed the required time of the virus to attain the maximal level of NA mRNA at 4 – 5 h p.i., which means that approximately 10^5 copies of NA mRNA per ng cDNA were used as template in qPCR.

In addition, assuming that 10^6 MDCK cells were used per sample one can roughly estimate the maximum NA mRNA level corresponding to about 10^4 copies per infected cell. This is in agreement with data reported for MDCK cells infected with an influenza A virus reassortant (A/NWS/33HA-G70cΔNAMviA, H1N9). In this study 10^5 copies of total viral mRNA per cell 7 h p.i. were detected by a ribonuclease protection assay [209].

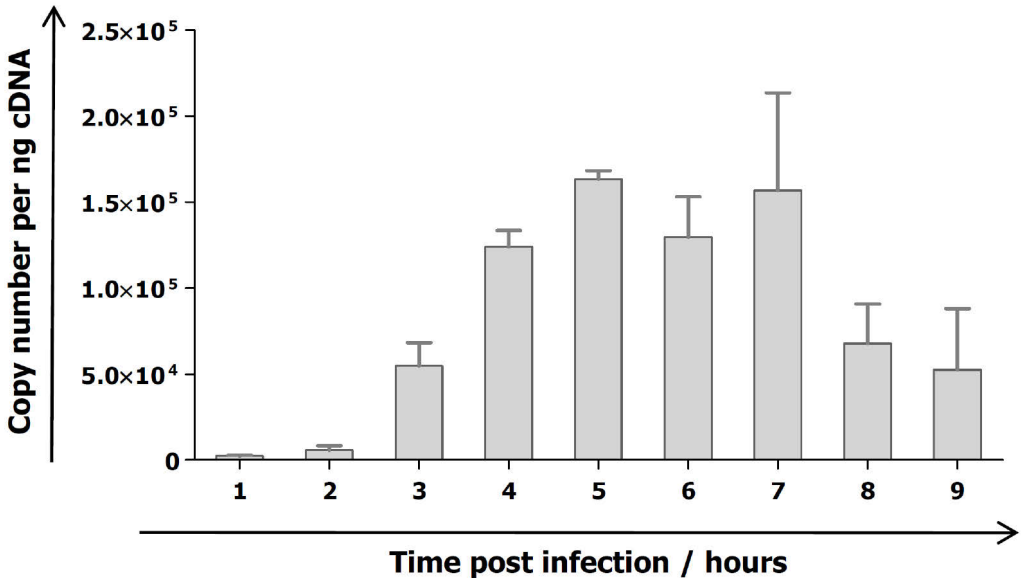

Figure 15: Time course of the NA mRNA copy number per ng cDNA of influenza A/PR/8 infected MDCK cells. The calculation relies on the calibration curve (Figure 14) obtained from the RT-qPCR analysis. Mean ±SEM of three independent experiments is plotted.

The viral mRNA expression levels decreased at prolonged times after infection illustrating the switch from transcription to replication mode.

4.1.4 Verification of Influenza A Infection

For fluorescence intensity data analysis the cells were selected manually from images (see chapter 4.1.6). Hence, it is important to determine the percentage of infected cells. Infection of MDCK cells with influenza A/PR/8, followed by specific labelling with an anti-NP (H1N1) antibody as well as a secondary goat anti-mouse antibody was performed as described in chapters 3.2.3 and 3.2.5 5 h p.i. The confocal laser scanning microscopy images depicted in figure 16 indicate an infection efficiency of ~98% by the near quantitative staining.

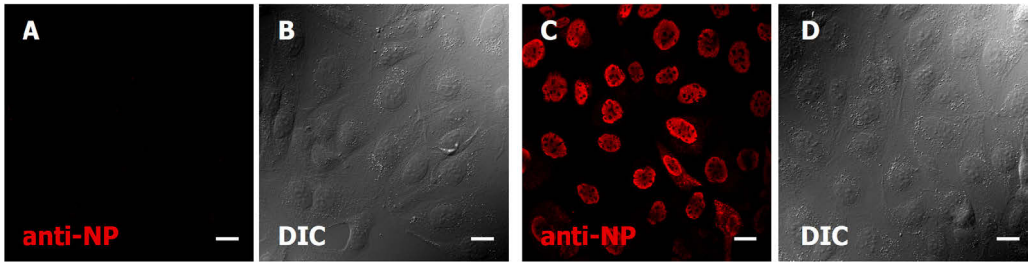

Figure 16: Confocal laser scanning microscopy images of fixed MDCK cells stained with an anti-NP (H1N1) antibody. (A, B) Non-infected MDCK cells and (C, D) influenza A/PR/8 infected MDCK cells (5 h p.i.) were labelled with an anti-NP (H1N1) antibody to determine the infection efficiency. Non-infected cells showed no fluorescence signal. In contrast the infected sample showed a strong nuclear NP staining. Images were acquired with an inverted confocal laser scanning microscope using a 60x oil-immersion objective at room temperature. Alexa 568 (anti-NP) was excited employing a 559 nm laser. White bars correspond to 10 µm. DIC = differential interference contrast

4.1.5 Verification of Cell Viability

FIT-PNAs were transferred into living MDCK cells using streptolysin O. As a consequence of the SLO treatment and reversible permeabilisation of the plasma membrane the cell viability might be impaired in cell damage and death. Here, a cell vitality test based on propidium iodide, which is excluded by intact cells, was employed to address this important issue. As demonstrated in figure 17 propidium iodide was excluded from both MDCK cells treated with SLO and untreated MDCK cells showing just minor fluorescence inside the cells. In contrast, cells incubated at acidic conditions exhibited a strong propidium iodide signal.

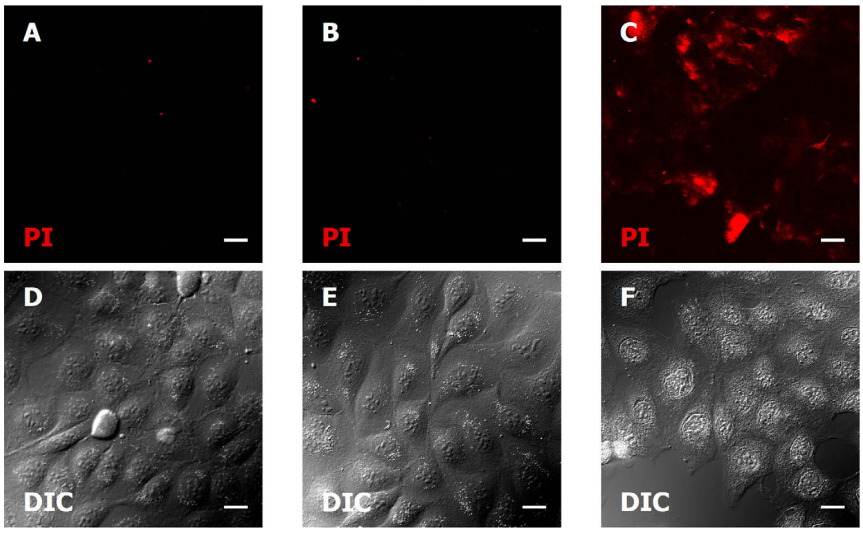

Figure 17: Confocal laser scanning microscopy images of living MDCK cells stained with propidium iodide (PI). (A, D) Untreated MDCK cells, (B, E) SLO-treated MDCK cells and (C, F) HCl-treated cells were incubated with PI for 10 min to determine the cell viability. Untreated and SLO-treated cells showed minor fluorescence signals. In contrast, the HCl-treated sample demonstrated a positive PI incorporation. Images were acquired with an inverted confocal laser scanning microscope using a 60x water objective at room temperature. PI was excited employing a 559 nm laser. White bars correspond to 10 µm. DIC = differential interference contrast

4.1.6 Detection of Neuraminidase mRNA in Living Infected MDCK Cells

Detailed information about a certain biological process requires preferably an easy examinable system that closely mimics in vivo conditions. Working in cell culture provides both: a living biological system and easy handling. For influenza A infection MDCK cells are the most prominent cell culture model system [210]. Employing this cell line the formation and localisation of NA mRNA was followed with the help of a sequence specific FIT-PNA. The probe 1a introduced in chapter 4.1.1 was extended by PEGylation to enhance the solubility in the cell cytoplasm and to prevent segregation or nuclear import [211, 212]. The linkage of a poly-ethylene glycol residue had just minor effects on its fluorescence responsiveness [183].

FIT-PNAs were transferred into living infected (and non-infected) MDCK cells grown on 35 mm glass bottom dishes enabled by SLO mediated plasma membrane permeabilisation (see chapter 3.2.2.3).

Considering the result of maximum NA mRNA level obtained by the above described RT-qPCR (see chapters 3.2.4.3 and 3.2.4.4) images in figure 18 were acquired 4.5 h p.i. to obtain the maximum enhancement of fluorescence. A first visual inspection indicated a strong increase in fluorescence for the influenza A infected cells in comparison to non-infected cells. Neither Semliki Forest Virus (SFV) [213, 214] infected cells nor cells infected with influenza A but stained with VSV L protein specific FIT-PNA 1d evinced similar fluorescence patterns. The probe 1d fluoresced upon hybridisation with specific VSV L mRNA in infected BHK-21 cells (see chapter 4.4), but is virtually non-responsive in influenza infected cells. These control experiments proved that the increased fluorescence is due to specific complex formation of FIT-PNA 1b with NA mRNA, but not to virus infection per se or unspecific binding processes mediated by proteins or nucleic acids.

The signal distribution inside influenza A infected MDCK cells appeared non-random. It is conceivably that due to regulatory, developmental and economical

aspects the (viral) mRNA is localised in subcellular compartments utilizing cellular transport mechanisms [211].

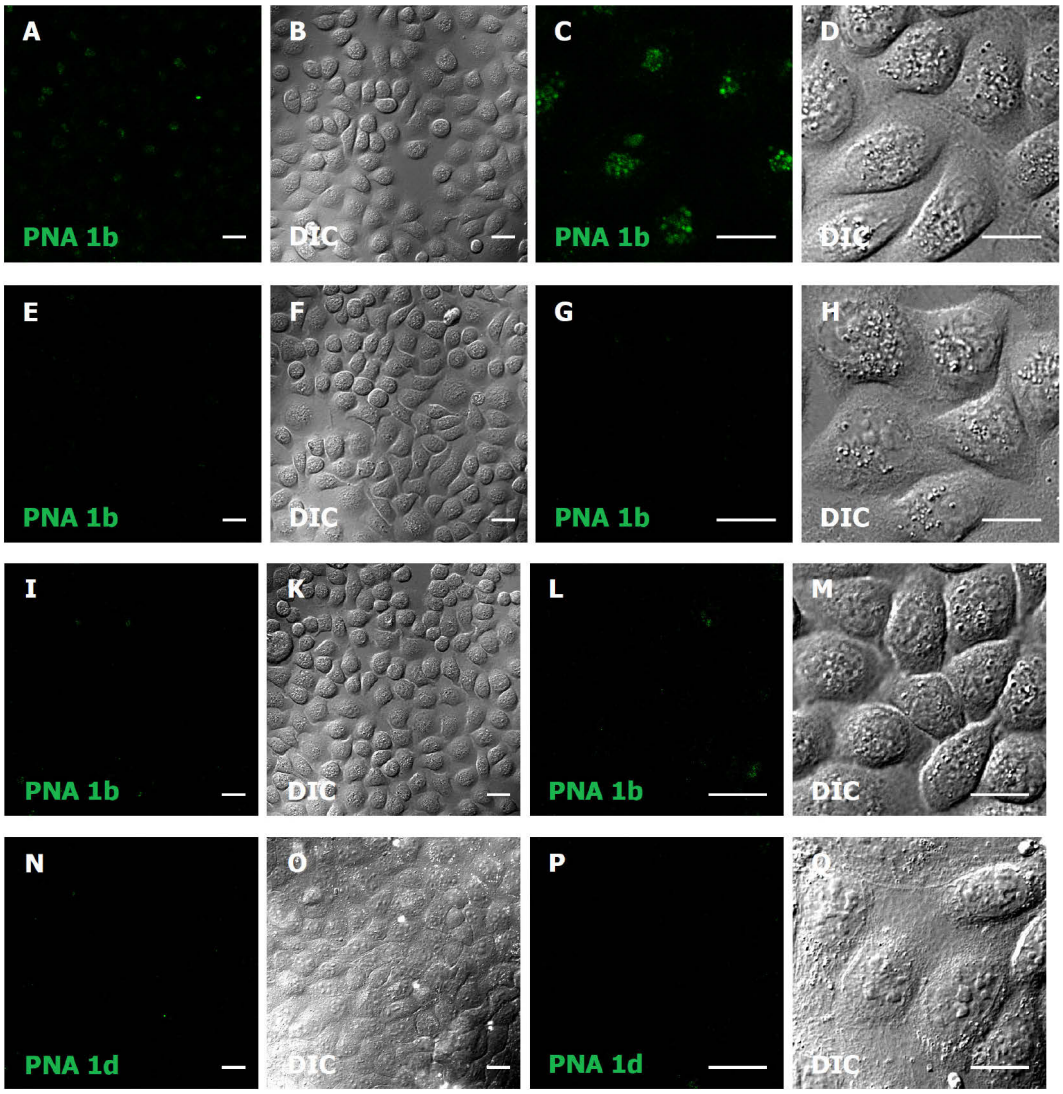

Figure 18: Confocal laser scanning microscopy images of living MDCK cells stained with FIT-PNAs. (A - D) Influenza A/PR/8 infected, (E - H) non-infected and (I - M) Semliki Forest Virus infected MDCK cells stained with FIT-PNA 1b (NA, H1N1) and (N – Q) influenza A/PR/8 infected cells stained with FIT-PNA 1d (L, VSV) at 4.5 h p.i. All control samples (E – Q) showed minor fluorescence signals. In contrast, the influenza A/PR/8 infected and with the NA mRNA specific FIT-PNA treated MDCK cells exhibited high TO fluorescence signals. Images were acquired with an inverted confocal laser scanning microscope using a 60x water objective at 37 °C. TO was excited employing a 488 nm laser. White bars correspond to 10 µm. DIC = differential interference contrast

An evaluation of FIT-PNA 1b performance compared to MB was realized by measuring MB 2 used in a previous viral mRNA imaging study [121] and comparing the fluorescence enhancement upon target binding in living infected MDCK cells. As illustrated in figure 19 the NA specific MB 2 showed just weak fluorescence signals. No significant difference between the infected and the non-infected cells could be visually observed.

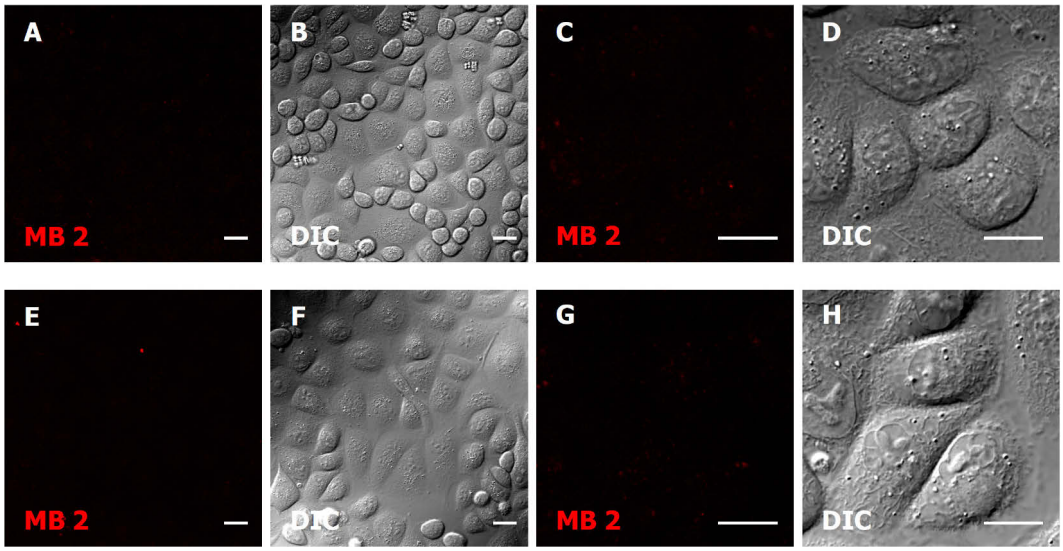

Figure 19: Confocal laser scanning microscopy images of living MDCK cells stained with MB 2. (A - D) Influenza A/PR/8 infected and (E - H) non-infected MDCK cells stained with MB 2 (NA, H1N1) at 4.5 h p.i. A comparison of both samples revealed no clear difference in fluorescence intensity. Images were acquired with an inverted confocal laser scanning microscope using a 60x water objective at 37 °C. TMR was excited employing a 559 nm laser. White bars correspond to 10 µm. DIC = differential interference contrast

For fluorescence intensity quantification an image analysis was performed using Image J. Regions of interest (ROI) including nucleus and cytoplasm were selected as depicted in figure 20 and the mean fluorescence intensity per area was calculated by the programme. The background fluorescence was subtracted for each image and all values were normalised to the corresponding control.

Images of influenza A infected MDCK cells stained with FIT-PNA 1b revealed a 4.5-fold enhancement of fluorescence compared to non-infected MDCK cells. Control experiments were performed and supported this finding. While SFV infected and FIT-PNA 1b treated cells showed a 1.1-fold increase in fluorescence,

for the influenza A infected but stained with FIT-PNA 1d MDCK cells no increase in fluorescence was observed.

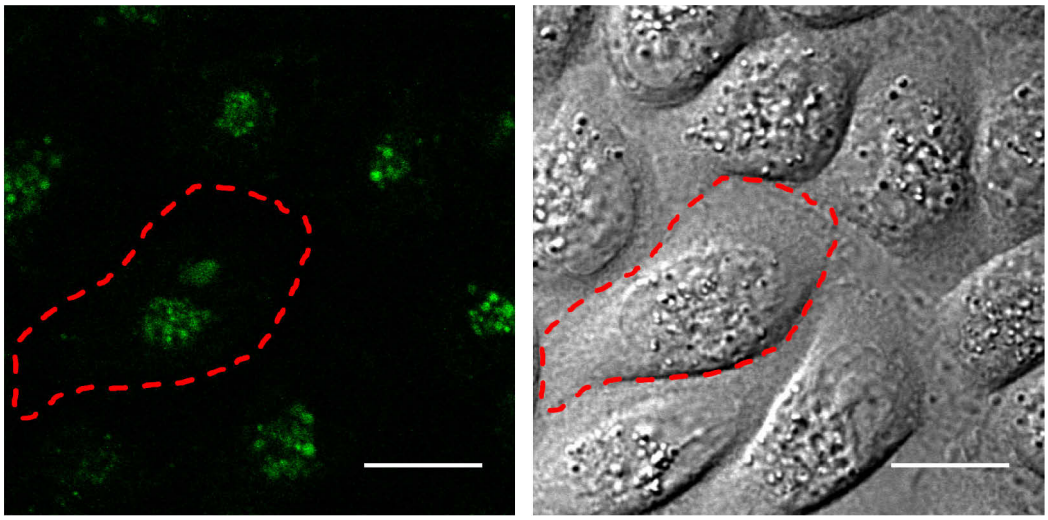

Figure 20: Image analysis using Image J for determining the enhancement factor. Row data images were used to calculate the mean fluorescence intensity of manually selected areas (ROI = region of interest). White bar corresponds to 10 µm.

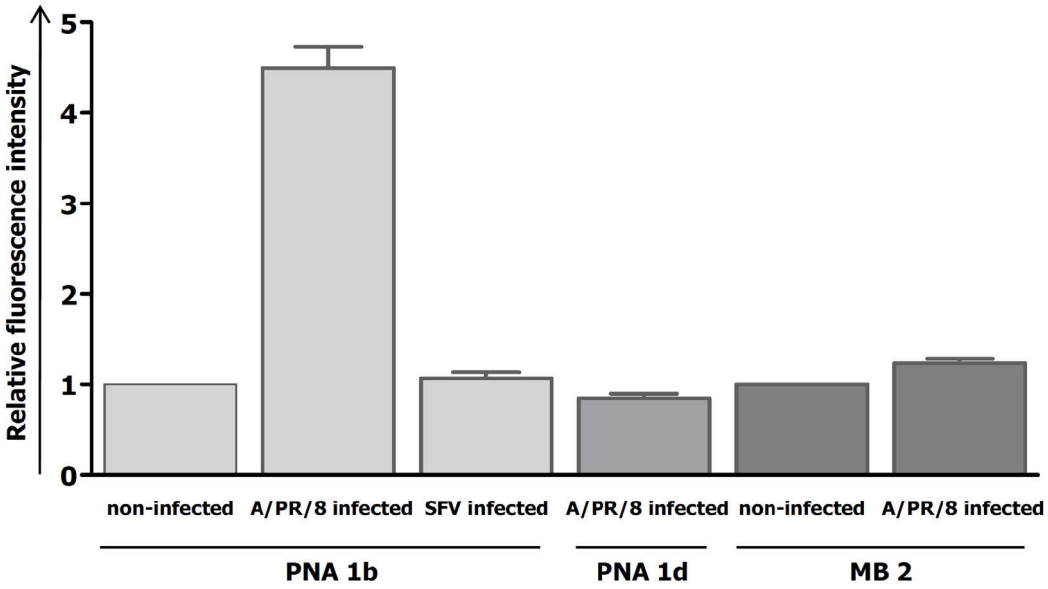

Figure 21: Relative fluorescence intensities of FIT-PNAs and MB 2 in living infected MDCK cells. The integrated fluorescence intensity values of influenza A/PR/8 NA specific FIT-PNA 1b, VSV L protein specific FIT-PNA 1d and influenza A/PR/8 NA specific MB 2 in MDCK cells infected with influenza A/PR/8 or infected with SFV, respectively, are shown. Normalized values are indicated as bars. Scatter bars correspond to SEM. Data represents three independent experiments with five cells per experiment (n=15).

4.1.7 FACS BASED DETECTION OF INFLUENZA A INFECTION

The FIT-PNA technique is applicable to a variety of diagnostic standard methods. This was demonstrated by utilizing the neuraminidase specific FIT-PNA 1b to detect influenza A infected MDCK cells in a FACS based approach (see figure 22). In contrast to the non-infected control, the influenza A/PR/8 infected cells showed an increased TO fluorescence signal. Furthermore, the shape of the intensity curve exhibited an additional maximum, which is called shoulder.

A second control using the X-31 influenza A strain (H3N2) was included into the FACS analysis. This strain lacks completely the target sequence of FIT-PNA 1b. Interestingly, the X-31 infected MDCK cells revealed a decrease in detected TO fluorescence compared to the non-infected control indicating the presence of a partial matching sequence in the cellular transcriptome. For verification of the presented results the experiment was repeated three-times independently. All replicates confirmed the results plotted in figure 22.

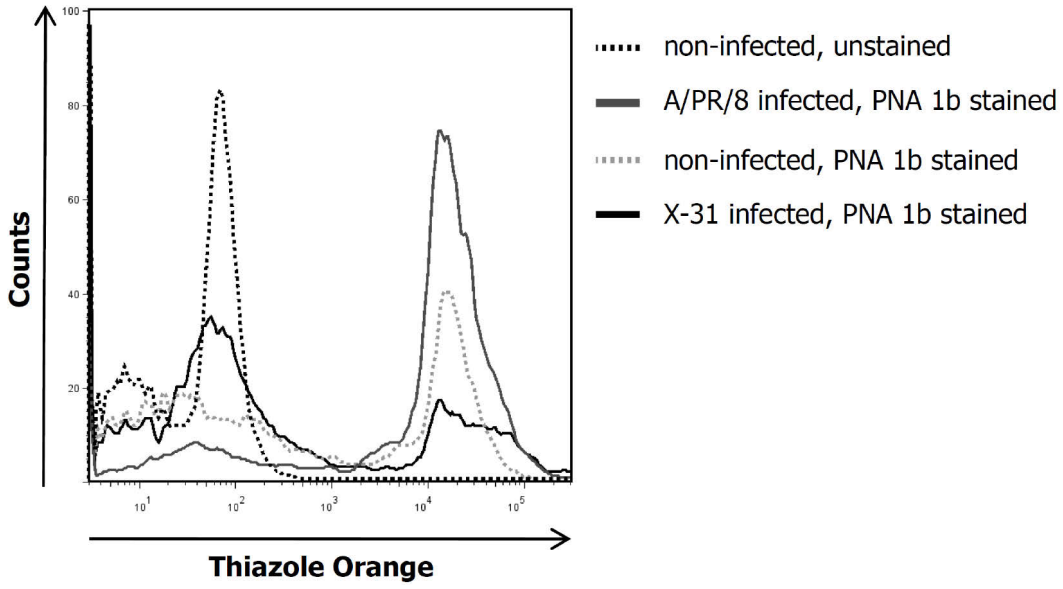

Figure 22: FACS analysis of influenza A infected MDCK cells using sequence specific FIT-PNA 1b. MDCK cells were infected with the influenza A/PR/8 and the X-31 strain (see 3.2.3). After 4.5 h incubation the cells were trypsinized and fixed in solution. Cell permeabilisation and delivery of FIT-PNA 1b was performed using saponin. The shown histogram presents non-gated data of 10000 counts. TO was excited at 494 nm and emission maximum was set to 519 nm.

4.2 Studies on the Matrix Protein 1 Transcript of Influenza A Virus

To investigate the progress of viral transcription is one of the most relevant issues in influenza A research. This mechanism is highly conserved throughout the different influenza A virus strains and thus holds great promise for new antiviral strategies. During the viral replication cycle the coordinated action of the distinct viral proteins contributes to virus entry, genome release into the cytoplasm, transcription, replication, protein biosyntheses, assembly and budding. Consequently, regulation of transcription in terms of function enforcement is conceivable. Are there any temporal differences in viral mRNA progression during the time course of replication?

For this purpose a second FIT-PNA specific to the matrix protein 1 (M1) of influenza A/PR/8 carrying a TO derivate called pyridinium benzothiazole (BO) as intercalating fluorophore was designed and examined.

4.2.1 Identification of a Suitable PNA

Based on the experience gained from the design of FIT-PNA 1b specific to NA mRNA the PNAs specific to M1 mRNA were composed with a centred base surrogate and a polyethylene glycol chain (PEG) to enhance the specific fluorescence signal and the solubility of the probe inside the cytosol, respectively.

The FIT-PNA probe with the maximum enhancement (third PNA sequence in table 5, figure 23) was chosen and named FIT-PNA 1c in the following.

Table 5: PNA oligomers used to identify suitable FIT-PNA 1c with corresponding enhancement factors upon hybridisation with complementary target RNA at 37 °C. Lys = Lysine

Sequence	Enhancement factor
H-Lys(PEG)-catg-Aeg(BO)-ctgattagtg	1.8
H-Lys(PEG)-catgt-Aeg(BO)-tgattagtg	2.1
H-Lys(PEG_2)-catgtctg-Aeg(BO)-ttagtg	5.7
H-Lys(PEG)-catgtctga-Aeg(BO)-tagtg	2.0

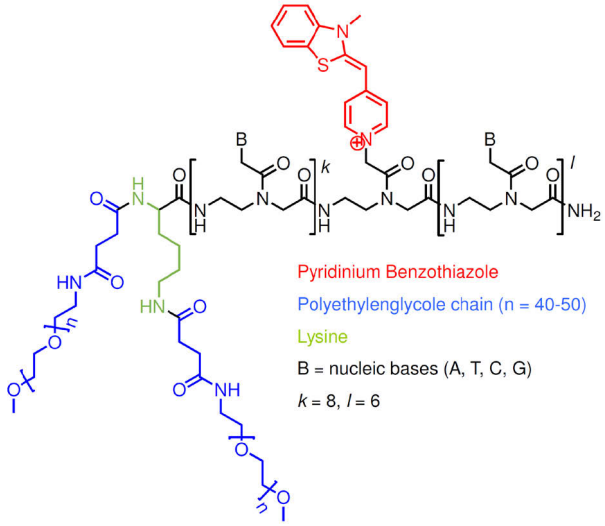

Figure 23: Chemical structure of PNA 1c.

Measurements with the synthetic target sequence (H1N1) and a mismatch control (H3N2) revealed an enhancement factor of 5.7 and 2.0, respectively.

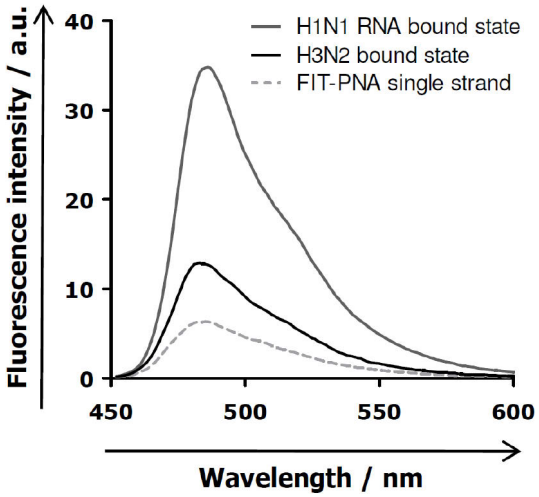

Figure 24: Fluorescence spectroscopic measurements of FIT-PNA 1c. Excitation wavelength was set to 440 nm. The fluorescence of FIT-PNA 1c in presence (solid, grey) and absence (dotted) of matched H1N1 RNA 3c and mismatched RNA target 4 (H3N2) was recorded from 450 nm to 600 nm at 37 °C. Conditions: 1 µM probe and 10 µM target in 100 mM NaCl, 10 mM NaH_2PO_4, pH 7.0.

4.2.2 Real-Time quantitative PCR

Similarly to the neuraminidase mRNA progression studies using quantitative Real-time PCR the synthesis of M1 mRNA during the replication cycle was estimated (for details please see chapter 4.1.3).

With one exception the RT-qPCR was performed following the described protocol (see chapter 3.2.4.3): the M1 specific FIT-PNA 1c was used as the detecting probe. Therefore excitation and emission conditions had to be adjusted to the BO fluorescence properties. The probe was excited using a 450/25 nm excitation filter and emission was recorded with the help of a 485/20 nm emission filter.

In this case, the increase in BO fluorescence directly correlated to the amplification of an M1 specific sequence in influenza A/PR/8 infected samples. For the non-template and the non-infected control samples no specific sequence amplification was observed.

Using the same principle as described above a 10-fold dilution series (see figure 25) of the amplicon was analysed to generate a calibration curve (see figure 26) and to quantify the amount of M1 mRNA molecules in infected MDCK cells (see figure 27).

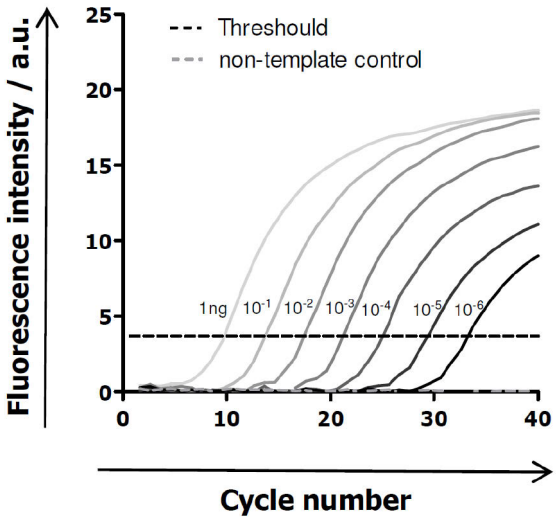

Figure 25: Amplification curve of a 101 bp in length sequence encoding for the M1 (H1N1) in a 10-fold dilution series. For conditions please review chapter 3.2.4.3. The mean of three independent experiments is plotted.

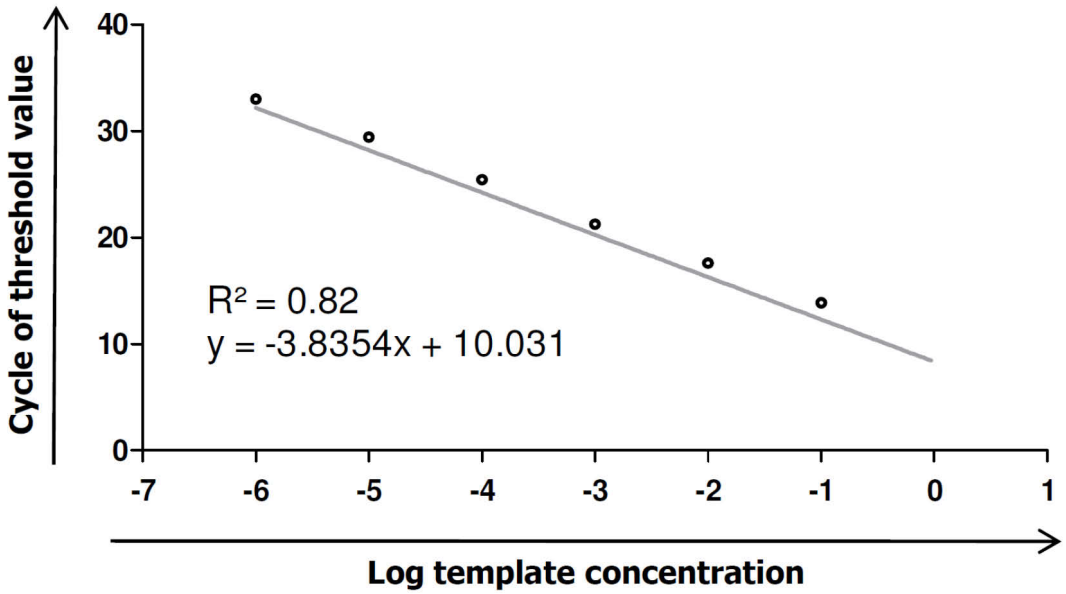

Figure 26: Logarithmic presentation of the calibration curve. Cycle of threshold values plotted against the logarithm of the template concentration ng/µl to estimate the specificity of the RT-qPCR (R^2).

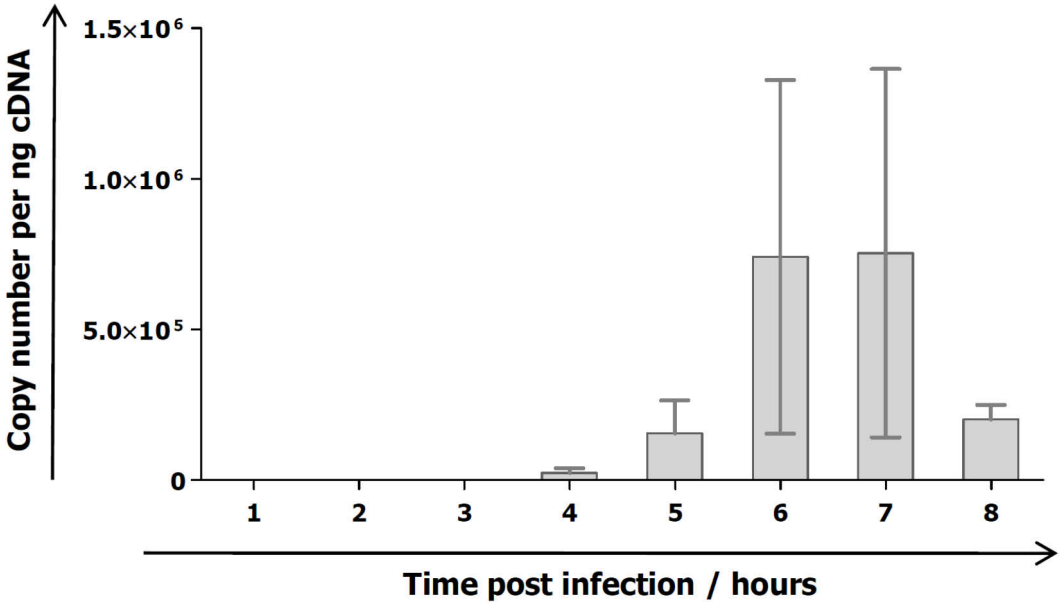

Figure 27: Time course of the M1 mRNA copy number per ng cDNA of influenza A/PR/8 infected MDCK cells. The calculation relies on the calibration curve (see figure 18) resulted from the RT-qPCR analysis. Mean ±SEM of three independent experiments is plotted.

4.2.3 Detection of Matrix protein 1 mRNA in Living Infected MDCK Cells

The applied staining protocol for the SLO-mediated delivery of FIT-PNA 1b was adjusted to the time requirements of the M1 mRNA progression as determined by the above described RT-qPCR analysis. Therefore imaging was performed at 5 h p.i.

Living influenza A/PR/8 infected MDCK cells 5 h p.i. showed an intense cytosolic fluorescence signal (see figure 28). The low fluorescence signals in the non-infected and SFV infected MDCK cells supported the sequence specificity of PNAs, especially of PNA 1c.

Interestingly, the intracellular fluorescence pattern differs from that of the FIT-PNA 1b based staining of NA mRNA. This phenomenon remains to be clarified by simultaneous detection of M1 mRNA and NA mRNA in living infected cells (see chapter 4.3).

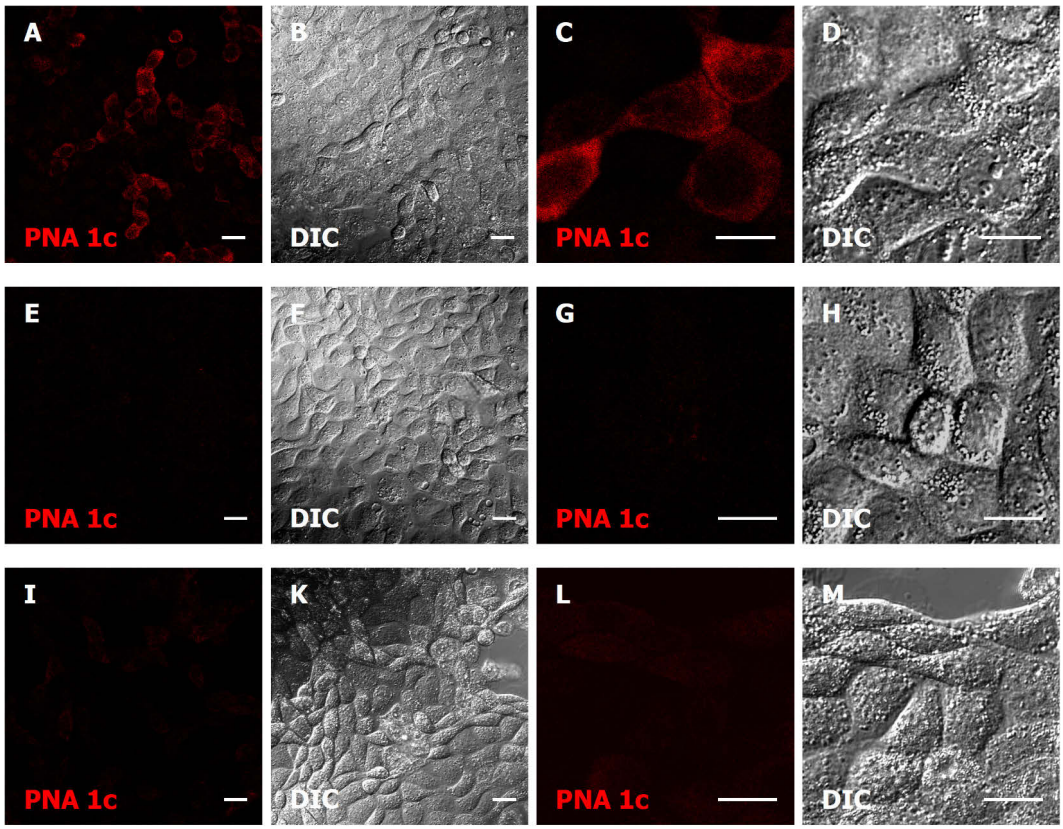

Figure 28: Confocal laser scanning microscopy images of living MDCK cells stained with FIT-PNA 1c. (A - D) Influenza A/PR/8 infected, (E - H) non-infected and (I - M) Semliki Forest Virus infected MDCK cells stained with FIT-PNA 1c (M1, H1N1) at 5 h p.i. The control samples (E-M) showed minor fluorescence signals. In contrast, the influenza A/PR/8 infected and with the M1 mRNA specific FIT-PNA treated MDCK cells exhibited high BO fluorescence signals. Images were acquired with an inverted confocal laser scanning microscope using a 60x water objective at 37 °C. BO was excited at 440 nm. White bars correspond to 10 µm. DIC = differential interference contrast

Image analysis for fluorescence intensity calculations was performed according to the procedure described for FIT-PNA 1b. The mean fluorescence intensity of BO in influenza A infected MDCK cells showed an enhancement factor of 6.97 compared to the non-infected control. In contrast, SFV infected MDCK cells revealed only a 1.2-fold increase of intensity (see figure 29).

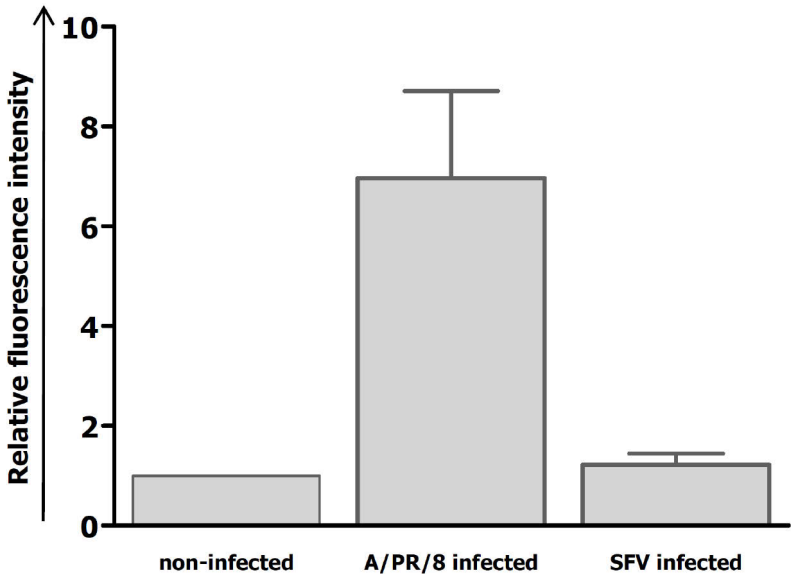

Figure 29: Relative fluorescence intensities of FIT-PNA 1c in living infected MDCK cells. The integrated fluorescence intensity values of influenza A/PR/8 M1 specific FIT-PNA 1c in MDCK cells infected with influenza A/PR/8 or infected with SFV, respectively, are graphed. Normalization was performed referring to the corresponding mean of the control (non-infected). Scatter bars correspond to SEM. Data represents three independent experiments with five cells per experiment (n=15).

4.3 Simultaneous Study on the Neuramindase and Matrix Protein 1 Transcripts

Another crucial benefit of the introduced probes using intercalating fluorophores for a sequence specific detection of viral mRNA in living infected cells is the possibility of a simultaneous visualisation of several mRNA species.

4.3.1 Imaging Conditions

Considering the emission spectra (see figure 30) of both fluorophores, thiazole orange and pyridium benzothiazole, the emission range was adjusted in order to prevent cross-talk between both channels (TO: 530 nm - 600 nm, BO: 460 nm - 490 nm).

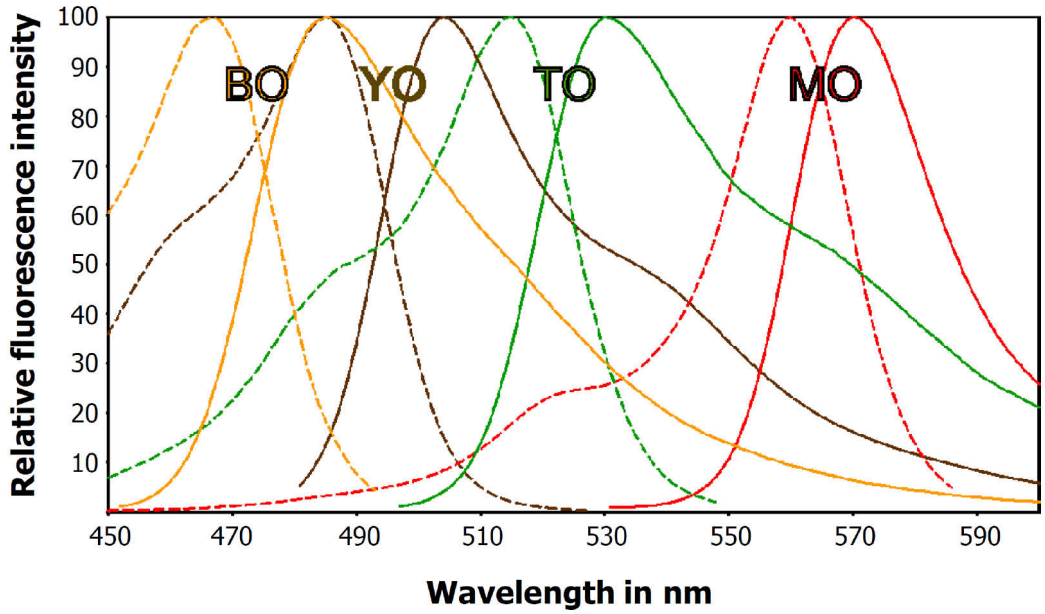

Figure 30: Relative fluorescence spectra of intercalating fluorophores. BO = pyridium benzothiazole organge, YO = oxazole yellow, TO = thiazole orange, MO = thiazole pyridine

However, the emission of BO could lead to an excitation of the TO fluorophore and thus to false positive signals. Therefore BO and TO were measured in the other respective channel (see figure 31). This control revealed that the cross-talk effect is negligible in the case of localisation studies. But it is recommended to perform the experiments for fluorescence enhancement calculations upon sequence specific hybridisation in living cells separately.

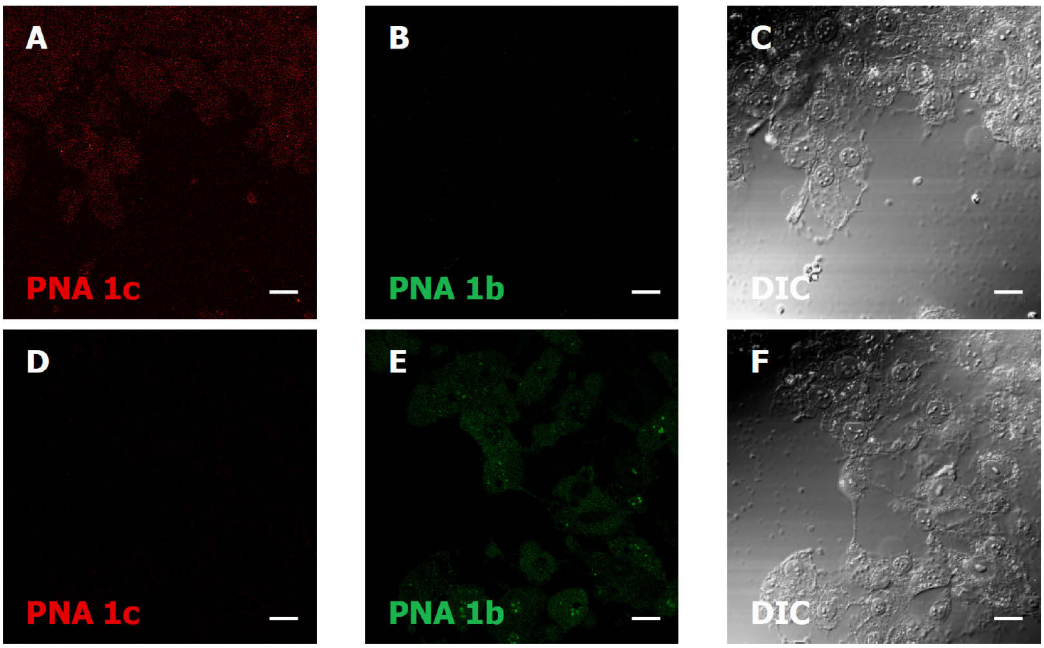

Figure 31: Confocal laser scanning microscopy images of living influenza A/PR/8 infected MDCK cells measured in the BO (Ex = 440 nm) and the TO (Ex = 484 nm) channel. MDCK cells were stained with (A-C) PNA 1c (BO, M1 specific) or (D-F) FIT-PNA 1b (TO, NA specific) and imaged at 5 h p.i. Each probe was excited by both channels sequentially. Images were acquired with an inverted confocal laser scanning microscope using a 60x water objective at 37 °C. White bars correspond to 10 µm. DIC = differential interference contrast

4.3.2 Simultaneous Detection of Neuraminidase and Matrix protein 1 mRNA in Living Infected MDCK Cells

As discussed earlier, the pattern of fluorescence signal due to specific binding of PNA 1c displayed variations in signal intensity as highlighted by white arrows in figure 32 (A, E, I). In contrast, the fluorescence signal of FIT-PNA 1b seemed to be as well distributed heterogeneously but lacks such regions of signal accumulation.

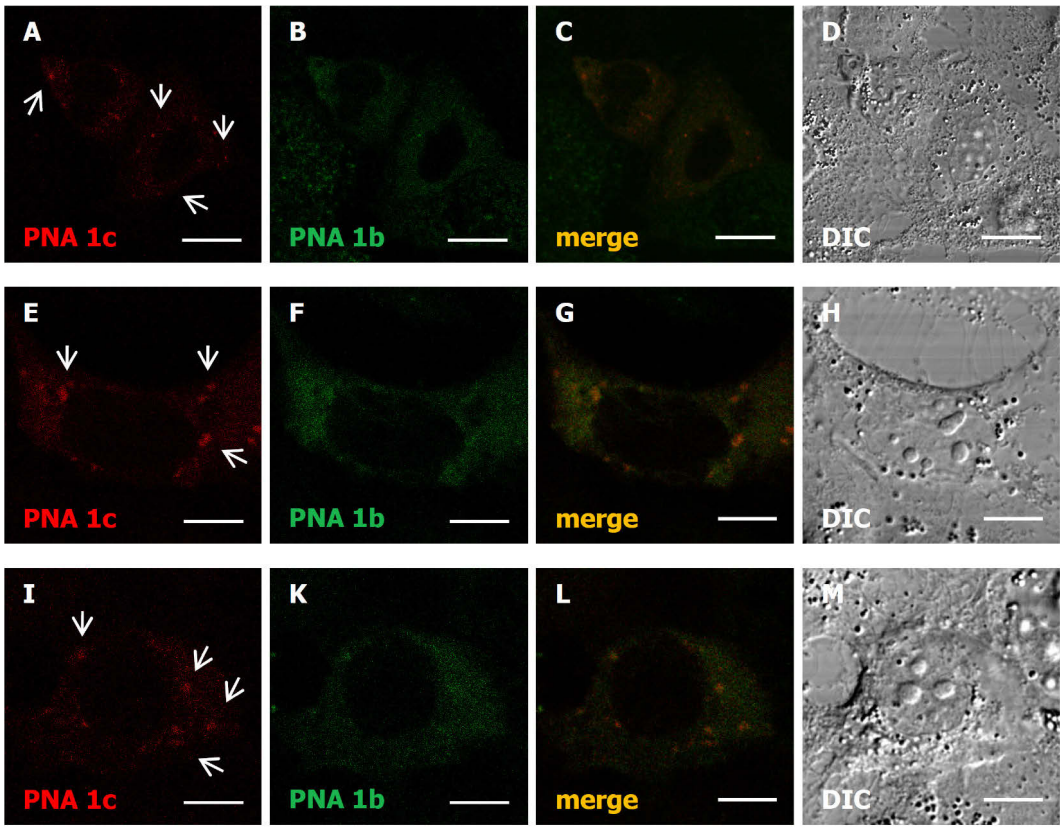

Figure 32: Confocal laser scanning microscopy images of living influenza A/PR/8 infected MDCK cells measured in the BO (Ex = 440 nm) and the TO (Ex = 484 nm) channel. MDCK cells were stained with PNA 1c (BO, M1 specific) and FIT-PNA 1b (TO, NA specific) and imaged at 5 h p.i. Each probe was excited for both channels sequentially. Arrows point at regions of high fluorescence intensity. Images were acquired with an inverted confocal laser scanning microscope using a 60x water objective at 37 °C. White bars correspond to 10 µm. DIC = differential interference contrast

4.4 Studies on the RNA-Dependent RNA Polymerase Transcript of Vesicular Stomatitis Virus

The sequence specific detection of viral mRNA inside the infected cells was implemented to investigate the Vesicular Stomatitis Virus (VSV) replication. This demonstrates the versatile application options of the FIT-PNA technique.

VSV belongs to the group of negative-sense single-stranded non-segmented RNA viruses (*mononegavirales*), precisely to the *Rhabodoviridae* family. It causes serious zootic vesicular disease in cattle, pigs, horses and numerous other species [215-218]. The genome is composed of a sequential arrangement of genes which are separated by non-coding intergenic regions. The RNA-dependent RNA polymerase (= L protein) is the most crucial protein of VSV [219]. It mediates the transcription of the negative ssRNA into positive strands mimicking cellular mRNA molecules. Mammalian cells lack such an enzyme making the L protein essential for VSV replication. The VSV specific FIT-PNA was designed to target the highly conserved region of the L protein situated at the 5´end of the viral genome [220-222].

4.4.1 Identification of a Suitable FIT-PNA

First, to design appropriate probes, *mfold* calculations were carried out with the help of the prediction tools on the Zuker webpage (see 3.1.10) to assess the secondary structure of the respective mRNA molecule (see figure 33).

To identify conserved regions, the L gene of experimentally used virus particles was sequenced by the Meixner GmbH (Berlin). The obtained sequence was aligned to the one given in the PubMed database (NC_001560, Indiana strain). Matched regions were assumed to be conserved or at least less susceptible for mutations.

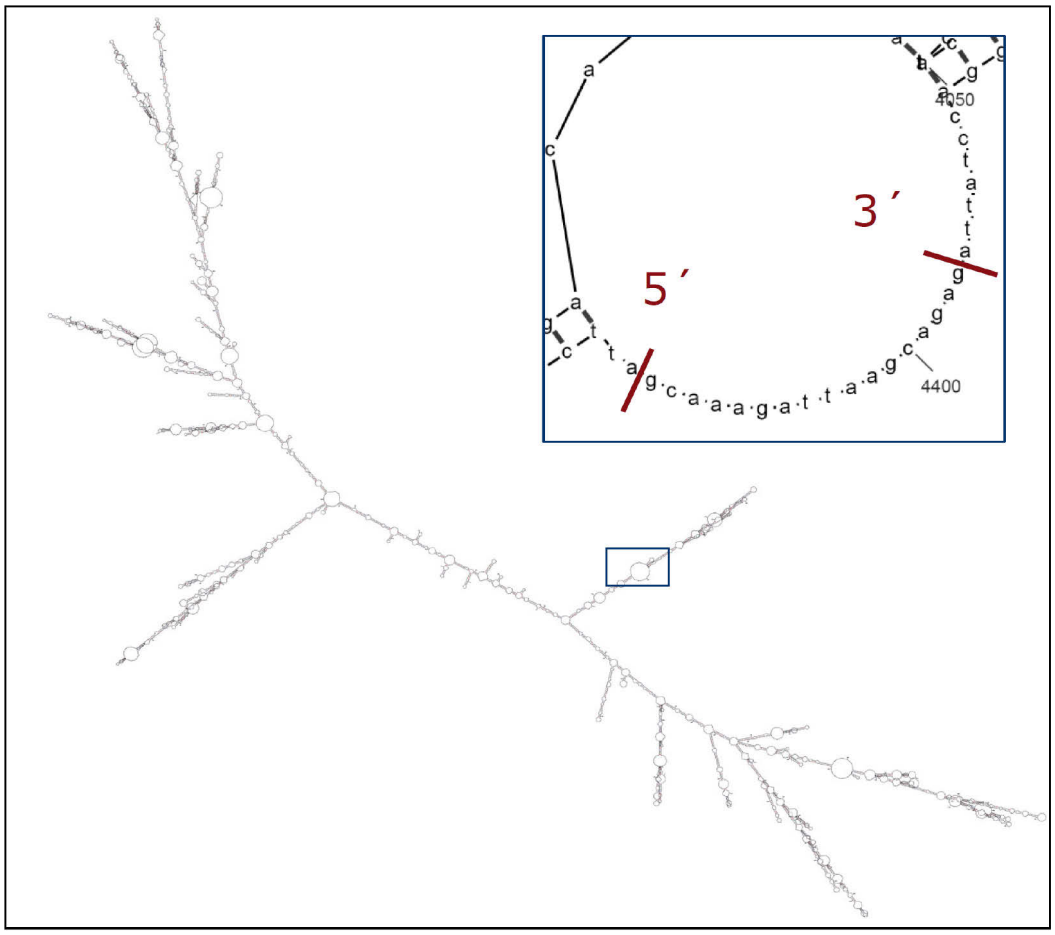

Figure 33: Secondary structure of the L protein mRNA (VSV) predicted by mfold. The structure was obtained using the mfold calculator. The inset shows a magnification of the target region used as template for the FIT-PNA design (sequence marked with red bars).

A single stranded sequence inside a conserved region was chosen and ten PNA oligomers (listed in table 6) were synthesized with changing position of the TO base surrogate. Furthermore, for solubility improvement, different amino acid residues were tested. The PNA with the maximum increase in fluorescence upon hybridisation with the target sequence (3.4 at 37 °C) will be named FIT-PNA 1d in the following.

Table 6: PNA oligomers used to identify suitable FIT-PNA 1d with corresponding enhancement factors upon hybridisation with complementary target at 37 °C. Lys = Lysine, Glu = Glutamic acid, Gly = Glycine

Sequence	Enhancement factor
H-Glu-cgttt-Aeg(TO)-taattcgtctc-Gly-NH_2	3.0
H-Lys-cgttt-Aeg(TO)-taattcgtctc-Lys-NH_2	3.1
H-Lys-cgttt-Aeg(TO)-taattcgtctc-Lys-NH_2	3.1
H-Glu-cgtttc-Aeg(TO)-aattcgtctc-Gly-NH_2	1.1
H-Glu-cgtttct-Aeg(TO)-attcgtctc-Gly-NH_2	3.4
H-Glu-cgtttcta-Aeg(TO)-ttcgtc-Gly-NH_2	3.2
H-Glu-cgtttcta-Aeg(TO)-ttcgtctc-Gly-NH_2	2.1
H-Glu-cgtttctaa-Aeg(TO)-tcgtc-Gly-NH_2	2.4
H-Glu-cgtttctaa-Aeg(TO)-tcgtctc-Gly-NH_2	2.0
H-Glu-cgtttctaat-Aeg(TO)-cgtctc-Gly-NH_2	0.45

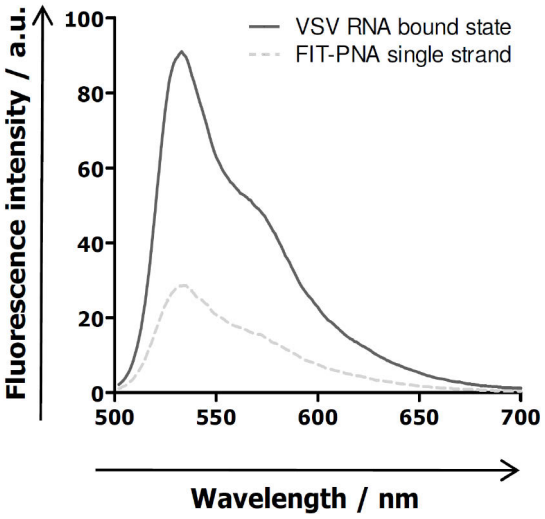

Figure 34: Fluorescence spectroscopic measurement of FIT-PNA 1d. Excitation wavelength was set to 485 nm. FIT-PNA 1c was measured in presence (solid) and absence (dotted) of matched target RNA 6 at 37 °C. Conditions: 1 µM probe and 10 µM target in 100 mM NaCl, 10 mM NaH_2PO_4, pH 7.0.

4.4.2 Verification of Vesicular Stomatitis Virus Infection

To determine the VSV infection the glycoprotein G of VSV [216] was visualized using a polyclonal antibody in combination with a Cy3 conjugated secondary goat anti-rabbit IgG antibody. The ICC was performed 3 h p.i. as described above (see chapters 3.2.3 and 3.2.5). The near quantitative staining of VSV infected BHK-21 cells revealed ~100% VSV G positive cells (see figure 35). Because the image analysis was performed manually, the percentage of infected cells is of great relevance.

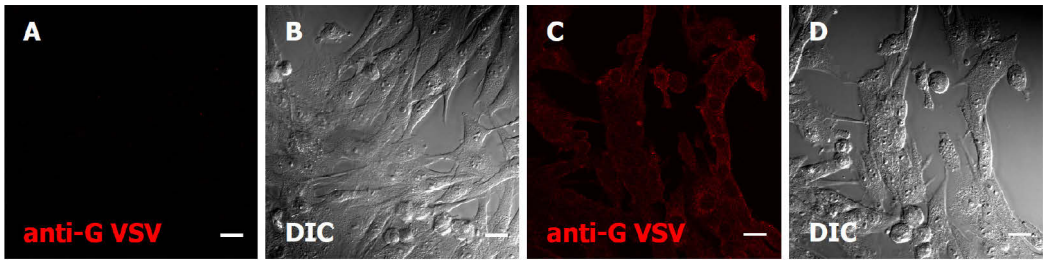

Figure 35: Confocal laser scanning microscopy images of fixed BHK-21 cells stained with an anti-G (VSV) antibody. (A, B) Non-infected BHK-21 cells and (C, D) VSV infected BHK-21 cells (3 h p.i.) were labelled with an anti-G (VSV) polyclonal antibody to determine the percentage of infected cells. Non-infected cells showed no fluorescence signal. In contrast the infected sample showed a strong G (VSV) staining. Images were acquired with an inverted confocal laser scanning microscope using a 60x oil-immersion objective at room temperature. Cy3 (goat anti-rabbit IgG) was excited employing a 559 nm laser. White bars correspond to 10 µm. DIC = differential interference contrast

4.4.3 Detection of L Protein mRNA in Fixed BHK-21 Cells

To apply the SLO-mediated FIT-PNA delivery failed for BHK-21 cells. In contrast to the intercellular adhesion of epithelial MDCK cells, fibroblasts lack strong connections to neighboring cells and thus were not able to survive the plasma membrane permeabilisation. Therefore BHK-21 cells were subjected to fixation and Triton X-100 treatment to transfer FIT-PNA probes into the cytoplasm.

Hence, it was not possible to carry out a continuous time-resolved measurement of the fluorescence progression during the VSV replication cycle due to the aforementioned delivery problem. The time course illustrated in figure 36 repre-

sents samples where the replication cycle was interrupted at various time points (0 min, 30 min, 60 min, 90 min, 120 min, 150 min) post infection by fixation.

After staining with the VSV L protein specific FIT-PNA 1d, an increase in TO fluorescence was observed for the samples at 60 min p.i. and 90 min p.i. (see figure 36 A) compared to the starting point (0 min p.i.). At 120 min p.i. the fluorescence signal returned to its basic intensity. A comparison to non-infected control cells (see figure 36 B) or SFV infected cells (see figure 36 C) showed minor non-significant changes in fluorescence intensities over the same time scale indicating that probe 1d selectively responded to viral mRNA and fluorescence enhancement was not due to unexpected degradation and/or binding processes.

It is known, that during the fixation, preferentially the lysine residues of the proteins were cross-linked by paraformaldehyde preserving secondary and even tertiary structures. Whether there is an influence on the secondary structure of the viral mRNA which has an impact on the accessibility of the target sequence cannot be ruled out.

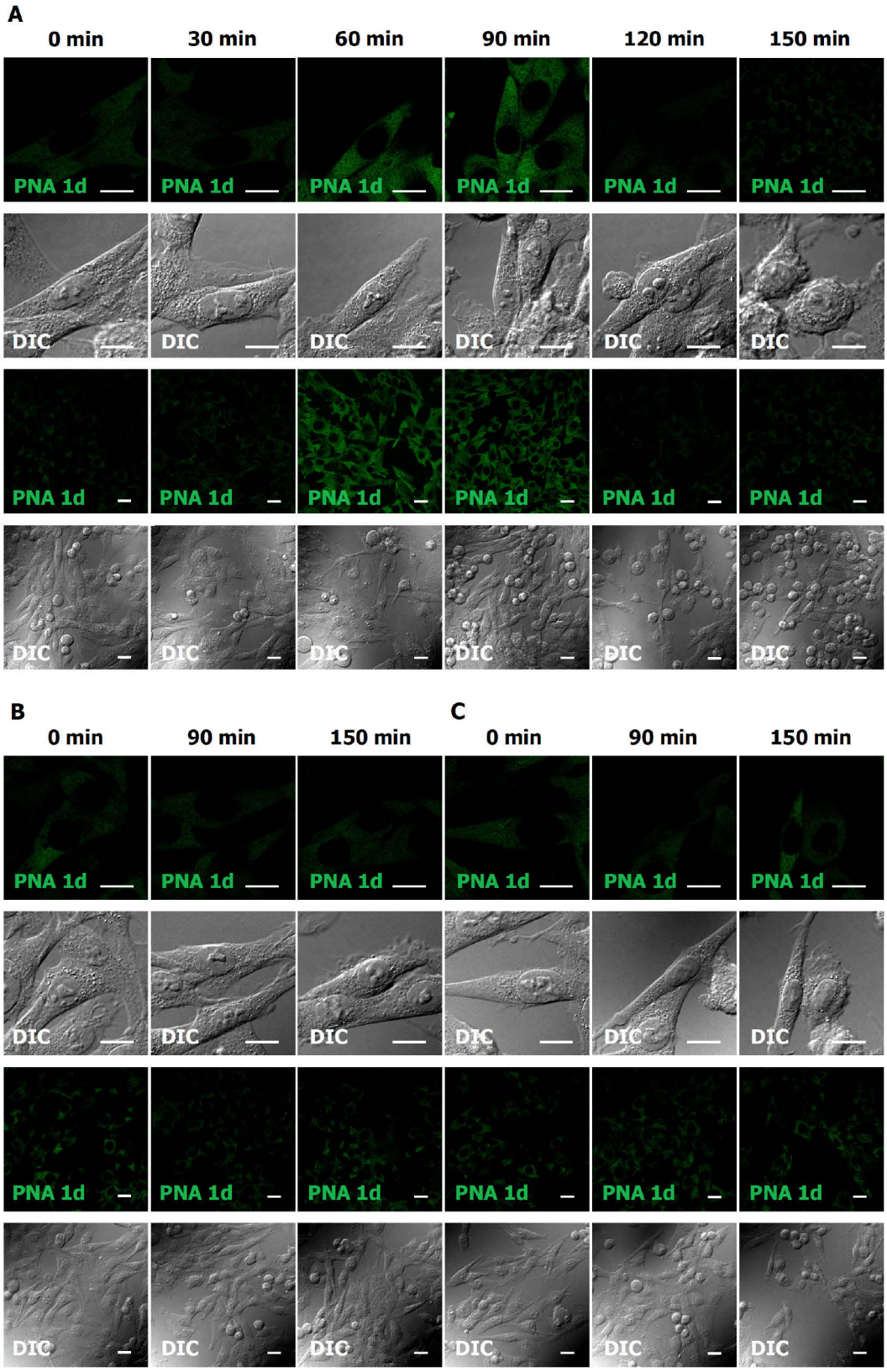
A
0 min
30 min
60 min
90 min
120 min
150 min
PNA 1d
DIC
B
0 min
90 min
150 min
C
0 min
90 min
150 min

Figure 36: Confocal laser scanning microscopy images of fixed BHK-21 cells stained with FIT-PNA 1d in a 150 min time course. (A) VSV infected, (B) non-infected and (C) Semliki Forest Virus infected BHK-21 cells stained with FIT-PNA 1d (L Protein, VSV). The samples were fixed and stained at the indicated time point p.i. All control samples (B, C) showed minor variation in fluorescence signals. In contrast, the VSV infected BHK-21 cells exhibited an enhancement of TO fluorescence intensity 60 – 90 min p.i. Images were acquired with an inverted confocal laser scanning microscope using a 60x oil-immersion objective at 37 °C. TO was excited employing a 488 nm laser. White bars correspond to 10 µm. DIC = differential interference contrast

For quantitative analysis the method described in chapter 4.1.6 was applied to determine the fluorescence enhancement. Importantly, in this study the nucleus was not included in the calculation of the mean fluorescence intensity.

Data analysis verified the visual observation. For the non-infected and SFV infected BHK-21 cells stained with the FIT-PNA 1d specific to VSV L protein mRNA no significant change in fluorescence intensity was determined (figure 37, upper right and lower left graph, respectively). An additional control was included, namely VSV infected BHK-21 cells stained with FIT-PNA 1b (NA mRNA, H1N1). These cells exhibited no significant fluorescence intensity over the time course as the aforementioned controls demonstrating again the specificity of the FIT-PNA 1d.

In contrast, upon normalization to the corresponding basic fluorescence intensity (0 min p.i.) the VSV infected BHK-21 cells which were treated with the specific FIT-PNA 1d revealed a 1.6 fold enhancement in fluorescence 90 min p.i.

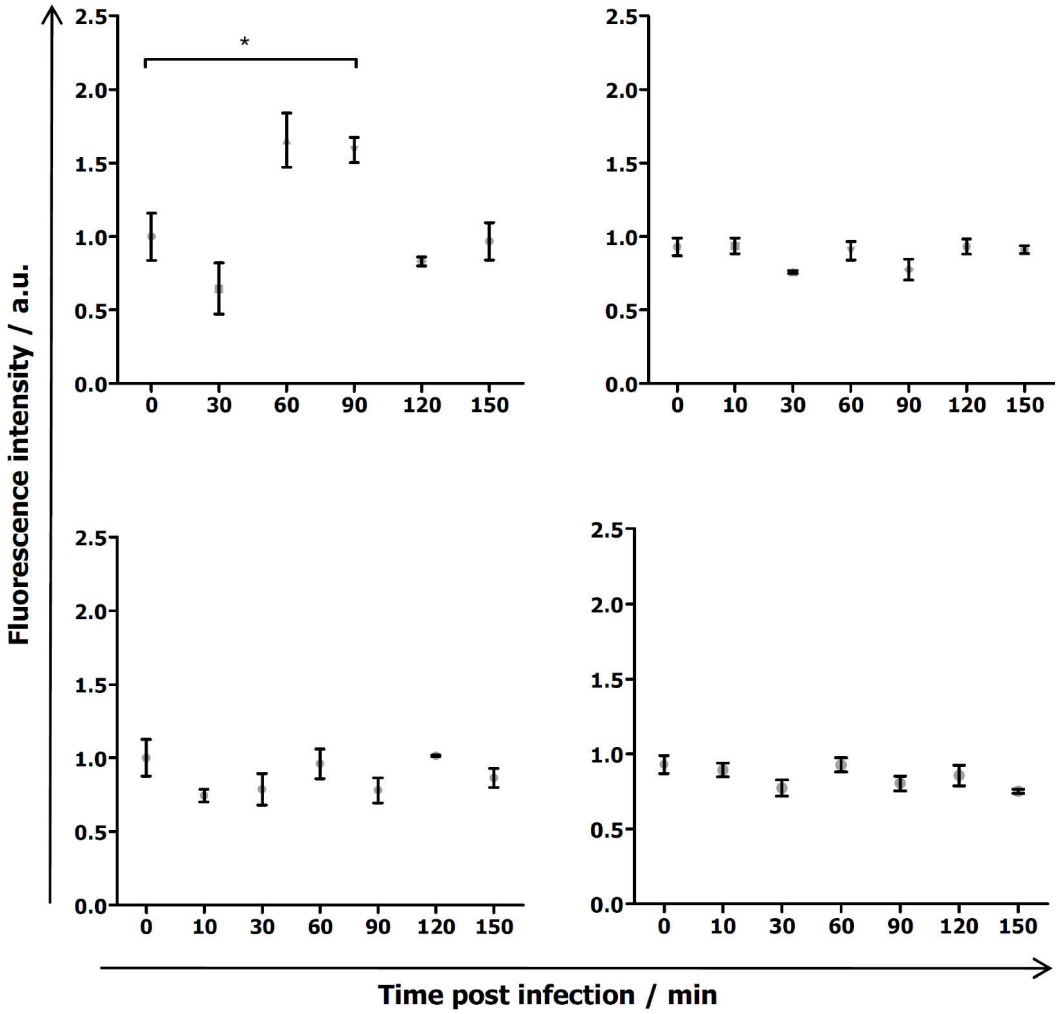

Figure 37: Fluorescence intensity of VSV L specific FIT-PNA 1c in fixed BHK-21 cells. The absolute fluorescence intensity of VSV infected (upper left), non-infected (upper right), and SFV infected (lower left) fixed BHK-21 cells stained with FIT-PNA 1d as well as VSV infected BHK-21 cells stained with FIT-PNA 1b (NA, H1N1) is graphed for various time points p.i. from 0 to 150 min p.i. CLSM images were analysed following the procedure described in chapter 4.1.6 excluding the cell nucleus. The mean fluorescence intensity per area was normalized to the intensity at time 0 min p.i. and plotted with SEM. Data represent three independent experiments with three cells per time point and sample. (p = 0.0174)*

4.5 Proteomic Studies of Influenza A Infected MDCK Cells on a Systems Level using Stable Isotope Labelling of Amino Acids in Cell Culture (SILAC)

Global quantitative analysis of host cell proteomes among others is destined to revolutionize the understanding of viral host interaction. The impact on the host cell proteome upon influenza A infection was analysed using SILAC in combination with LC-MS (see chapter 3.2.8). Samples of infected MDCK cells 0 to 8 h p.i. were investigated.

As a result of an alignment to the dog protein data set, GO annotations and an applied hypergeometric test (see chapter 3.2.9) the identified proteins were clustered by their specific abundance variation (see figure 38). In general, the protein abundance increased for the majority of identified proteins comparing the cell proteome status at 8 h p.i. with the starting situation (0 h p.i.).

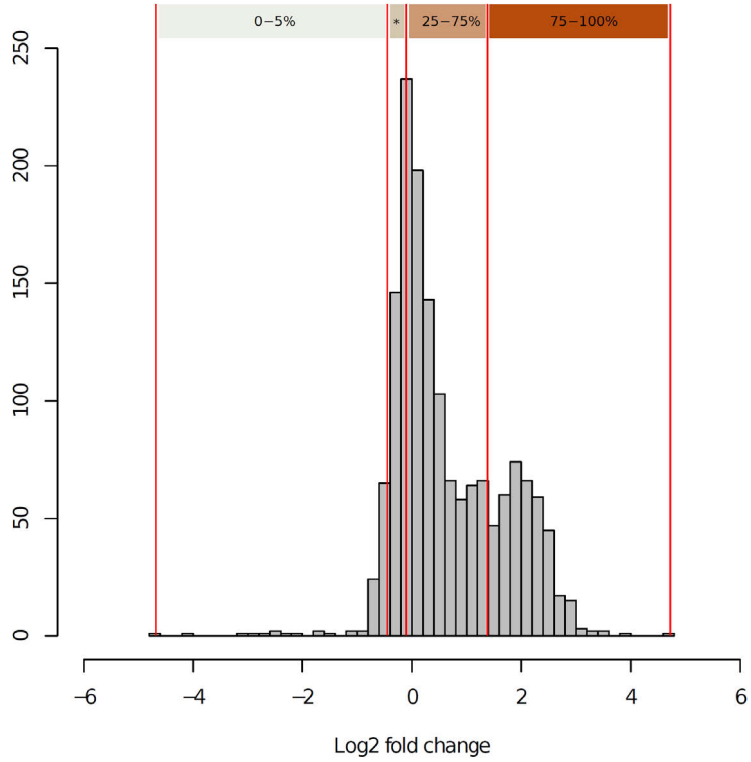

Figure 38: Fold-change distribution of the MDCK proteome upon 8 h infection by influenza A virus. The total protein amount is plotted against the Log2 fold change in protein abundance for each cluster. The histogram is divided into four quantiles according to the relative protein expression (0 – 5 %, 5 – 25 %, 25 -75 %, 75 – 100 %). *5-25%

The presented clusters were assigned to higher-order groups according to their relative expression into 4 quantiles: 0 - 5 %, 5 – 25 %, 25 – 75 % and 75 – 100 %. A classification into quantiles enabled the evaluation with respect to the magnitude of abundance variation. Each quantile was assessed separately for over-represented biological processes based on the gene ontology pathway analysis and the resulting categories were clustered concerning their z-transformed p values in a so called heat map (see figure 39). This enabled the visual interpretation of the infected MDCK cell phenotype after 8 h p.i. in terms of functional modules on a systems level.

Selection of the most prominent biological processes of each quantile resulted in a simplified visual interpretation. In the first category (0 – 5 %), proteins which are responsible for lipid metabolism, like lipoprotein biosynthesis, amino acid lipidation as well as phospholipid, membrane lipid and glycolipid metabolism, were over-represented. Interestingly, also cell adhesion mediating proteins were registered. These proteins were stronger down-regulated than the remaining 95 %. The second category (5 – 25 %) is dominated by proteins involved in ion homeostasis of the cell. The two first categories indicated that 25 % of all proteins were down-regulated. Remarkably, for the main fraction of the identified proteins the estimated abundance remained constant or showed only moderate up-regulation upon influenza A virus infection. Proteins related to RNA biosynthetic processes, like mRNA processing, RNA localisation and splicing, RNA metabolism, as well as factors responsible for positive regulation of gene expression were over-represented in this third quantile.

The fourth quantile "75-100%" included proteins which were higher up-regulated than the remaining 75 % of all proteins. Considering their GO annotation these proteins were categorized to the following cellular functions: programmed cell death, immune response and protein transport/localisation/modification.

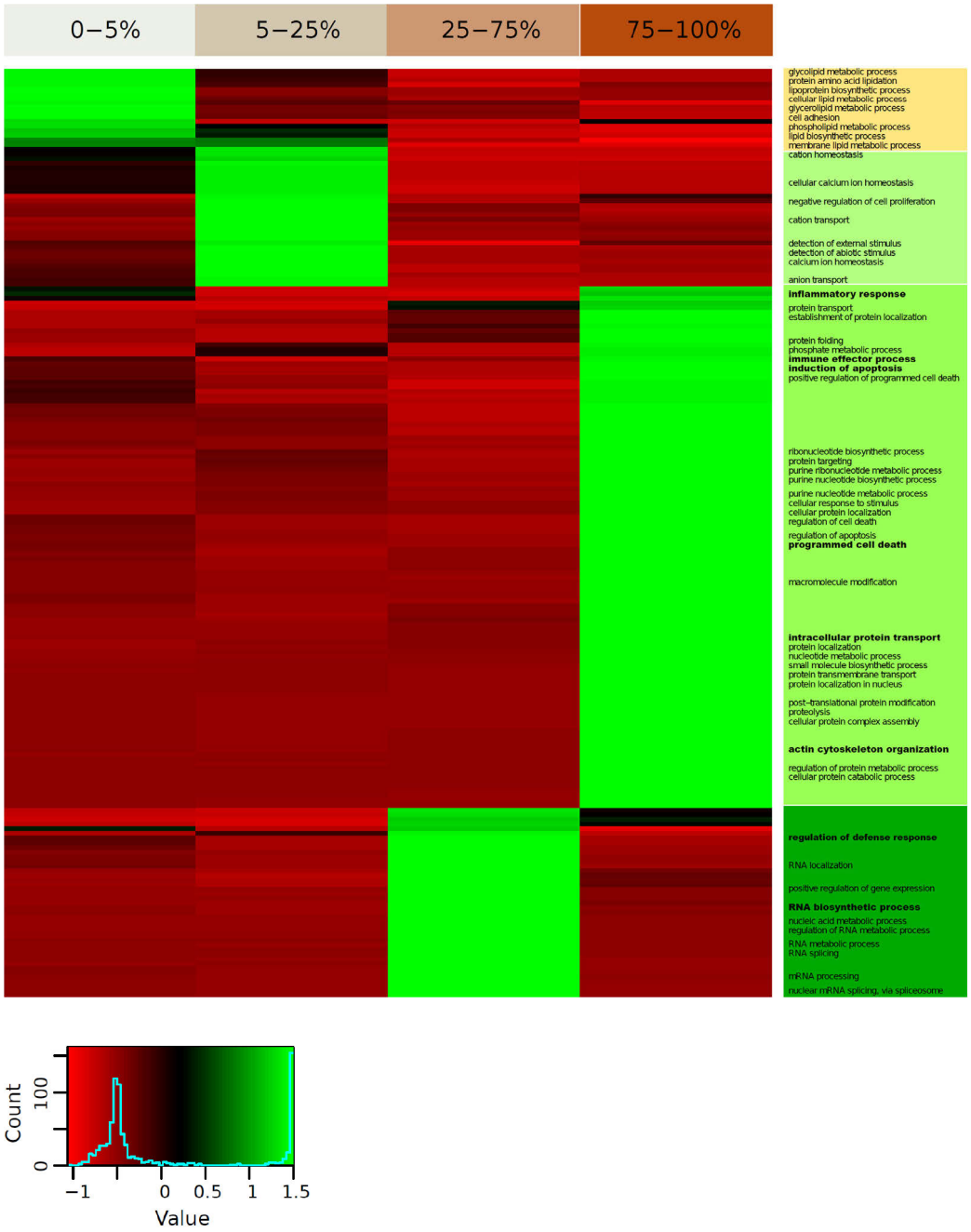

Figure 39: Functional phenotyping of the influenza A/PR/8 infected MDCK cell proteome. Quantiles resulting from the quantification histogram (see figure 38) are indicated at the top of the heat map. Each quantile was separately analysed for gene ontology pathways and clustered for the z-transformed p values. The most prominent representatives of all over-represented biological processes of each quantile were selected and annotated. At the bottom left a histogram of the z-transformed p-values is plotted.

Further, an *mfuzz* clustering was performed resulting in cellular protein groups showing the same dynamics in protein level change during the influenza A virus infection. This method relies on the characterization of single GO terms over the whole time course based on their membership value. (see figure 40, cluster 1-6). While the heat map enabled an absolute evaluation of the protein abundance change in MDCK cells after 8 h p.i., the *mfuzz* clustering provided for a detailed time-resolved analysis.

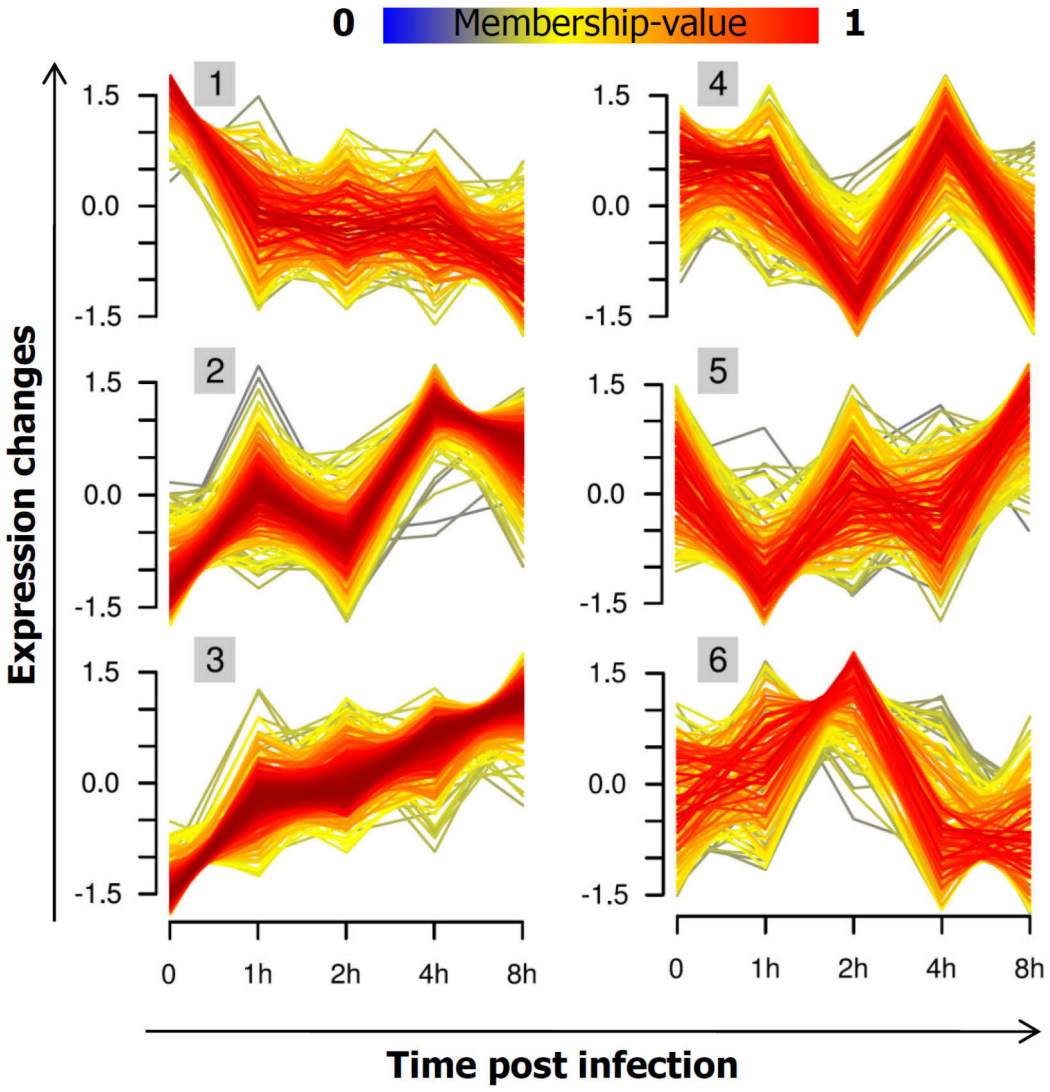

Figure 40: Fuzzy c-means clustering of the cellular proteins over the infection time course (0 – 8 h p.i.). Proteins were analysed according to their expression pattern. The time range is not displayed linear due to program restrictions with respect to plotting.

Generally the *mfuzz* clustering in the first instance revealed 6 groups with a certain expression pattern. Interestingly, for most of the clusters the important time point seemed to be 2 h p.i. indicating the viral impact on cellular processes or the cellular response to viral infection.

For the transcription of the viral genome, the usage of cap structures originating from cellular mRNA molecules as initiation primers is essential. This mechanism realized by the viral polymerase complex is named cap snatching and results in the premature degradation of cellular mRNA molecules. This may hint at the causal correlation of the expression pattern graphed as cluster 1. Here, processes of the lipid metabolism and mitochondrion organization (inter alia, ATP syntheses coupled electron transport chain) were over-represented and decreased in abundance over the time course of infection.

Cluster 2 showed a comparable expression pattern like cluster 3 but with greater value alterations of expression. Even on the functional level these two clusters seemed to be connected. Proteins of cluster 2 were involved in gene expression processes (e.g. positive regulation of gene expression, negative and positive regulation of transcription from RNA polymerase II promoter and transcription in general). All these proteins control or establish protein expression and thus are required for all regulated proteins during the analysed time range.

A consistent increase in protein level 0 – 8 h p.i. was found for all GO terms assigned to cluster 3. They represent three main functional subgroups: processes related to apoptosis (ubiquitination, proteolysis, actin filament and microtubule organization), to RNA metabolism (RNA splicing, localisation, transport) and to antiviral response (defence response to virus, regulation of immune effector response). The finding is in accordance with the expected reaction of the host cell faced with a viral infection.

Proteins involved in chromosome organization, DNA packaging, chromatin assembly and disassembly, and nucleosome assembly were over-represented in cluster 4. Despite the causal correlation to the physiological reaction of the in-

duced apoptosis in influenza A virus infected cells, Garcia-Robles *et al.* 2005 [223] revealed that in purified nucleosomes the RNP complexes bind to the histone tails and M1 to the globular domain of the histone octamer. The hypothesis that viral proteins alter the chromatin structure is supported by the findings of Takizawa *et al.* 2006 [224] who observed that vRNPs associate partially with the dense chromatin where viral transcription and replication takes place.

Although due to the cap snatching mechanism a wide range of cellular mRNA molecules might be destroyed, the cell integrity seemed to be intact until 8 h p.i. This conclusion is based on the protein composition of cluster 5 including mainly house-keeping genes.

Cluster 6 clearly demonstrated the demand on a time-dependent analysis to reveal the detailed information about the protein abundance changes upon influenza A virus infection. The heat map (see figure 39) indicated a reduction in proteins responsible for ion homoeostasis while the time-dependent functional cluster analysis showed an increase in abundance until 2 h p.i. followed by a drastic decrease which is evinced by the heat map.

For detailed information concerning the cluster composition please review table 7.

Figure 41 elucidates the dynamic process of protein abundance change upon influenza A virus infection for specified protein groups which are the influenza A virus proteins, virus-host interaction partners identified in a previous RNAi screen [83] and proteins exhibiting GO annotations assigned to antiviral response.

The curves of the diagrams were generated with values which were normalized to the mean of each data set. This enables the logarithmic presentation of the protein abundance change. The abundance change of the viral proteins was referred to 1 h p.i. due to the fact that these proteins are not present in the control sample (0 h p.i.). Whereas the NP and the NS1 protein showed a strong increase in the first 2 hours the PB1 and NA protein only increased slightly. Proteins like

M1 and HA exhibited a more linear protein progression during the recorded time scale (Figure 33 A).

Karlas *et al.* 2010 [83] estimated 6 host factors crucial for influenza A virus replication as verified by an RNA interference approach in combination with an indirect NP-luciferase-reporter assay. The results of this study are limited to the absolute determination of negative effects on viral replication after 24 h. In the presented work 5 out of these virus host interaction partners were identified in the SILAC experiment enabling a time-resolved analysis of the dynamic processes in the early stage of infection. For example, the COPG (coat protein gamma) protein abundance strongly increased starting at 2 h p.i. by nearly 1 magnitude. COPG belongs to the COP proteins which mediate the biosynthetic transport from the endoplasmatic reticulum to the golgi apparatus, up to the trans-golgi network [225]. The transmembrane viral proteins require this transport mechanism for an efficient posttranslational modification of the HA and the NA protein.

In figure 41 C proteins which were annotated to the GO term antiviral defence and/or response were analysed in their abundance change during the time course 0 – 8 h p.i. The protein level of the majority of these antiviral proteins remained essentially constant over the whole recorded time-scale. While proteins like SERPIN B6 (serin protease inhibitor) [226], CAD (carbamyl phosphate synthetase II, aspartate transcarbamylase, and dihydroorotase; pyrimidine biosynthesis pathway) [227] and SF1 (splicing factor 1) [228] increased in abundance, the ZER 1 protein (recruitment of ubiquitin ligase complex) [229] dramatically decreased after 2 h p.i. for more than 4 magnitudes until 4 h p.i. and recovered in the following.

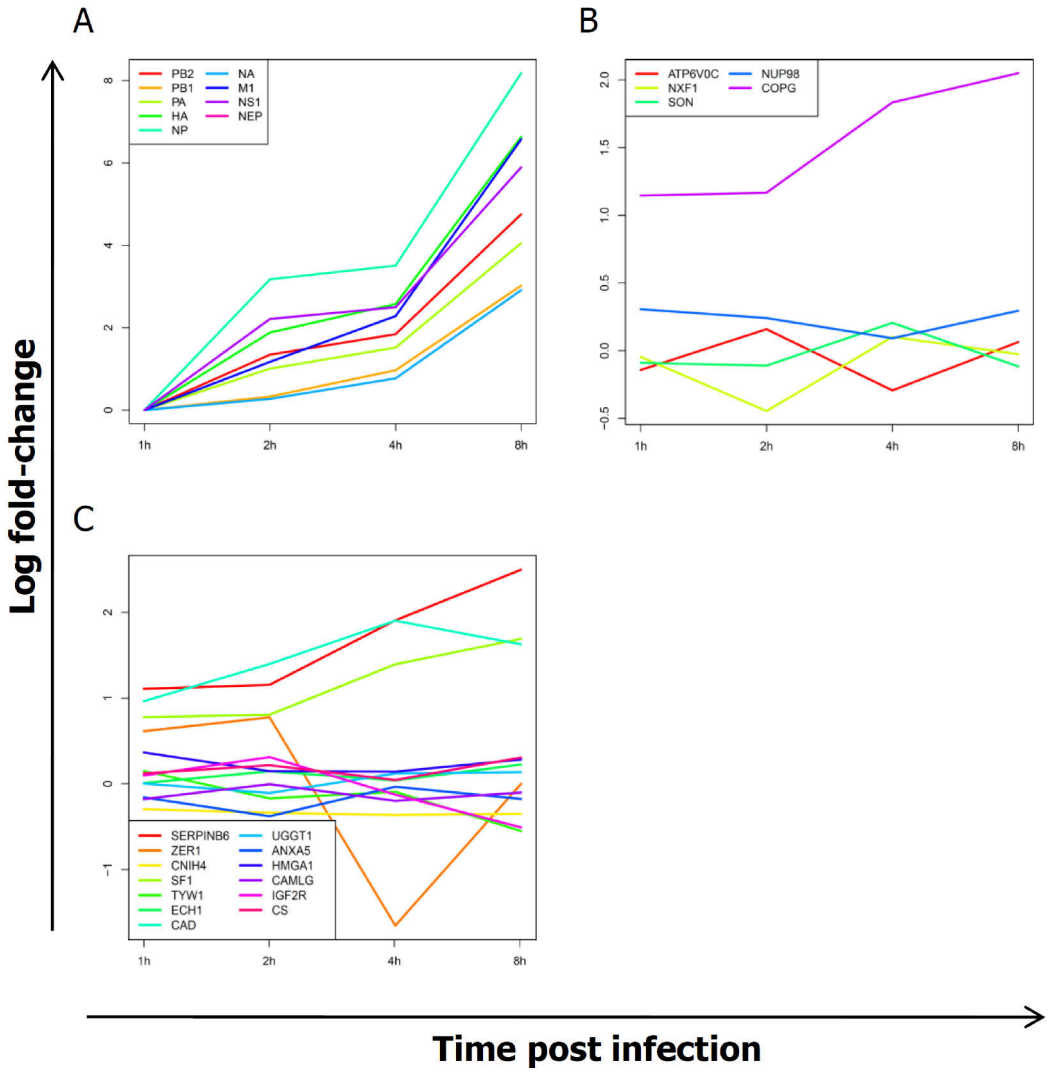

Figure 41: Logarithmic presentation of the protein abundance fold change of functional clusters upon the time course of influenza A virus infection (0 – 8 h p.i). in MDCK cells. (A) Influenza A proteins, (B) cellular interaction partners crucial for efficient replication and (C) proteins involved in antiviral defence. The time range is not displayed linear due to program restrictions with respect to plotting.

Table 7: Gene ontology pathways enriched in fuzzy c-means clusters illustrated in figure 40.

Cluster 1
sphingolipid biosynthetic process
ATP synthesis coupled electron transport
electron transport chain
transmembrane transport
lipid biosynthetic process
membrane lipid metabolic process
behavioral fear response
sphingomyelin biosynthetic process
photorespiration
response to endoplasmic reticulum stress
learning
ER-nucleus signaling pathway
neutral lipid metabolic process
protein targeting to mitochondrion
cation transport
mitochondrial respiratory chain complex assembly
energy derivation by oxidation of organic compounds
ceramide metabolic process
triglyceride metabolic process
mitochondrial electron transport, NADH to ubiquinone
glycerol ether metabolic process
sphingosine biosynthetic process
sphinganine biosynthetic process
Cluster 2
regulation of BMP signaling pathway
translational elongation
mRNA metabolic process
rRNA processing
transcription

DNA metabolic process

regulation of long-term neuronal synaptic plasticity

regulation of cellular biosynthetic process

regulation of cell cycle

positive regulation of gene expression

nucleocytoplasmic transport

negative regulation of post-embryonic development

positive regulation of gene-specific transcription from RNA polymerase II promoter

positive regulation of transcription, DNA-dependent

regulation of metabolic process

macromolecule biosynthetic process

positive regulation of nucleobase, nucleoside, nucleotide and nucleic acid metabolic process

regulation of gene expression, epigenetic

regulation of macromolecule biosynthetic process

mRNA processing

ribosomal large subunit biogenesis

negative regulation of transcription from RNA polymerase II promoter

negative regulation of nitrogen compound metabolic process

negative regulation of transcription

negative regulation of biosynthetic process

regulation of RNA stability

positive regulation of cellular biosynthetic process

gene expression

cellular protein metabolic process

mitotic spindle elongation

nucleic acid metabolic process

cellular macromolecule metabolic process

cell cycle phase

spindle organization

primary metabolic process

microtubule-based process

ribosome assembly
mRNA stabilization
RNA biosynthetic process
ribosomal small subunit assembly
RNA splicing
mitotic cell cycle
regulation of nucleobase, nucleoside, nucleotide and nucleic acid metabolic process
regulation of gene expression
regulation of transcription, DNA-dependent
negative regulation of RNA metabolic process
cellular nitrogen compound metabolic process
positive regulation of macromolecule biosynthetic process
RNA processing
Cluster 3
positive regulation of ubiquitin-protein ligase activity involved in mitotic cell cycle
positive regulation of ligase activity
positive regulation of protein ubiquitination
negative regulation of ubiquitin-protein ligase activity involved in mitotic cell cycle
negative regulation of ligase activity
teasomal ubiquitin-dependent protein catabolic process
anaphase-promoting complex-dependent pro
regulation of protein catabolic process
regulation of actin filament length
cellular protein complex assembly
cellular macromolecule metabolic process
cellular macromolecule localisation
positive regulation of macromolecule metabolic process
regulation of apoptosis
monosaccharide metabolic process
negative regulation of protein complex disassembly
imaginal disc development

establishment or maintenance of cell polarity
macromolecular complex subunit organization
actin filament polymerization
glucose metabolic process
protein localisation
cellular macromolecular complex disassembly
negative regulation of macromolecule metabolic process
protein import into nucleus
hexose catabolic process
regulation of cell death
protein depolymerization
regulation of multi-organism process
regulation of mRNA processing
glycolsis
alcohol catabolic process
regulation of cellular metabolic process
actin filament-based process
vesicle coating
cellular component disassembly
regulation of cellular component biogenesis
response to acid
response to DNA damage stimulus
regulation of cellular component organization
regulation of actin filament depolymerization
cardiac myofibril assembly
germ cell development
protein transmembrane transport
microtubule cytoskeleton organization
response to stimulus
protein localisation in organelle
alpha-beta T cell differentiation
negative regulation of protein transport

cell differentiation
response to other organism
regulation of cellular catabolic process
primary metabolic process
actomyosin structure organization
negative regulation of microtubule polymerization or depolymerization
activation of pro-apoptotic gene products
leukocyte mediated cytotoxicity
regulation of RNA splicing
RNA localisation
sexual reproduction
anatomical structure formation involved in morphogenesis
positive regulation of programmed cell death
actin filament capping
organ development
nuclear mRNA splicing, via spliceosome
RNA splicing, via transesterification reactions
death
negative regulation of protein polymerization
regulation of response to biotic stimulus
protein complex biogenesis
cell motility
regulation of cell shape
leukocyte mediated immunity
cell division
positive regulation of cellular component organization
cardiac cell development
regulation of mitosis
production of molecular mediator involved in inflammatory response
post-embryonic morphogenesis
regulation of establishment of protein localisation
cell projection assembly

ameboidal cell migration
tissue development
intracellular protein transport
regulation of alternative nuclear mRNA splicing, via spliceosome
defence response to virus
regulation of defence response to virus by virus
regulation of biological process
cellular carbohydrate catabolic process
translational initiation
negative regulation of organelle organization
proteolysis
regulation of actin filament-based process
negative regulation of cellular process
negative regulation of molecular function
regulation of protein metabolic process
regulation of cytoskeleton organization
protein modification by small protein conjugation
cell cycle process
mitotic cell cycle
regulation of protein modification process
negative regulation of protein ubiquitination
regulation of ubiquitin-protein ligase activity
proteasomal protein catabolic process
post-translational protein modification
ubiquitin-dependent protein catabolic process
macromolecule catabolic process
negative regulation of cellular protein metabolic process
regulation of catalytic activity
actin filament organization
cellular protein catabolic process
positive regulation of molecular function
positive regulation of cellular process

modification-dependent macromolecule catabolic process
macromolecule modification
positive regulation of cellular protein metabolic process
Cluster 4
nucleosome assembly
DNA packaging
chromatin assembly or disassembly
chromosome organization
peptidyl-proline modification
peptidyl-proline hydroxylation to 4-hydroxy-L-proline
skin development
acidic amino acid transport
glycoprotein metabolic process
anterior/posterior pattern formation
regulation of embryonic development
organic anion transport
cholesterol metabolic process
Cluster 5
cellular ketone metabolic process
organic acid metabolic process
glutamine family amino acid catabolic process
branched chain family amino acid catabolic process
isocitrate metabolic process
succinate metabolic process
regulation of acetyl-CoA biosynthetic process from pyruvate
cellular respiration
lipid oxidation
protein homotetramerization
regulation of cofactor metabolic process
glutamine family amino acid biosynthetic process
metabolic process
carboxylic acid catabolic process

cellular amino acid metabolic process
small molecule catabolic process
oxidation reduction
generation of precursor metabolites and energy
carboxylic acid metabolic process
glutamate metabolic process
amine catabolic process
fatty acid metabolic process
coenzyme catabolic process
cellular lipid catabolic process
cofactor biosynthetic process
2-oxoglutarate metabolic process
tricarboxylic acid cycle
acetyl-CoA biosynthetic process
fatty acid beta-oxidation
succinyl-CoA metabolic process
cofactor metabolic process
lipid metabolic process
acetyl-CoA metabolic process
amine metabolic process
cellular catabolic process
Cluster 6
ion transport
metal ion transport
response to copper ion
regulation of smooth muscle cell proliferation
chloride transport
iron ion transport
regulation of necrotic cell death
response to retinoic acid
drug transmembrane transport
positive regulation of endothelial cell migration

indole and derivative metabolic process
intermediate filament organization
indolalkylamine metabolic process
negative regulation of cytokine production
positive regulation of calcium ion transport

5. DISCUSSION

In the present work essential steps of the replication cycle of influenza A virus were investigated. For this purpose a new imaging technique was established and a recently invented quantitative method for proteome studies applied. The presented results give new insights into the progress of viral replication and provide a deeper understanding of the viral-host interaction.

In the first chapters a sequence specific technique for viral mRNA imaging in living infected cells was introduced. This technique is based on the combination of PNA molecules with intercalating fluorophores. The most crucial advantage is that the fluorescent moiety apart from other probes is inserted as a base substitution. This leads to the highly specific generation of fluorescence signals assigned to viral mRNA molecules. For the first time, viral mRNA was investigated in a sequence specific manner in mammalian cells using FIT-PNAs.

To demonstrate the wide application spectrum of the presented technique influenza A virus infection was further determined via FACS analysis and a VSV derived transcript was studied in infected cells using a specific PNA probe.

The last chapter focuses on the progression of influenza A virus translation and the viral impact on the host cell proteome. Both, the viral and the cellular proteome were quantitatively assessed using mass spectrometry in concert with SILAC. The non-radioactive labelling of essential amino acids in newly synthesized proteins enables a time-resolved quantitative study upon influenza A virus infection. The results provide detailed information about the impact of viral action on cellular processes and viral-host interactions during the early stages of replication on a systems level.

Collectively, this work implies data on the influenza A virus replication which set a basis for computational modelling, the development of new antiviral strategies and a deeper understanding of the viral host-dependency.

5.1 HYBRIDISATION AND FLUORESCENCE PROPERTIES OF FIT-PNAS

PNA molecules exhibit a stronger binding affinity to RNA than RNA or DNA to their respective counterparts [150]. Nielson *et al.* 1994 explained this by pointing at the main structural property of PNA molecules which is the peptide backbone. Apart from DNA or RNA molecules PNAs are uncharged and thus lack the charge repulsion effect [159]. Moreover, the backbone substitution prevents endonuclease mediated degradation [153] and thus provides a stable labelling during the imaging time range. The nuclease and protease resistance of the used FIT-PNA was assessed in cell lysate in the absence of the target sequence (see figure 12). The fluorescence of the FIT-PNA was virtually unchanged indicating that the structure was not destroyed by cleavage. The influence of nucleases was shown by measuring MB 2 under the same conditions. After 5 hours incubation in cell lysate, the fluorescence of this probe increased by more than 40% reflecting a strong decrease in sensitivity. Consequently, this experiment revealed the favoured biostability of PNA molecules over DNA Molecular Beacons.

FIT-PNAs possess a highly specific sequence discrimination shown by Socher *et al.* 2008 [182] in a study detecting single nucleotide polymorphisms in a real-time PCR approach. This is in good agreement with the results of this work since the applied PNAs exhibited high sequence sensitivity. FIT-PNA 1b which was designed to target a 17 bases in length sequence in the NA mRNA exhibits an 11-fold enhancement in fluorescence intensity upon hybridisation with the artificial RNA target 3b (see 3.1.9). Even a 12-fold increase was reached for the measurement at 60 °C with the DNA target 5 (see 3.1.9.). Previous studies with artificial target sequences reported a maximal possible enhancement by a factor of 20 [170]. However, one has to keep in mind, that the quantum efficiency of the intercalating fluorophore, thiazole orange and its derivates, strongly depends on

the environment. The five nucleic bases (thymine, guanine, cytosine, adenine, and uracil) produce distinct spatial properties which influence the position of the heterocycles and thus the basis for maximal fluorescence enhancement [172, 173]. Whether there is a preference for the substituted nucleic base remains to be clarified. Jarikote *et al.* 2007 [180] provides clues for the PNA sequence design. But to date, the ideal sequence cannot be predicted theoretically due to the complexity of altering parameters like the interaction with neighbouring base pairs in combination with the sequence length. This effect is reflected by experiments using the sequence of the swine H1N1/Mexico/2009 strain which is shortened in length but the remaining target is sequence identical and the analogues sequence of the H3N2/X-31 strain which exhibits seven continuous matched base pairs situated in close proximity to the TO base surrogate. While the FIT-PNA 1b hybridised to the H1N1/2009 target confirmed the high enhancement in fluorescence, it stayed virtually unchanged in combination with the H3N2/X-31 target sequence (see figure 11).

PNA 1c (M1) showed a minor increase (factor 5.7) in fluorescence hybridised to the complementary artificial target sequence in comparison to the unspecific target sequence (factor 2) (see figure 34). One could argue that the TO and the BO do not share the same sensitivity properties caused by their varying structure as the BO lacks one carbon ring but the results obtained in living cells revealed a higher enhancement factor for the BO probe compared to the TO probe. The difference in sensitivity of PNA 1b and 1c is also not contributed to the nucleic base composition as for both probes the AT:GC ratio is 1.7. It is likely, that the position of the fluorophore plays a more sophisticated role for the sensitivity as demonstrated by the results in table 4, 5 and 6. For example, the estimated maximal enhancement factor of FIT-PNA 1d (L, VSV) was 3.4. But if the TO base surrogate was shifted only one position to the N-terminal end it lost nearly 70% sensitivity (factor 1.1). In general, a centred position for the intercalating fluorophore substitution is recommended whereas variations cannot be excluded.

Moreover, one has to deal with the given target sequence possibilities in biological applications, e.g. specific mRNA imaging in living cells. This limits the design of the PNA sequence. In this case the problematic issue is the accessibility of the target sequence for the detecting probe. Secondary structures of mRNA molecules exhibit double stranded regions which produce single stranded loops as side effect. All PNAs used in this work were directed to single stranded regions of the corresponding mRNA species.

Fang *et al.* 2010 [230] reported about a method to generate a native mRNA antisense-accessible sites library (MASL) for designing mRNA imaging probes. This technique is based on the identification of antisense-accessible sites using RT-ROL (reverse transcription with random oligonucleotides libraries). Albeit it is only demonstrated to work for mouse macrophages this technique provides for a powerful tool to simplify the PNA sequence selection.

An essential drawback of FIT-PNAs is the low quantum yield of thiazole orange and its derivates (0.1-0.4) compared to fluorescent proteins (e.g. EGFP 0.6). However, the target specific increase in fluorescence enables the discrimination of bound and unbound probe. Fluorescent proteins in combination with the MS2 technique are suitable for imaging of mRNA in yeast but tend to form aggregates resulting in false-positive signals [116].

Notably, these assumptions on hybridisation and fluorescence features of PNA probes are based on measurements in buffered solutions excluding interfering factors which are present in living cells. These factors include binding of RNA/DNA binding proteins, false-positive signals evoked by competitive target sequences of cellular mRNA molecules and the cytosol itself creating the fluorophore environment.

5.2 FIT-PNAs IN REAL-TIME QUANTITATIVE PCR

In 1993 Kary Mullis was awarded with the Nobel prize in Chemistry for the invention of the polymerase chain reaction [231]. Essentially, this technique allows the amplification of any nucleic acid sequence generating identical copies. But for analytical purposes the original PCR was limited since the amount of the product was the same independent from the template concentration. Higuchi *et al.* 1992 [232] improved the standard PCR enabling the simultaneous amplification and product monitoring during the course of the reaction. This is based on the detection of the increase in fluorescence of the reporter dye which is proportional with the amount of specific product. Among the several chemistries which have been developed TaqMan probes® and SYBR-Green I® are the most common used detecting agents [233].

Typical applications for real-time qPCR include analysis of gene expression, chromosome aberration and single nucleotide polymorphism [234]. In this work the amount of influenza A virus NA and M1 mRNA per infected cell was determined based on a specific real-time qPCR. To enhance the detection specificity the reaction was performed utilizing the FIT-PNAs 1a and 1c which were designed to target the NA and M1 mRNA, respectively, and were essentially used in mRNA imaging in living infected cells. This is a great advantage over Molecular Beacons [126, 148] or Locked Nucleic Acids [235]: although they can be applied to qPCR or imaging, a single probe is restricted to one application due to the fact that their functionality is temperature-dependent.

For the qPCR approach performed in this work the primer pairs were designed to amplify a 101bp in length sequence in which the target region of the PNA was included. Therefore the increase in fluorescence of TO and BO correlated with the amount of specific product and enabled an accurate and sensitive quantitative data analysis.

Assuming a certain reaction efficiency (one doubling of molecules per amplification cycle), the number of specific cDNA molecules which were initially present in

the sample at the cycle of threshold was determined. The time course of samples 0 – 8 h p.i. revealed a maximum of NA copy number at 4.5 h p.i. whereas for the M1 the maximal amount was reached 5 h p.i. (see chapters 4.1.3. and 4.2.2.). Despite this slight difference in both cases the amount stayed virtually constant until 7 h p.i. and decreased in the following. The lowering of the mRNA abundance might indicate the switch from the transcription to the replication mode.

Shapiro *et al.* 1987 [66] generally concluded that the synthesis of viral mRNAs largely determines the translation rate of the encoded proteins. Thus, alterations in the temporal appearance of individual mRNA molecules are surmised. Apart from the NS1 which was proved to be transcribed in the early phase of the viral replication cycle for NA and M1 only a slight difference in the onset of transcription was determined. Notably, based on a rough estimation of the maximal amount of an mRNA species per infected cell revealed a higher concentration for M1 ($\sim 10^6$ copies/infected cell) compared to NA ($\sim 10^5$ copies/infected cell). This is in good agreement with the viral particle composition: approximately 3000 copies of M1 form the viral core, while only 100 molecules of NA are embedded in the viral envelope [236].

Summarizing, it can be surmised that the amount of a particular mRNA is more crucial for the encoded viral protein abundance than a temporal control of the transcript synthesis.

These results may not exclude alterations evoked by strain specificities and cell population heterogeneity. The variability of the studied biological systems gives rise to considerable uncertainty. That is why these data cannot be in detail related to other influenza A virus strains or cell lines. In fact the time course gives an impression of the dynamics of the infection and the amount of produced viral mRNA. This point requires further studies concerning the remaining influenza A segments which might reveal larger differences in temporal progression and mRNA concentration in infected cells.

Moreover the application of single cell PCR approaches to the determination of mRNA copy numbers might reveal variations in infection efficiency and progression due to cell heterogeneity.

5.3 Parallel Imaging of Viral mRNAs in Living Infected Cells

To date, most insights in nucleic acid research in living systems are based on two techniques which focus on a sequence specific detection in concert with a fluorescence signal increase: the MS 2 technique [114, 115] and Molecular Beacons [125]. Indeed, these strategies are limited to special applications (e.g. imaging in yeast) or exhibit certain disadvantages (e.g. susceptibility to nucleases), respectively. The introduction of FIT-PNAs [170] into the field of mRNA imaging in living cells improved the method spectrum. The FIT-PNA technique is neither restricted to a certain cell type nor suffering from drawbacks which other probes are faced with [116, 147, 148].

In the present work for the first time FIT-PNAs were employed for viral mRNA imaging in living infected cells using CLSM [183].

In living influenza A virus infected MDCK cells FIT-PNA 1b showed a 4.5-fold increase in fluorescence at 4.5.h p.i. upon binding to the NA mRNA target sequence. Control experiments with non-infected and SFV infected cells confirmed the high sensitivity of the probe as in these samples no significant fluorescence was detected (see chapter 4.1.6). These findings revealed that the increase in fluorescence of FIT-PNA 1b was due to target hybridisation and not evoked by the binding of proteins or unspecific hybridisation to any viral mRNA.

A second influenza A virus mRNA species was targeted by a PNA molecule carrying BO as intercalating fluorophore. This M1 specific PNA 1c reached an enhancement of 6.97 at 5 h p.i. in comparison to the non-infected control. The result deviated to the measurement with the complementary artificial target RNA furnishing only a 5.7-fold increase. As discussed afore previous studies provided evidence for the impact of the environment on the fluorescence properties of the

intercalating dyes. Svanvik *et al.* 2001 [237] determined the quantum yield influencing factors of TO using light-up probes which demands to be further assessed for the remaining TO derivates. Importantly, both probes show comparable fluorescence enhancement factors upon specific target binding enabling simultaneous detection of the NA and M1 mRNA species in the same cell (see chapter 4.1.6 and 4.2.3). To date, imaging of mRNA in living cells was restricted to one sort of mRNA molecules. With the help of the FIT-PNA technique alterations in localisation, transport or turnover-rates of different RNA molecules can be investigated including dynamic processes in living cells. In particular, this is of great relevance for the understanding of viral-host interaction and the mechanisms behind viral hijacking of host cell processes.

For this purpose, the emission range of TO and BO were adjusted to prevent cross-talk between the two emission channels. TO was measured from 510 nm to 540 nm individually and from 530 nm to 600 nm in combination with the BO probe. Because TO has its emission peak at 530 nm, the shift did not dramatically influence the brightness of the probe. BO emission was recorded from 470 nm to 500 nm in individual measurements but was shifted 10 nm to lower wavelengths with negligible impact on the fluorescence intensity.

Whether the derivates of TO besides BO, oxazole yellow (YO) and thiazole pyridine (MO) (see chapter 4.3.1, figure 30), provide for the same applicability in PNA molecules remains to be clarified. It is likely, that several combinations might be problematic due to fluorescence interference effects. Therefore the adjustment of the recorded emission range has to be performed careful to prevent cross-talk between the emission channels.

Simultaneous CLSM imaging of the NA mRNA and the M1 mRNA upon influenza A virus infection 5 h p.i. in living cells revealed alterations in the fluorescence patterns. Despite the observation of a certainly not homogenous distribution in both cases, for the M1 mRNA distinct regions of increased fluorescence were detected (see figure 32, white arrows).

This leads to the assumption that the heterogenous distribution of the NA and M1 mRNA is based on a certain localisation due to regulatory and economical reasons. Martin *et al.* 2009 [211] reviewed the localisation of cellular mRNA molecules in distinct subcellular compartments. The viral replication is a fine tuned process which requires temporal and spatial control of gene expression. Therefore a controlled localisation of viral transcripts at the rough endoplasmatic reticulum or polysomes to enhance the translation rate of viral transcripts could be surmised.

This is also reflected by the work of Davey *et al.* 2011 [80] who described a mechanism how viruses hijack for example the host intracellular transport machinery (see Introduction). It is assumed that viruses mimic cellular motifs, named SLiMs (short linear motifs), as proved for the influenza A protein PB2 mimicking the nuclear localisation signal of the cellular importin α to enter the host nucleus and for NS1 to alter the host immune response [80].

In respect to the described binding activity of the NS1 to a wide range of RNA molecules [54] and the influence on the cellular mRNA export as well as viral mRNA translation [57, 58] it is conceivable that the NS1 controls also the transport and localisation of the viral mRNA molecules by entering host cell proteins using SLiMs.

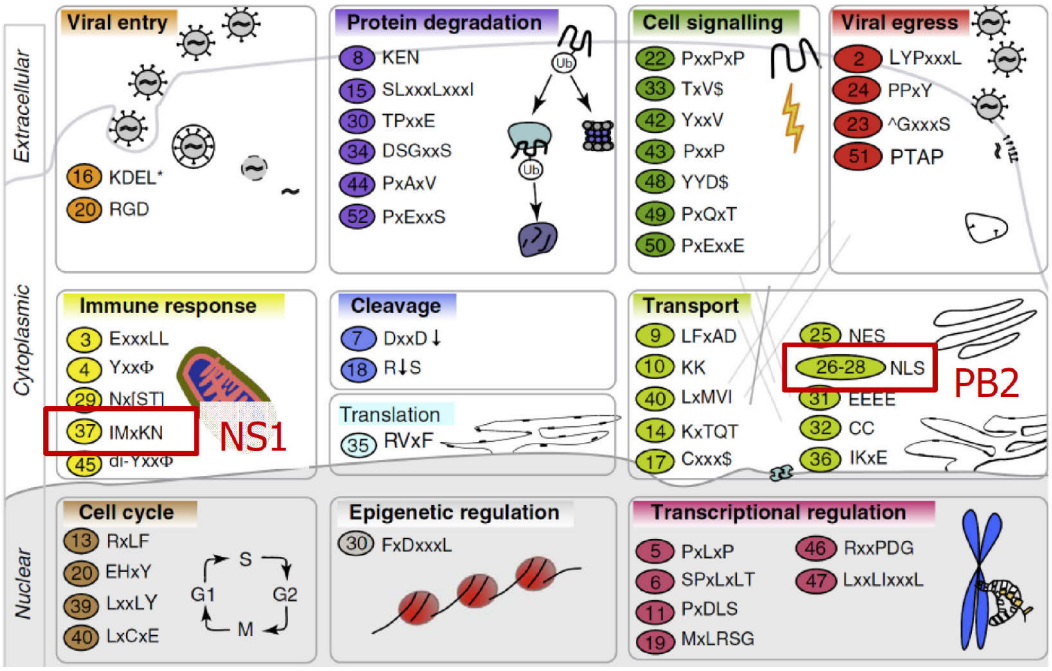

Figure 42: Overview of SLiMs roughly classified by function. (modified from Davey et al. 2011) The numbering scheme corresponds to the examples provided in Davey et al. 2011. Motifs which are used by influenza A protein PB2 and NS1 to interact with cellular proteins are highlighted in red.

Besides that, viral mRNA is assumed to hold a key position in the influenza A virus infection induced host cell apoptosis as described previously by Morris *et al.* 1999 [238]. Induction of apoptosis after the last round of progeny virus synthesis may prevents reinfection of cells already been infected [209]. The ability to adjust the efficiency of infection by regulating transcription and replication gives important clues on the virulence and pathogenicity of pandemic influenza A strains. The FIT-PNA technique can be used to study the temporal and spatial progression of transcription and is therefore the method of choice.

A comparison of the images acquired with FIT-PNA 1b in influenza A infected MDCK cells 4.5 h p.i. (see chapter 4.1.6) and 5 h p.i. (see chapter 4.3.2) revealed a difference in the fluorescence signal localisation. At 4.5 h p.i. the signal was mainly concentrated in the nucleus whereas at 5 h p.i. it appeared more cytosolic. This demonstrates the dynamics of the mRNA localisation and will be fur-

ther assessed in ongoing studies in terms of real-time monitoring of single infected cells. In contrast, MBs enter the nucleus but accumulate there due to binding of RNA/DNA binding proteins. Therefore they are not longer capable for further target detection in the cytosol and are not suitable to monitor viral mRNA transport in living infected host cells.

Whether the binding of the PNA has an impact on the lifetime of the viral transcript or the translation efficiency into viral proteins requires further investigation. Previous studies in nuclear medicine described antisense-strategies with PNA molecules [152, 154] and thus, demonstrated the applicability of PNAs as antisense agents. It is likely, that the underlying mechanism of the eventually produced gene knock-down is comparable to that of small interfering RNAs or micro RNAs [83, 88].

Nevertheless, the risk to modify the native localisation, transport and dynamics of (viral) mRNA is not given as it occurs by using GFP tags in tandem repeats (MS2 technique). Hence, the fluorescent probe is very small and does not require molecular modifications of the target or the transgenic expression of the selected gene leading to a non-physiological over-expression. With the help of the FIT-PNA technique the mRNA progression can be followed in real-time in living cells.

A crucial aspect in working with PNA molecules is the transfer into the cytosol of living cells. Due to their uncharged character [150] PNAs do not interact with standard transfection reagents in which the binding to the shuttle agent is based on electrostatical effects (e.g. Lipofectamine, Invitrogen). In this work a sufficient PNA delivery was carried out utilizing streptolysin O mediating a reversible plasma membrane penetration (see chapter 3.2.2.3). For MDCK cells this method did not reduce cell viability as shown with a cell viability test using propidium iodide (see figure 17).

5.4 IMAGING OF VIRAL mRNA IN FIXED CELLS

Apart from epithelial derived cell lines (MDCK) exhibiting strong connections to neighbouring cells, fibroblasts lack intercellular adhesion and thus were not able to survive the SLO mediated plasma membrane permeabilisation. For the present study of VSV L mRNA, the BHK-21 cells were subjected to fixation and Triton X-100 treatment to deliver FIT-PNA 1d into the cytoplasm. Cell-penetrating peptides (CPPs) might be an attractive tool to solve the delivery problem into living cells concerning fibroblast or SLO sensitive cell lines. Liu *et al.* 2010 [239] suggested CPPs for the transfer of quantum dots (luminescent semiconductor nanocrystals) in biomedical approaches whereas Shim and Kwon *et al.* 2010 [240] described CPPs for the targeted delivery of siRNAs *in vivo*. CPPs are short peptides enriched in basic amino acids that penetrate the plasma membrane in a receptor- and energy-independent manner. Octa-arginine or nona-arginine achieved the highest delivery efficiency in this context [241]. The peptide can be linked covalently or non-covalently to the cargo and showed minor cytotoxicity [242]. Due to their peptide backbone PNA molecules can be easily modified with additional peptide chains. Thus, it is highly recommended to test the applicability of CPPs to the delivery of PNA molecules.

Besides the drawback that imaging in living cells could not be carried out, interesting information about the progression of the VSV L mRNA were acquired (see chapter 4.4.2., figure 36). At 60 min p.i. the fluorescence of TO increased in comparison to the starting point (0 min p.i.). The quantitative analysis revealed that the high fluorescence signal stayed constant for approximately 30 min and decreased in the following samples (until 150 min p.i.). Although the enhancement factor was low the high sensitivity of the probe generated a clear discrimination to the non-infected and the SFV infected controls showing no significant increase in fluorescence (see chapter 4.4.2., figure 36).

To date, apart from the pathological characteristics and clinical signs less is known about the temporal progression of VSV replication. Investigation of the L

mRNA in BHK-21 cells gave first insights into the time course of VSV transcription. Interestingly, the production of this particular VSV mRNA was detected approximately 1 h after infection. This is much faster compared to the results obtained for influenza A virus where the mRNA synthesis started approximately 3 h p.i. This brings up two questions: Why is the VSV transcription faster compared to influenza A virus? And what are the mechanisms behind?

The present data just allow speculations as detailed information about the temporal progression of VSV replication are lacking. Whether the VSV exhibits a more efficient entry or uncoating process leading to an earlier onset of transcription or the polymerases differ in their function remains to be clarified. Thus, since in general the genome composition of VSV (non-segmented) and influenza A virus (segmented) differ from each other it is conceivable that this causes the alteration in transcription rate. Another aspect one has to keep in mind is the amount of novel synthesized virus particles determining the abundance of viral proteins and thus the transcription rate.

Generally, although BHK-21 and MDCK cells are both of mammalian origin it has to be assumed that these cell lines differ in their biological status which might result in variations in infection progression.

5.5 Global Proteome Analysis of Influenza A Virus Infected MDCK Cells Using SILAC

SILAC is a simple and accurate approach for expression proteomics on a systems level enabling an automated simultaneous identification and quantification of complex protein mixtures [186]. In contrast to ICAT (isotope-coded affinity tag) labelling which is the most well established method in quantitative proteomics by mass spectrometry to date, SILAC does not require multiple fractionation and affinity purification steps and is therefore suitable to small amounts of proteins and the direct comparison of varying states [186]. This is crucial for the presented work as the starting material (number of cells, virus stock) was limited.

Assuming that after a certain number of cell doublings, each argine and lysine will have been replaced by its isotopic analogue, MDCK cells were tested for the efficiency of incorporation. The measurement revealed an incorporation of ~99.8% for cells maintained seven passages in SILAC medium (data not shown). As there is no chemical difference between the labelled and the natural amino acids the cells behaved exactly like a control cell population.

The SILAC technique was readily applied to the determination of muscle cell differentiation [186], phenotypic comparison of immortalized cell lines with their cognate primary cells [194] and investigations of the impact on the host cell proteome upon virus infection [200, 202].

In the present work SILAC was applied to compare the gene expression profile of influenza A virus infected and non-infected MDCK cells on a proteome level. In particular, the viral impact on the host proteome was investigated in the first stages of the infection in an 8 h time-scale. Hence, this study focuses on the influence on viral transcription and replication as well as cellular antiviral processes it is not expected to identify host factors involved in virus assembly, budding or release.

The functional phenotyping of the MDCK proteome after 8 h p.i. provided an unbiased global portrait of representative biological functions (see figure 39). The most prominent category of proteins expressed at higher levels in influenza A infected MDCK cells were related to inflammatory response, induction of apoptosis, immune effector processes, intracellular protein transport and actin cytoskeleton organisation (see also figure 40, cluster 3). Biologically, these reactions coincide with the expected processes in an infected cell and are in good agreement with the findings of a previous study on influenza A virus (A/PR/8) infection in human lung A549 cells at 24 h p.i. [243]. On the one hand the virus hijacks the cellular transport machinery and induces cell death as assumed by Davey *et al.* 2011 and Morris *et al.* 1999, respectively [80, 238]. On the other hand, the attacked cells recruit defence mechanisms. These proteins responsible for antiviral

response were graphed in figure 41 C illustrating the abundance progression in detail. Surprisingly, most of the proteins showed no drastic alterations in protein level over the whole time-scale indicating that they are either activated after 8 h p.i. or completely not included in this specific defence reaction. Further, it is conceivable to surmise that they were blocked by viral host-shutoff processes.

Other proteins like SERPIN B6, CAD and SF1 increased by more than 2 magnitudes in protein abundance until 8 h p.i. SERPIN B6 belongs to the serpin superfamily and controls inflammation and tumor suppression. Cathepsin G, an antiviral agent in neutrophilic polymorphonuclear granules, is one of its targets [226]. CAD (carbamyl phosphate synthetase II, aspartate transcarbamylase, and dihydro-orotase) catalysis the first 3 steps of the pyrimidine biosynthesis and SF1 regulates the splicing of distinct cellular mRNA molecules. The most impressive pattern in the recorded abundance change was shown for the ZER 1 protein with a fast decrease after 2 h p.i. over 4 magnitudes. It recruits the ubiquitin ligase complex while interacting with CUL-2 inducing ubiquitination of special substrates including transcription factors. Whether this has any antiviral effect cannot be ruled out by the given data set but enrichment of proteins related to ubiquitination was already identified by König *et al.* 2010 [82] employing an arrayed short-interfering RNA screen of 19,000 human genes.

The reduction of specific host proteins as shown in the functional cluster 1 and 6 (see figure 40) representing mainly cellular lipid metabolism and ion homoeostasis, respectively, might be contributed to the enhanced abundance and thus, activity of proteasomal proteins which were assembled in cluster 4.

The host cell gene expression is critical for influenza A virus replication since the cap structures of polymerase II transcripts are required for priming of viral transcription and the cellular splicing machinery is crucial to produce the alternative splicing variants M2 and NS2 (NEP) [243]. This is reflected by the strongly regulated abundance of proteins assigned to cluster 2 (see figure 40) during the infection time range. Assuming that the maximal level of proteins responsible for

positive regulation of transcription from polymerase II promoters correlates with the availability of cap structures this finding is in perfect accordance with the 30 – 60 min delayed maximal concentration of NA and M1 mRNA molecules (please review chapter 4.1.3. and 4.2.2.) estimated for influenza A virus infected MDCK cells.

Moreover, the influenza A virus proteins (except the M2 protein) were included in this proteomic study. Generally, the level of a certain viral protein logically correlates with its function during the replication cycle or the required copy number present in progeny virus particles: For the NP and the NS1 a strong increase in abundance was revealed in the first 2 hours of infection. This is in good agreement with the corresponding function as the level of NP is assumed to regulate the switch from the transcription to the replication mode and the NS1 activity is surmised to impede cellular antiviral defence mechanisms [32, 59]. Contrary, the PB1 and NA protein increased slightly in abundance over the whole measured time-range. Caused by the fact that these proteins are not responsible for regulatory mechanisms during the viral replication there might be no requirement for a highly controlled translation rate (for details please review Introduction). Highly abundant structural proteins like the HA and the M1 [236] showed a comparable linear progression until 8 h p.i. but with larger slope resulting in a three-times higher protein amount.

It has to be admitted that the impact of physiological alterations in the cell`s protein expression cannot be excluded for all presented results. This effect is assessed in ongoing studies investigating also samples of influenza A virus infected MDCK cells 8 – 12 h p.i. and non-infected cells over the same time-range. Besides, it is likely, that by far the majority of the discussed issues concerning influenza A virus induced modifications of the host cell proteome will be verified in further studies.

Summarizing, SILAC is the method of choice for detailed investigation of dynamic protein progression during infection as it provides for reliable results and includes

also less abundant proteins which are difficult to detect in less sensitive detection methods like ICAT, ICC or Western Blotting. Besides, no chemical modifications or specific antibodies are required enabling a high throughput analysis of thousands of proteins in parallel. Thus, abundance alterations caused by biological variations of samples are minimized making a direct comparison of differently treated samples possible. The presented experimental strategy is improvable by choosing the time point 8 h p.i. as reference. It is likely, that the usage of 1 h p.i. as reference value implied aberrations concerning the exact viral protein amount caused by inaccurate protein determination. Therefore the above presented data interpretation is based on the overall relation of the viral proteins to each other and not on detailed numerical values.

The field of proteomics is becoming more quantitative than qualitative [205] enlarging the obtained data sets wherein thousands of details are included complicating the causal interpretation. Therefore, if specific antibodies are available targeted studies on specific virus-host interaction partners identified in previous siRNA screens in combination with immunoprecipitation assays give more direct information.

CONCLUSION AND FUTURE PERSPECTIVES

The present work includes new insights into the transcription and translation of the influenza A virus and points the way to an quantitative and temporal characterization of new as well as previously described virus-host interaction pathways and hypotheses behind the mystery how viruses control cellular processes.

Apart from a previous proteomic study using SILAC to analyse the global changes in host protein abundance upon influenza A virus infection [244] 12 h p.i. this work revealed a strong regulation of distinct proteins rather than a complete decrease in host cell protein levels. In particular, the dynamics in protein expression during the first 6 to 8 h of the viral infection (see figure 40) indicate strong viral host interaction mechanisms where the virus hijacks cellular processes and resources to efficiently replicate. The question how the in this work identified strong regulation of antiviral response proteins like SERPIN B6, CAD, SF1 and /or ZER 1 is controlled and imbedded into this interaction network remains to be further investigated.

The innovative FIT-PNA technique enables detailed temporal, spatial and quantitative investigation on different viral mRNA molecules in living cells simultaneously. This sequence specific method is applicable to a wide range of viruses, in particular with mRNA intermediate step, and nucleic acid variants. The relevance of these probes for nucleic acid imaging is reflected by the article in ChemBioChem written by Jens Tilsner and Cristina Flors 2011 [245] highlighting our publication on influenza A virus mRNA imaging in living infected cells using FIT-PNAs [183]. They assume that studies in cellular complex environments benefit from the high specificity and increased sensitivity of FIT-PNAs and conclude that these probes might be suitable for single-molecule approaches.

For the first time a time-resolved analysis of the cellular and viral proteomic dynamics in the early stages of influenza A virus infection in MDCK cells was performed. The recently by Schwanhäußer *et al.* 2009 [246] described pulsed SILAC technique might improve the flexibility and temporal resolution. This method enables the direct and quantitative determination of protein translation and turnover rates on a proteome-wide scale. In concert with data obtained from single cell studies using FIT-PNAs this global approach might complete an overall description of the host and influenza A proteome dynamics in time and space.

Further studies could focus on the detailed analysis of functional protein phosphorylation, nucleic and cytosolic protein fractionation, other cell types and virus strains. In particular, pandemic variants compared to seasonal flu causing strains might identify unique features of highly pathogenic viruses and help to improve antiviral therapies.

Whether the presented results obtained in an immortalized cell line can be applied to the *in vivo* situation remains to be clarified. Pan *et al.* [194] ruled out that the lack of tissue architecture and a heterogeneous population of different cell types in cell culture generally impedes cell-cell interaction and other functions based on tissue context. Therefore cells in culture might acquire a molecular phenotype varied from cells *in vivo* that requires a careful choice of the most appropriate experimental system.

An improvement of the quantitative analysis to determine the fluorescence intensity of FIT-PNAs in cells might be achieved by automation of the measurement. This requires the identification of cells by the software and the recognition of cell borders to distinguish between the cytosol and the background.

BIBLIOGRAPHY

1. CHEUNG, T.K. AND L.L. POON, *BIOLOGY OF INFLUENZA A VIRUS.* ANN N Y ACAD SCI, 2007. **1102**: P. 1-25.
2. KROSSOY, B., ET AL., THE PUTATIVE POLYMERASE SEQUENCE OF INFECTIOUS SALMON ANEMIA VIRUS SUGGESTS A NEW GENUS WITHIN THE ORTHOMYXOVIRIDAE. J VIROL, 1999. **73**(3): P. 2136-42.
3. FOUCHIER, R.A., ET AL., CHARACTERIZATION OF A NOVEL INFLUENZA A VIRUS HEMAGGLUTININ SUBTYPE (H16) OBTAINED FROM BLACK-HEADED GULLS. J VIROL, 2005. **79**(5): P. 2814-22.
4. LAVER, W.G., ET AL., *INFLUENZA VIRUS NEURAMINIDASE WITH HEMAGGLUTININ ACTIVITY.* VIROLOGY, 1984. **137**(2): P. 314-23.
5. BURLEIGH, L.M., ET AL., INFLUENZA A VIRUSES WITH MUTATIONS IN THE M1 HELIX SIX DOMAIN DISPLAY A WIDE VARIETY OF MORPHOLOGICAL PHENOTYPES. J VIROL, 2005. **79**(2): P. 1262-70.
6. ELLEMAN, C.J. AND W.S. BARCLAY, THE M1 MATRIX PROTEIN CONTROLS THE FILAMENTOUS PHENOTYPE OF INFLUENZA A VIRUS. VIROLOGY, 2004. **321**(1): P. 144-53.
7. JIN, H., ET AL., INFLUENZA VIRUS HEMAGGLUTININ AND NEURAMINIDASE CYTOPLASMIC TAILS CONTROL PARTICLE SHAPE. EMBO J, 1997. **16**(6): P. 1236-47.
8. ROBERTS, P.C., R.A. LAMB, AND R.W. COMPANS, THE M1 AND M2 PROTEINS OF INFLUENZA A VIRUS ARE IMPORTANT DETERMINANTS IN FILAMENTOUS PARTICLE FORMATION. VIROLOGY, 1998. **240**(1): P. 127-37.
9. ROBERTS, P.C. AND R.W. COMPANS, *HOST CELL DEPENDENCE OF VIRAL MORPHOLOGY.* PROC NATL ACAD SCI U S A, 1998. **95**(10): P. 5746-51.
10. RUIGROK, R.W., L.J. CALDER, AND S.A. WHARTON, *ELECTRON MICROSCOPY OF THE INFLUENZA VIRUS SUBMEMBRANAL STRUCTURE.* VIROLOGY, 1989. **173**(1): P. 311-6.
11. BAUDIN, F., ET AL., STRUCTURE OF INFLUENZA VIRUS RNP. I. INFLUENZA VIRUS NUCLEOPROTEIN MELTS SECONDARY STRUCTURE IN PANHANDLE RNA AND EXPOSES THE BASES TO THE SOLVENT. EMBO J, 1994. **13**(13): P. 3158-65.
12. JENNINGS, P.A., ET AL., DOES THE HIGHER ORDER STRUCTURE OF THE INFLUENZA VIRUS RIBONUCLEOPROTEIN GUIDE SEQUENCE REARRANGEMENTS IN INFLUENZA VIRAL RNA? CELL, 1983. **34**(2): P. 619-27.
13. MURTI, K.G., R.G. WEBSTER, AND I.M. JONES, LOCALIZATION OF RNA POLYMERASES ON INFLUENZA VIRAL RIBONUCLEOPROTEINS BY IMMUNOGOLD LABELING. VIROLOGY, 1988. **164**(2): P. 562-6.
14. O'NEILL, R.E., J. TALON, AND P. PALESE, THE INFLUENZA VIRUS NEP (NS2 PROTEIN) MEDIATES THE NUCLEAR EXPORT OF VIRAL RIBONUCLEOPROTEINS. EMBO J, 1998. **17**(1): P. 288-96.
15. JONES, I.M., P.A. REAY, AND K.L. PHILPOTT, NUCLEAR LOCATION OF ALL THREE INFLUENZA POLYMERASE PROTEINS AND A NUCLEAR SIGNAL IN POLYMERASE PB2. EMBO J, 1986. **5**(9): P. 2371-6.
16. BRAAM, J., I. ULMANEN, AND R.M. KRUG, MOLECULAR MODEL OF A EUCARYOTIC TRANSCRIPTION COMPLEX: FUNCTIONS AND MOVEMENTS OF INFLUENZA P PROTEINS DURING CAPPED RNA-PRIMED TRANSCRIPTION. CELL, 1983. **34**(2): P. 609-18.

17. PLOTCH, S.J., ET AL., A UNIQUE CAP(M7GPPPXM)-DEPENDENT INFLUENZA VIRION ENDONUCLEASE CLEAVES CAPPED RNAS TO GENERATE THE PRIMERS THAT INITIATE VIRAL RNA TRANSCRIPTION. CELL, 1981. **23**(3): P. 847-58.
18. PLOTCH, S.J., M. BOULOY, AND R.M. KRUG, TRANSFER OF 5'-TERMINAL CAP OF GLOBIN MRNA TO INFLUENZA VIRAL COMPLEMENTARY RNA DURING TRANSCRIPTION IN VITRO. PROC NATL ACAD SCI U S A, 1979. **76**(4): P. 1618-22.
19. POOLE, E., ET AL., FUNCTIONAL DOMAINS OF THE INFLUENZA A VIRUS PB2 PROTEIN: IDENTIFICATION OF NP- AND PB1-BINDING SITES. VIROLOGY, 2004. **321**(1): P. 120-33.
20. POCH, O., ET AL., IDENTIFICATION OF FOUR CONSERVED MOTIFS AMONG THE RNA-DEPENDENT POLYMERASE ENCODING ELEMENTS. EMBO J, 1989. **8**(12): P. 3867-74.
21. GONZALEZ, S., T. ZURCHER, AND J. ORTIN, IDENTIFICATION OF TWO SEPARATE DOMAINS IN THE INFLUENZA VIRUS PB1 PROTEIN INVOLVED IN THE INTERACTION WITH THE PB2 AND PA SUBUNITS: A MODEL FOR THE VIRAL RNA POLYMERASE STRUCTURE. NUCLEIC ACIDS RES, 1996. **24**(22): P. 4456-63.
22. CHEN, W., ET AL., A NOVEL INFLUENZA A VIRUS MITOCHONDRIAL PROTEIN THAT INDUCES CELL DEATH. NAT MED, 2001. **7**(12): P. 1306-12.
23. SANZ-EZQUERRO, J.J., ET AL., *THE PA INFLUENZA VIRUS POLYMERASE SUBUNIT IS A PHOSPHORYLATED PROTEIN.* J GEN VIROL, 1998. **79 (PT 3)**: P. 471-8.
24. DE LA LUNA, S., C. MARTINEZ, AND J. ORTIN, MOLECULAR CLONING AND SEQUENCING OF INFLUENZA VIRUS A/VICTORIA/3/75 POLYMERASE GENES: SEQUENCE EVOLUTION AND PREDICTION OF POSSIBLE FUNCTIONAL DOMAINS. VIRUS RES, 1989. **13**(2): P. 143-55.
25. FODOR, E. AND M. SMITH, THE PA SUBUNIT IS REQUIRED FOR EFFICIENT NUCLEAR ACCUMULATION OF THE PB1 SUBUNIT OF THE INFLUENZA A VIRUS RNA POLYMERASE COMPLEX. J VIROL, 2004. **78**(17): P. 9144-53.
26. NIETO, A., ET AL., NUCLEAR TRANSPORT OF INFLUENZA VIRUS POLYMERASE PA PROTEIN. VIRUS RES, 1992. **24**(1): P. 65-75.
27. SKEHEL, J.J., ET AL., CHANGES IN THE CONFORMATION OF INFLUENZA VIRUS HEMAGGLUTININ AT THE PH OPTIMUM OF VIRUS-MEDIATED MEMBRANE FUSION. PROC NATL ACAD SCI U S A, 1982. **79**(4): P. 968-72.
28. VINES, A., ET AL., THE ROLE OF INFLUENZA A VIRUS HEMAGGLUTININ RESIDUES 226 AND 228 IN RECEPTOR SPECIFICITY AND HOST RANGE RESTRICTION. J VIROL, 1998. **72**(9): P. 7626-31.
29. STEINHAUER, D.A., ROLE OF HEMAGGLUTININ CLEAVAGE FOR THE PATHOGENICITY OF INFLUENZA VIRUS. VIROLOGY, 1999. **258**(1): P. 1-20.
30. WEBBY, R.J., ET AL., RESPONSIVENESS TO A PANDEMIC ALERT: USE OF REVERSE GENETICS FOR RAPID DEVELOPMENT OF INFLUENZA VACCINES. LANCET, 2004. **363**(9415): P. 1099-103.
31. ALBO, C., A. VALENCIA, AND A. PORTELA, IDENTIFICATION OF AN RNA BINDING REGION WITHIN THE N-TERMINAL THIRD OF THE INFLUENZA A VIRUS NUCLEOPROTEIN. J VIROL, 1995. **69**(6): P. 3799-806.
32. SHAPIRO, G.I. AND R.M. KRUG, INFLUENZA VIRUS RNA REPLICATION IN VITRO: SYNTHESIS OF VIRAL TEMPLATE RNAS AND VIRION RNAS IN THE ABSENCE OF AN ADDED PRIMER. J VIROL, 1988. **62**(7): P. 2285-90.
33. MARTIN, K. AND A. HELENIUS, NUCLEAR TRANSPORT OF INFLUENZA VIRUS RIBONUCLEOPROTEINS: THE VIRAL MATRIX PROTEIN (M1) PROMOTES EXPORT AND INHIBITS IMPORT. CELL, 1991. **67**(1): P. 117-30.
34. WHITTAKER, G., M. BUI, AND A. HELENIUS, *NUCLEAR TRAFFICKING OF INFLUENZA VIRUS RIBONULEOPROTEINS IN HETEROKARYONS.* J VIROL, 1996. **70**(5): P. 2743-56.
35. NEUMANN, G., M.R. CASTRUCCI, AND Y. KAWAOKA, *NUCLEAR IMPORT AND EXPORT OF INFLUENZA VIRUS NUCLEOPROTEIN.* J VIROL, 1997. **71**(12): P. 9690-700.

36. VARGHESE, J.N. AND P.M. COLMAN, THREE-DIMENSIONAL STRUCTURE OF THE NEURAMINIDASE OF INFLUENZA VIRUS A/TOKYO/3/67 AT 2.2 A RESOLUTION. J MOL BIOL, 1991. **221**(2): P. 473-86.
37. LIU, C., ET AL., INFLUENZA TYPE A VIRUS NEURAMINIDASE DOES NOT PLAY A ROLE IN VIRAL ENTRY, REPLICATION, ASSEMBLY, OR BUDDING. J VIROL, 1995. **69**(2): P. 1099-106.
38. PALESE, P., ET AL., CHARACTERIZATION OF TEMPERATURE SENSITIVE INFLUENZA VIRUS MUTANTS DEFECTIVE IN NEURAMINIDASE. VIROLOGY, 1974. **61**(2): P. 397-410.
39. LI, S., ET AL., GLYCOSYLATION OF NEURAMINIDASE DETERMINES THE NEUROVIRULENCE OF INFLUENZA A/WSN/33 VIRUS. J VIROL, 1993. **67**(11): P. 6667-73.
40. MATROSOVICH, M.N., ET AL., NEURAMINIDASE IS IMPORTANT FOR THE INITIATION OF INFLUENZA VIRUS INFECTION IN HUMAN AIRWAY EPITHELIUM. J VIROL, 2004. **78**(22): P. 12665-7.
41. RUIGROK, R.W., ET AL., *MEMBRANE INTERACTION OF INFLUENZA VIRUS M1 PROTEIN.* VIROLOGY, 2000. **267**(2): P. 289-98.
42. WATANABE, K., ET AL., MECHANISM FOR INHIBITION OF INFLUENZA VIRUS RNA POLYMERASE ACTIVITY BY MATRIX PROTEIN. J VIROL, 1996. **70**(1): P. 241-7.
43. YE, Z., D. ROBINSON, AND R.R. WAGNER, *NUCLEUS-TARGETING DOMAIN OF THE MATRIX PROTEIN (M1) OF INFLUENZA VIRUS.* J VIROL, 1995. **69**(3): P. 1964-70.
44. HUANG, X., ET AL., EFFECT OF INFLUENZA VIRUS MATRIX PROTEIN AND VIRAL RNA ON RIBONUCLEOPROTEIN FORMATION AND NUCLEAR EXPORT. VIROLOGY, 2001. **287**(2): P. 405-16.
45. ARZT, S., ET AL., STRUCTURE OF A KNOCKOUT MUTANT OF INFLUENZA VIRUS M1 PROTEIN THAT HAS ALTERED ACTIVITIES IN MEMBRANE BINDING, OLIGOMERISATION AND BINDING TO NEP (NS2). VIRUS RES, 2004. **99**(2): P. 115-9.
46. HOLSINGER, L.J. AND R.A. LAMB, INFLUENZA VIRUS M2 INTEGRAL MEMBRANE PROTEIN IS A HOMOTETRAMER STABILIZED BY FORMATION OF DISULFIDE BONDS. VIROLOGY, 1991. **183**(1): P. 32-43.
47. PINTO, L.H., L.J. HOLSINGER, AND R.A. LAMB, *INFLUENZA VIRUS M2 PROTEIN HAS ION CHANNEL ACTIVITY.* CELL, 1992. **69**(3): P. 517-28.
48. NEIRYNCK, S., ET AL., A UNIVERSAL INFLUENZA A VACCINE BASED ON THE EXTRACELLULAR DOMAIN OF THE M2 PROTEIN. NAT MED, 1999. **5**(10): P. 1157-63.
49. WHARTON, S.A., ET AL., ROLE OF VIRION M2 PROTEIN IN INFLUENZA VIRUS UNCOATING: SPECIFIC REDUCTION IN THE RATE OF MEMBRANE FUSION BETWEEN VIRUS AND LIPOSOMES BY AMANTADINE. J GEN VIROL, 1994. **75 (PT 4)**: P. 945-8.
50. LIU, W., H. LI, AND Y.H. CHEN, N-TERMINUS OF M2 PROTEIN COULD INDUCE ANTIBODIES WITH INHIBITORY ACTIVITY AGAINST INFLUENZA VIRUS REPLICATION. FEMS IMMUNOL MED MICROBIOL, 2003. **35**(2): P. 141-6.
51. WATANABE, T., ET AL., INFLUENZA A VIRUS CAN UNDERGO MULTIPLE CYCLES OF REPLICATION WITHOUT M2 ION CHANNEL ACTIVITY. J VIROL, 2001. **75**(12): P. 5656-62.
52. TAKEDA, M., ET AL., INFLUENZA A VIRUS M2 ION CHANNEL ACTIVITY IS ESSENTIAL FOR EFFICIENT REPLICATION IN TISSUE CULTURE. J VIROL, 2002. **76**(3): P. 1391-9.
53. ALONSO-CAPLEN, F.V. AND R.M. KRUG, REGULATION OF THE EXTENT OF SPLICING OF INFLUENZA VIRUS NS1 MRNA: ROLE OF THE RATES OF SPLICING AND OF THE NUCLEOCYTOPLASMIC TRANSPORT OF NS1 MRNA. MOL CELL BIOL, 1991. **11**(2): P. 1092-8.
54. QIU, Y. AND R.M. KRUG, THE INFLUENZA VIRUS NS1 PROTEIN IS A POLY(A)-BINDING PROTEIN THAT INHIBITS NUCLEAR EXPORT OF MRNAS CONTAINING POLY(A). J VIROL, 1994. **68**(4): P. 2425-32.
55. MARION, R.M., ET AL., INFLUENZA VIRUS NS1 PROTEIN INTERACTS WITH VIRAL TRANSCRIPTION-REPLICATION COMPLEXES IN VIVO. J GEN VIROL, 1997. **78 (PT 10)**: P. 2447-51.

56. Nemeroff, M.E., et al., Influenza virus NS1 protein interacts with the cellular 30 kDa subunit of CPSF and inhibits 3'end formation of cellular pre-mRNAs. Mol Cell, 1998. **1**(7): p. 991-1000.
57. Chen, Z., Y. Li, and R.M. Krug, Influenza A virus NS1 protein targets poly(A)-binding protein II of the cellular 3'-end processing machinery. EMBO J, 1999. **18**(8): p. 2273-83.
58. de la Luna, S., et al., Influenza virus NS1 protein enhances the rate of translation initiation of viral mRNAs. J Virol, 1995. **69**(4): p. 2427-33.
59. Cheung, C.Y., et al., Induction of proinflammatory cytokines in human macrophages by influenza A (H5N1) viruses: a mechanism for the unusual severity of human disease? Lancet, 2002. **360**(9348): p. 1831-7.
60. Richardson, J.C. and R.K. Akkina, NS2 protein of influenza virus is found in purified virus and phosphorylated in infected cells. Arch Virol, 1991. **116**(1-4): p. 69-80.
61. Neumann, G., M.T. Hughes, and Y. Kawaoka, Influenza A virus NS2 protein mediates vRNP nuclear export through NES-independent interaction with hCRM1. EMBO J, 2000. **19**(24): p. 6751-8.
62. Herz, C., et al., Influenza virus, an RNA virus, synthesizes its messenger RNA in the nucleus of infected cells. Cell, 1981. **26**(3 Pt 1): p. 391-400.
63. Desselberger, U., et al., The 3' and 5'-terminal sequences of influenza A, B and C virus RNA segments are highly conserved and show partial inverted complementarity. Gene, 1980. **8**(3): p. 315-28.
64. Hay, A.J., J.J. Skehel, and J. McCauley, *Characterization of influenza virus RNA complete transcripts.* Virology, 1982. **116**(2): p. 517-22.
65. Robertson, J.S., M. Schubert, and R.A. Lazzarini, *Polyadenylation sites for influenza virus mRNA.* J Virol, 1981. **38**(1): p. 157-63.
66. Shapiro, G.I., T. Gurney, Jr., and R.M. Krug, Influenza virus gene expression: control mechanisms at early and late times of infection and nuclear-cytoplasmic transport of virus-specific RNAs. J Virol, 1987. **61**(3): p. 764-73.
67. Bouloy, M., S.J. Plotch, and R.M. Krug, Both the 7-methyl and the 2'-O-methyl groups in the cap of mRNA strongly influence its ability to act as primer for influenza virus RNA transcription. Proc Natl Acad Sci U S A, 1980. **77**(7): p. 3952-6.
68. Shih, S.R. and R.M. Krug, Surprising function of the three influenza viral polymerase proteins: selective protection of viral mRNAs against the cap-snatching reaction catalyzed by the same polymerase proteins. Virology, 1996. **226**(2): p. 430-5.
69. Fodor, E., D.C. Pritlove, and G.G. Brownlee, *The influenza virus panhandle is involved in the initiation of transcription.* J Virol, 1994. **68**(6): p. 4092-6.
70. Plotch, S.J. and R.M. Krug, Influenza virion transcriptase: synthesis in vitro of large, polyadenylic acid-containing complementary RNA. J Virol, 1977. **21**(1): p. 24-34.
71. Singer, M.F. and P. Leder, *Messenger RNA: an evaluation.* Annu Rev Biochem, 1966. **35**: p. 195-230.
72. Shimizu, K., et al., Regulation of influenza virus RNA polymerase activity by cellular and viral factors. Nucleic Acids Res, 1994. **22**(23): p. 5047-53.
73. Vreede, F.T., T.E. Jung, and G.G. Brownlee, Model suggesting that replication of influenza virus is regulated by stabilization of replicative intermediates. J Virol, 2004. **78**(17): p. 9568-72.
74. Olson, A.C., E. Rosenblum, and R.D. Kuchta, Regulation of influenza RNA polymerase activity and the switch between replication and transcription by the

CONCENTRATIONS OF THE VRNA 5' END, THE CAP SOURCE, AND THE POLYMERASE. BIOCHEMISTRY, 2010. **49**(47): P. 10208-15.

75. BOUVIER, N.M. AND P. PALESE, *THE BIOLOGY OF INFLUENZA VIRUSES.* VACCINE, 2008. **26 SUPPL 4**: P. D49-53.
76. TUMPEY, T.M., ET AL., CHARACTERIZATION OF THE RECONSTRUCTED 1918 SPANISH INFLUENZA PANDEMIC VIRUS. SCIENCE, 2005. **310**(5745): P. 77-80.
77. GAMBOTTO, A., ET AL., *HUMAN INFECTION WITH HIGHLY PATHOGENIC H5N1 INFLUENZA VIRUS.* LANCET, 2008. **371**(9622): P. 1464-75.
78. SNIJDER, B., ET AL., POPULATION CONTEXT DETERMINES CELL-TO-CELL VARIABILITY IN ENDOCYTOSIS AND VIRUS INFECTION. NATURE, 2009. **461**(7263): P. 520-3.
79. SHAPIRA, S.D., ET AL., A PHYSICAL AND REGULATORY MAP OF HOST-INFLUENZA INTERACTIONS REVEALS PATHWAYS IN H1N1 INFECTION. CELL, 2009. **139**(7): P. 1255-67.
80. DAVEY, N.E., G. TRAVE, AND T.J. GIBSON, *HOW VIRUSES HIJACK CELL REGULATION.* TRENDS BIOCHEM SCI, 2011. **36**(3): P. 159-69.
81. WATANABE, T., S. WATANABE, AND Y. KAWAOKA, *CELLULAR NETWORKS INVOLVED IN THE INFLUENZA VIRUS LIFE CYCLE.* CELL HOST MICROBE, 2010. **7**(6): P. 427-39.
82. KONIG, R., ET AL., HUMAN HOST FACTORS REQUIRED FOR INFLUENZA VIRUS REPLICATION. NATURE, 2010. **463**(7282): P. 813-7.
83. KARLAS, A., ET AL., GENOME-WIDE RNAI SCREEN IDENTIFIES HUMAN HOST FACTORS CRUCIAL FOR INFLUENZA VIRUS REPLICATION. NATURE, 2010. **463**(7282): P. 818-22.
84. KRISHNAN, M.N., ET AL., RNA INTERFERENCE SCREEN FOR HUMAN GENES ASSOCIATED WITH WEST NILE VIRUS INFECTION. NATURE, 2008. **455**(7210): P. 242-5.
85. BRASS, A.L., ET AL., THE IFITM PROTEINS MEDIATE CELLULAR RESISTANCE TO INFLUENZA A H1N1 VIRUS, WEST NILE VIRUS, AND DENGUE VIRUS. CELL, 2009. **139**(7): P. 1243-54.
86. LE QUESNE J, C.C., *MICRO-RNAS AND BREAST CANCER.* MOL ONCOL, 2010. **4**(3): P. 230-41.
87. BHATTI, I., ET AL., *SMALL RNA: A LARGE CONTRIBUTOR TO CARCINOGENESIS?* J GASTROINTEST SURG, 2009. **13**(7): P. 1379-88.
88. SINGH, S.K., ET AL., *MICRORNAS--MICRO IN SIZE BUT MACRO IN FUNCTION.* FEBS J, 2008. **275**(20): P. 4929-44.
89. KOTA, S.K. AND S. BALASUBRAMANIAN, *CANCER THERAPY VIA MODULATION OF MICRO RNA LEVELS: A PROMISING FUTURE.* DRUG DISCOV TODAY, 2010. **15**(17-18): P. 733-40.
90. LAITALA-LEINONEN, T., UPDATE ON THE DEVELOPMENT OF MICRORNA AND SIRNA MOLECULES AS REGULATORS OF CELL PHYSIOLOGY. RECENT PAT DNA GENE SEQ, 2010. **4**(2): P. 113-21.
91. KABESCH, M., S. MICHEL, AND J. TOST, *EPIGENETIC MECHANISMS AND THE RELATIONSHIP TO CHILDHOOD ASTHMA.* EUR RESPIR J, 2010. **36**(4): P. 950-61.
92. SCHLAUDER, S.M., A. AHMAD, AND T.D. HORN, *DICER AND MICRO-RNAS IN CUTANEOUS DISEASE.* J CUTAN PATHOL, 2009. **36**(5): P. 607-10.
93. VISONE, R., F. PETROCCA, AND C.M. CROCE, *MICRO-RNAS IN GASTROINTESTINAL AND LIVER DISEASE.* GASTROENTEROLOGY, 2008. **135**(6): P. 1866-9.
94. HUDDER, A. AND R.F. NOVAK, MIRNAS: EFFECTORS OF ENVIRONMENTAL INFLUENCES ON GENE EXPRESSION AND DISEASE. TOXICOL SCI, 2008. **103**(2): P. 228-40.
95. BICHENKOVA, E.V., ET AL., DNA-MOUNTED SELF-ASSEMBLY: NEW APPROACHES FOR GENOMIC ANALYSIS AND SNP DETECTION. BIOCHIM BIOPHYS ACTA, 2011. **1809**(1): P. 1-23.
96. SETHI, S., MOLECULAR DIAGNOSIS OF RESPIRATORY TRACT INFECTION IN ACUTE EXACERBATIONS OF CHRONIC OBSTRUCTIVE PULMONARY DISEASE. CLIN INFECT DIS, 2011. **52 SUPPL 4**: P. S290-5.
97. STRAMER, S.L., ET AL., *NUCLEIC ACID TESTING TO DETECT HBV INFECTION IN BLOOD DONORS.* N ENGL J MED, 2011. **364**(3): P. 236-47.
98. OH, J.K., ET AL., TYPE-SPECIFIC HUMAN PAPILLOMAVIRUS DISTRIBUTION IN INVASIVE CERVICAL CANCER IN KOREA, 1958-2004. ASIAN PAC J CANCER PREV, 2010. **11**(4): P. 993-1000.

99. LI, X., ET AL., DETECTION AND SUBTYPING OF INFLUENZA A VIRUS BASED ON A SHORT OLIGONUCLEOTIDE MICROARRAY. DIAGN MICROBIOL INFECT DIS, 2009. **65**(3): P. 261-70.
100. HUANG, Y., ET AL., MULTIPLEX ASSAY FOR SIMULTANEOUSLY TYPING AND SUBTYPING INFLUENZA VIRUSES BY USE OF AN ELECTRONIC MICROARRAY. J CLIN MICROBIOL, 2009. **47**(2): P. 390-6.
101. GE, Y., ET AL., DETECTION OF NOVEL SWINE ORIGIN INFLUENZA A VIRUS (H1N1) BY REAL-TIME NUCLEIC ACID SEQUENCE-BASED AMPLIFICATION. J VIROL METHODS, 2009.
102. DONG, H., ET AL., DETECTION OF HUMAN NOVEL INFLUENZA A (H1N1) VIRUSES USING MULTI-FLUORESCENT REAL-TIME RT-PCR. VIRUS RES. **147**(1): P. 85-90.
103. JAYAGOPAL, A., ET AL., HAIRPIN DNA-FUNCTIONALIZED GOLD COLLOIDS FOR THE IMAGING OF MRNA IN LIVE CELLS. J AM CHEM SOC, 2010. **132**(28): P. 9789-96.
104. BAO, G., W.J. RHEE, AND A. TSOURKAS, *FLUORESCENT PROBES FOR LIVE-CELL RNA DETECTION.* ANNU REV BIOMED ENG, 2009. **11**: P. 25-47.
105. RHEE, W.J. AND G. BAO, SIMULTANEOUS DETECTION OF MRNA AND PROTEIN STEM CELL MARKERS IN LIVE CELLS. BMC BIOTECHNOL, 2009. **9**: P. 30.
106. RAJ, A., ET AL., IMAGING INDIVIDUAL MRNA MOLECULES USING MULTIPLE SINGLY LABELED PROBES. NAT METHODS, 2008. **5**(10): P. 877-9.
107. MANOLAKOS, E., ET AL., CHARACTERIZATION OF 23 SMALL SUPERNUMERARY MARKER CHROMOSOMES DETECTED AT PRE-NATAL DIAGNOSIS: THE VALUE OF FLUORESCENCE IN SITU HYBRIDIZATION. MOL MED REPORT, 2010. **3**(6): P. 1015-22.
108. SANTANGELO, P.J., *MOLECULAR BEACONS AND RELATED PROBES FOR INTRACELLULAR RNA IMAGING.* WILEY INTERDISCIP REV NANOMED NANOBIOTECHNOL. **2**(1): P. 11-9.
109. KIHARA, T., ET AL., DEVELOPMENT OF A NOVEL METHOD TO DETECT INTRINSIC MRNA IN A LIVING CELL BY USING A MOLECULAR BEACON-IMMOBILIZED NANONEEDLE. BIOSENS BIOELECTRON, 2010. **26**(4): P. 1449-54.
110. TSIEN, R.Y., CONSTRUCTING AND EXPLOITING THE FLUORESCENT PROTEIN PAINTBOX (NOBEL LECTURE). ANGEW CHEM INT ED ENGL, 2009. **48**(31): P. 5612-26.
111. SNAPP, E.L., *FLUORESCENT PROTEINS: A CELL BIOLOGIST'S USER GUIDE.* TRENDS CELL BIOL, 2009. **19**(11): P. 649-55.
112. BIN WU, K.D.P., TIMOTHE´E LIONNET, ROBERT H SINGER AND AND V.V. VERKHUSHA, *MODERN FLUORESCENT PROTEINS AND IMAGING TECHNOLOGIES TO STUDY GENE EXPRESSION,NUCLEAR LOCALIZATION,AND DYNAMICS.* CURRENT OPINION IN CELL BIOLOGY, 2011. **23**: P. 1-8.
113. RAJ, A. AND A. VAN OUDENAARDEN, *SINGLE-MOLECULE APPROACHES TO STOCHASTIC GENE EXPRESSION.* ANNU REV BIOPHYS, 2009. **38**: P. 255-70.
114. BERTRAND, E., ET AL., *LOCALIZATION OF ASH1 MRNA PARTICLES IN LIVING YEAST.* MOL CELL, 1998. **2**(4): P. 437-45.
115. BEACH, D.L., E.D. SALMON, AND K. BLOOM, *LOCALIZATION AND ANCHORING OF MRNA IN BUDDING YEAST.* CURR BIOL, 1999. **9**(11): P. 569-78.
116. WEIL, T.T., R.M. PARTON, AND I. DAVIS, *MAKING THE MESSAGE CLEAR: VISUALIZING MRNA LOCALIZATION.* TRENDS CELL BIOL, 2010. **20**(7): P. 380-90.
117. GOLDING, I., ET AL., REAL-TIME KINETICS OF GENE ACTIVITY IN INDIVIDUAL BACTERIA. CELL, 2005. **123**(6): P. 1025-36.
118. KEPLER, T.B. AND T.C. ELSTON, STOCHASTICITY IN TRANSCRIPTIONAL REGULATION: ORIGINS, CONSEQUENCES, AND MATHEMATICAL REPRESENTATIONS. BIOPHYS J, 2001. **81**(6): P. 3116-36.
119. RAJ, A., ET AL., *STOCHASTIC MRNA SYNTHESIS IN MAMMALIAN CELLS.* PLOS BIOL, 2006. **4**(10): P. E309.
120. LENNON, F.E., ET AL., USE OF MOLECULAR BEACONS TO IMAGE EFFECTS OF TITANIUM SURFACE MICROSTRUCTURE ON BETA1 INTEGRIN EXPRESSION IN LIVE OSTEOBLAST-LIKE CELLS. BIOMATERIALS, 2010. **31**(30): P. 7640-7.

121. WANG, W., ET AL., IMAGING AND CHARACTERIZING INFLUENZA A VIRUS MRNA TRANSPORT IN LIVING CELLS. NUCLEIC ACIDS RES, 2008. **36**(15): P. 4913-28.
122. ALAN, L., ET AL., *FLUORESCENT IN SITU HYBRIDIZATION OF MITOCHONDRIAL DNA AND RNA.* ACTA BIOCHIM POL, 2010. **57**(4): P. 403-8.
123. BRATU, D.P., ET AL., *VISUALIZING THE DISTRIBUTION AND TRANSPORT OF MRNAS IN LIVING CELLS.* PROC NATL ACAD SCI U S A, 2003. **100**(23): P. 13308-13.
124. CHEN, A.K., M.A. BEHLKE, AND A. TSOURKAS, AVOIDING FALSE-POSITIVE SIGNALS WITH NUCLEASE-VULNERABLE MOLECULAR BEACONS IN SINGLE LIVING CELLS. NUCLEIC ACIDS RES, 2007. **35**(16): P. E105.
125. TYAGI, S. AND F.R. KRAMER, *MOLECULAR BEACONS: PROBES THAT FLUORESCE UPON HYBRIDIZATION.* NAT BIOTECHNOL, 1996. **14**(3): P. 303-8.
126. BONNET, G., ET AL., *THERMODYNAMIC BASIS OF THE ENHANCED SPECIFICITY OF STRUCTURED DNA PROBES.* PROC NATL ACAD SCI U S A, 1999. **96**(11): P. 6171-6.
127. LI, Y., X. ZHOU, AND D. YE, *MOLECULAR BEACONS: AN OPTIMAL MULTIFUNCTIONAL BIOLOGICAL PROBE.* BIOCHEM BIOPHYS RES COMMUN, 2008. **373**(4): P. 457-61.
128. SANDHYA, S., W. CHEN, AND A. MULCHANDANI, MOLECULAR BEACONS: A REAL-TIME POLYMERASE CHAIN REACTION ASSAY FOR DETECTING ESCHERICHIA COLI FROM FRESH PRODUCE AND WATER. ANAL CHIM ACTA, 2008. **614**(2): P. 208-12.
129. VET, J.A. AND S.A. MARRAS, DESIGN AND OPTIMIZATION OF MOLECULAR BEACON REAL-TIME POLYMERASE CHAIN REACTION ASSAYS. METHODS MOL BIOL, 2005. **288**: P. 273-90.
130. YE, Q., ET AL., REAL-TIME FLUORESCENT QUANTITATIVE IMMUNO-PCR METHOD FOR DETERMINATION OF FLUORANTHENE IN WATER SAMPLES WITH A MOLECULAR BEACON. J ENVIRON SCI (CHINA), 2010. **22**(5): P. 796-800.
131. OH, Y.H., ET AL., RAPID DETECTION OF THE EPIDERMAL GROWTH FACTOR RECEPTOR MUTATION IN NON-SMALL-CELL LUNG CANCER FOR ANALYSIS OF ACQUIRED RESISTANCE USING MOLECULAR BEACONS. J MOL DIAGN, 2010. **12**(5): P. 644-52.
132. MENG, X.C., ET AL., RAPID AND DIRECT QUANTITATIVE DETECTION OF VIABLE BIFIDOBACTERIA IN PROBIOTIC YOGURT BY COMBINATION OF ETHIDIUM MONOAZIDE AND REAL-TIME PCR USING A MOLECULAR BEACON APPROACH. J DAIRY RES, 2010. **77**(4): P. 498-504.
133. SHI, M.M., ENABLING LARGE-SCALE PHARMACOGENETIC STUDIES BY HIGH-THROUGHPUT MUTATION DETECTION AND GENOTYPING TECHNOLOGIES. CLIN CHEM, 2001. **47**(2): P. 164-72.
134. WABUYELE, M.B., ET AL., APPROACHING REAL-TIME MOLECULAR DIAGNOSTICS: SINGLE-PAIR FLUORESCENCE RESONANCE ENERGY TRANSFER (SPFRET) DETECTION FOR THE ANALYSIS OF LOW ABUNDANT POINT MUTATIONS IN K-RAS ONCOGENES. J AM CHEM SOC, 2003. **125**(23): P. 6937-45.
135. LI, Y.Q., ET AL., SIMULTANEOUS DETECTION OF DUAL SINGLE-BASE MUTATIONS BY CAPILLARY ELECTROPHORESIS USING QUANTUM DOT-MOLECULAR BEACON PROBE. BIOSENS BIOELECTRON, 2011. **26**(5): P. 2317-22.
136. LIU, X.P., J.L. HOU, AND J.H. LIU, A NOVEL SINGLE NUCLEOTIDE POLYMORPHISM DETECTION OF A DOUBLE-STRANDED DNA TARGET BY A RIBONUCLEOTIDE-CARRYING MOLECULAR BEACON AND THERMOSTABLE RNASE HII. ANAL BIOCHEM, 2010. **398**(1): P. 83-92.
137. TAN W, F.X., LI J, LIU X, MOLECULAR BEACONS: A NOVEL DNA PROBE FOR NUCLEIC ACID AND PROTEIN STUDIES. CHEMISTRY, 2000. **6**(7): P. 1107-11.
138. RICHES, L.C., A.M. LYNCH, AND N.J. GOODERHAM, A MOLECULAR BEACON APPROACH TO DETECTING RAD52 EXPRESSION IN RESPONSE TO DNA DAMAGE IN HUMAN CELLS. TOXICOL IN VITRO, 2010. **24**(2): P. 652-60.
139. MOLENAAR, C., ET AL., LINEAR 2' O-METHYL RNA PROBES FOR THE VISUALIZATION OF RNA IN LIVING CELLS. NUCLEIC ACIDS RES, 2001. **29**(17): P. E89-9.

140. Dirks, R.W., C. Molenaar, and H.J. Tanke, *Methods for visualizing RNA processing and transport pathways in living cells.* Histochem Cell Biol, 2001. **115**(1): p. 3-11.
141. Wu, Y., et al., Nucleic acid beacons for long-term real-time intracellular monitoring. Anal Chem, 2008. **80**(8): p. 3025-8.
142. Kubota, T., et al., Hybridization-sensitive fluorescent probe for long-term monitoring of intracellular RNA. Bioconjug Chem, 2009. **20**(6): p. 1256-61.
143. Cui, Z.Q., et al., Visualizing the dynamic behavior of poliovirus plus-strand RNA in living host cells. Nucleic Acids Res, 2005. **33**(10): p. 3245-52.
144. Meyvis, T.K., et al., Fluorescence recovery after photobleaching: a versatile tool for mobility and interaction measurements in pharmaceutical research. Pharm Res, 1999. **16**(8): p. 1153-62.
145. Bottiroli, G., A.C. Croce, and R. Ramponi, Fluorescence resonance energy transfer imaging as a tool for in situ evaluation of cell morphofunctional characteristics. J Photochem Photobiol B, 1992. **12**(4): p. 413-6.
146. Förster, T., Zwischenmolekulare Energiewanderung und Fluoreszenz. Annalen der Physik. Annalen der Physik, 1948. **437**(1-2): p. 55–75.
147. Vet, J.A., et al., Multiplex detection of four pathogenic retroviruses using molecular beacons. Proc Natl Acad Sci U S A, 1999. **96**(11): p. 6394-9.
148. Marras, S.A., F.R. Kramer, and S. Tyagi, *Multiplex detection of single-nucleotide variations using molecular beacons.* Genet Anal, 1999. **14**(5-6): p. 151-6.
149. Nielsen, P.E., et al., Sequence-selective recognition of DNA by strand displacement with a thymine-substituted polyamide. Science, 1991. **254**(5037): p. 1497-500.
150. Egholm, M., et al., PNA hybridizes to complementary oligonucleotides obeying the Watson-Crick hydrogen-bonding rules. Nature, 1993. **365**(6446): p. 566-8.
151. Agrawal, S., *Antisense oligonucleotides: towards clinical trials.* Trends Biotechnol, 1996. **14**(10): p. 376-87.
152. Good, L. and P.E. Nielsen, *Progress in developing PNA as a gene-targeted drug.* Antisense Nucleic Acid Drug Dev, 1997. **7**(4): p. 431-7.
153. Demidov, V.V., et al., Stability of peptide nucleic acids in human serum and cellular extracts. Biochem Pharmacol, 1994. **48**(6): p. 1310-3.
154. Knudsen, H. and P.E. Nielsen, *Antisense properties of duplex- and triplex-forming PNAs.* Nucleic Acids Res, 1996. **24**(3): p. 494-500.
155. Good, L. and P.E. Nielsen, Antisense inhibition of gene expression in bacteria by PNA targeted to mRNA. Nat Biotechnol, 1998. **16**(4): p. 355-8.
156. Good, L. and P.E. Nielsen, Inhibition of translation and bacterial growth by peptide nucleic acid targeted to ribosomal RNA. Proc Natl Acad Sci U S A, 1998. **95**(5): p. 2073-6.
157. Marwick, C., First "antisense" drug will treat CMV retinitis. JAMA, 1998. **280**(10): p. 871.
158. Bonham, M.A., et al., An assessment of the antisense properties of RNase H-competent and steric-blocking oligomers. Nucleic Acids Res, 1995. **23**(7): p. 1197-203.
159. Nielsen, P.E., M. Egholm, and O. Buchardt, *Peptide nucleic acid (PNA). A DNA mimic with a peptide backbone.* Bioconjug Chem, 1994. **5**(1): p. 3-7.
160. Doyle, D.F., et al., Inhibition of gene expression inside cells by peptide nucleic acids: effect of mRNA target sequence, mismatched bases, and PNA length. Biochemistry, 2001. **40**(1): p. 53-64.

161. Tian, X., et al., Receptor-mediated internalization of chelator-PNA-peptide hybridization probes for radioimaging or magnetic resonance imaging of oncogene mRNAs in tumours. Biochem Soc Trans, 2007. **35**(Pt 1): p. 72-6.
162. Tian, X., et al., *Tumor-targeting peptide-PNA-peptide chimeras for imaging overexpressed oncogene mRNAs.* Nucleosides Nucleotides Nucleic Acids, 2005. **24**(5-7): p. 1085-91.
163. Rao, P.S., et al., 99mTc-peptide-peptide nucleic acid probes for imaging oncogene mRNAs in tumours. Nucl Med Commun, 2003. **24**(8): p. 857-63.
164. Tian, X., et al., Noninvasive molecular imaging of MYC mRNA expression in human breast cancer xenografts with a [99mTc]peptide-peptide nucleic acid-peptide chimera. Bioconjug Chem, 2005. **16**(1): p. 70-9.
165. Chakrabarti, A., et al., Radiohybridization PET imaging of KRAS G12D mRNA expression in human pancreas cancer xenografts with [(64)Cu]DO3A-peptide nucleic acid-peptide nanoparticles. Cancer Biol Ther, 2007. **6**(6): p. 948-56.
166. Su, W., et al., Synthesis and cellular uptake of a MR contrast agent coupled to an antisense peptide nucleic acid--cell- penetrating peptide conjugate. Contrast Media Mol Imaging, 2007. **2**(1): p. 42-9.
167. Joshi, R., et al., MR contrast agent composed of cholesterol and peptide nucleic acids: design, synthesis and cellular uptake. Bioorg Med Chem Lett, 2010. **20**(7): p. 2238-41.
168. Heckl, S., et al., Intracellular visualization of prostate cancer using magnetic resonance imaging. Cancer Res, 2003. **63**(16): p. 4766-72.
169. Paroo, Z. and D.R. Corey, Imaging gene expression using oligonucleotides and peptide nucleic acids. J Cell Biochem, 2003. **90**(3): p. 437-42.
170. Seitz, O., F. Bergmann, and D. Heindl, A Convergent Strategy for the Modification of Peptide Nucleic Acids: Novel Mismatch-Specific PNA-Hybridization Probes. Angew Chem Int Ed Engl, 1999. **38**(15): p. 2203-2206.
171. Lee, L.G., C.H. Chen, and L.A. Chiu, *Thiazole orange: a new dye for reticulocyte analysis.* Cytometry, 1986. **7**(6): p. 508-17.
172. Nygren, J., N. Svanvik, and M. Kubista, *The interactions between the fluorescent dye thiazole orange and DNA.* Biopolymers, 1998. **46**(1): p. 39-51.
173. Rye, H.S., et al., Stable fluorescent complexes of double-stranded DNA with bis-intercalating asymmetric cyanine dyes: properties and applications. Nucleic Acids Res, 1992. **20**(11): p. 2803-12.
174. Privat, E., et al., Oligonucleotide-conjugated thiazole orange probes as "light-up" probes for messenger ribonucleic acid molecules in living cells. Photochem Photobiol, 2001. **74**(4): p. 532-41.
175. Berndl, S., et al., Imaging of RNA delivery to cells by thiazole orange as a fluorescent RNA base substitution. Org Biomol Chem, 2010. **8**(5): p. 997-9.
176. Kohler, O., D.V. Jarikote, and O. Seitz, Forced intercalation probes (FIT Probes): thiazole orange as a fluorescent base in peptide nucleic acids for homogeneous single-nucleotide-polymorphism detection. Chembiochem, 2005. **6**(1): p. 69-77.
177. Kohler, O. and O. Seitz, *Thiazole orange as fluorescent universal base in peptide nucleic acids.* Chem Commun (Camb), 2003(23): p. 2938-9.
178. Jarikote, D.V., Eur. J. Org. Chem. , 2005: p. 3187-3195.
179. Bethge, L., D.V. Jarikote, and O. Seitz, New cyanine dyes as base surrogates in PNA: forced intercalation probes (FIT-probes) for homogeneous SNP detection. Bioorg Med Chem, 2008. **16**(1): p. 114-25.
180. Jarikote, D.V., et al., Exploring base-pair-specific optical properties of the DNA stain thiazole orange. Chemistry, 2007. **13**(1): p. 300-10.

181. KARUNAKARAN, V., ET AL., LARGE DYNAMIC STOKES SHIFT OF DNA INTERCALATION DYE THIAZOLE ORANGE HAS CONTRIBUTION FROM A HIGH-FREQUENCY MODE. J AM CHEM SOC, 2006. **128**(9): P. 2954-62.
182. SOCHER, E., ET AL., FIT PROBES: PEPTIDE NUCLEIC ACID PROBES WITH A FLUORESCENT BASE SURROGATE ENABLE REAL-TIME DNA QUANTIFICATION AND SINGLE NUCLEOTIDE POLYMORPHISM DISCOVERY. ANAL BIOCHEM, 2008. **375**(2): P. 318-30.
183. KUMMER S, K.A., SOCHER E, BETHGE L, HERRMANN A, SEITZ O, *FLUORESCENCE IMAGING OF INFLUENZA H1N1 MRNA IN LIVING INFECTED CELLS USING SINGLE-CHROMOPHORE FIT-PNA.* ANGEW CHEM INT ED ENGL, 2011. **50**(8): P. 1931-4.
184. O'FARRELL, P.H., *HIGH RESOLUTION TWO-DIMENSIONAL ELECTROPHORESIS OF PROTEINS.* J BIOL CHEM, 1975. **250**(10): P. 4007-21.
185. PATTON, W.F. AND J.M. BEECHEM, RAINBOW'S END: THE QUEST FOR MULTIPLEXED FLUORESCENCE QUANTITATIVE ANALYSIS IN PROTEOMICS. CURR OPIN CHEM BIOL, 2002. **6**(1): P. 63-9.
186. ONG, S.E., ET AL., STABLE ISOTOPE LABELING BY AMINO ACIDS IN CELL CULTURE, SILAC, AS A SIMPLE AND ACCURATE APPROACH TO EXPRESSION PROTEOMICS. MOL CELL PROTEOMICS, 2002. **1**(5): P. 376-86.
187. ABBOTT, A., A POST-GENOMIC CHALLENGE: LEARNING TO READ PATTERNS OF PROTEIN SYNTHESIS. NATURE, 1999. **402**(6763): P. 715-20.
188. SCHNOLZER, M., P. JEDRZEJEWSKI, AND W.D. LEHMANN, PROTEASE-CATALYZED INCORPORATION OF 18O INTO PEPTIDE FRAGMENTS AND ITS APPLICATION FOR PROTEIN SEQUENCING BY ELECTROSPRAY AND MATRIX-ASSISTED LASER DESORPTION/IONIZATION MASS SPECTROMETRY. ELECTROPHORESIS, 1996. **17**(5): P. 945-53.
189. LAHM, H.W. AND H. LANGEN, MASS SPECTROMETRY: A TOOL FOR THE IDENTIFICATION OF PROTEINS SEPARATED BY GELS. ELECTROPHORESIS, 2000. **21**(11): P. 2105-14.
190. ODA, Y., ET AL., ACCURATE QUANTITATION OF PROTEIN EXPRESSION AND SITE-SPECIFIC PHOSPHORYLATION. PROC NATL ACAD SCI U S A, 1999. **96**(12): P. 6591-6.
191. GYGI, S.P., ET AL., QUANTITATIVE ANALYSIS OF COMPLEX PROTEIN MIXTURES USING ISOTOPE-CODED AFFINITY TAGS. NAT BIOTECHNOL, 1999. **17**(10): P. 994-9.
192. MANN, S.-E.O.M., A PRACTICAL RECIPE FOR STABLE ISOTOPE LABELING BY AMINO ACIDS IN CELL CULTURE (SILAC). NATURE PROTOCOLS, 2006. **1**(6).
193. AMANCHY, R., D.E. KALUME, AND A. PANDEY, STABLE ISOTOPE LABELING WITH AMINO ACIDS IN CELL CULTURE (SILAC) FOR STUDYING DYNAMICS OF PROTEIN ABUNDANCE AND POSTTRANSLATIONAL MODIFICATIONS. SCI STKE, 2005. **2005**(267): P. PL2.
194. PAN C, K.C., BOHL S, KLINGMUELLER U, MANN M., COMPARATIVE PROTEOMIC PHENOTYPING OF CELL LINES AND PRIMARY CELLS TO ASSESS PRESERVATION OF CELL TYPE-SPECIFIC FUNCTIONS. MOL CELL PROTEOMICS, 2009. **8**(3): P. 443-50.
195. CUOMO, A., ET AL., SILAC-BASED PROTEOMIC ANALYSIS TO DISSECT THE "HISTONE MODIFICATION SIGNATURE" OF HUMAN BREAST CANCER CELLS. AMINO ACIDS, 2010.
196. HARSHA, H.C., H. MOLINA, AND A. PANDEY, QUANTITATIVE PROTEOMICS USING STABLE ISOTOPE LABELING WITH AMINO ACIDS IN CELL CULTURE. NAT PROTOC, 2008. **3**(3): P. 505-16.
197. SOUFI, B., ET AL., STABLE ISOTOPE LABELING BY AMINO ACIDS IN CELL CULTURE (SILAC) APPLIED TO QUANTITATIVE PROTEOMICS OF BACILLUS SUBTILIS. J PROTEOME RES, 2010. **9**(7): P. 3638-46.
198. SURY, M.D., J.X. CHEN, AND M. SELBACH, *THE SILAC FLY ALLOWS FOR ACCURATE PROTEIN QUANTIFICATION IN VIVO.* MOL CELL PROTEOMICS, 2010. **9**(10): P. 2173-83.
199. WALTHER, D.M. AND M. MANN, ACCURATE QUANTIFICATION OF MORE THAN 4000 MOUSE TISSUE PROTEINS REVEALS MINIMAL PROTEOME CHANGES DURING AGING. MOL CELL PROTEOMICS, 2011. **10**(2): P. M110 004523.

200. EMMOTT, E., ET AL., QUANTITATIVE PROTEOMICS USING STABLE ISOTOPE LABELING WITH AMINO ACIDS IN CELL CULTURE REVEALS CHANGES IN THE CYTOPLASMIC, NUCLEAR, AND NUCLEOLAR PROTEOMES IN VERO CELLS INFECTED WITH THE CORONAVIRUS INFECTIOUS BRONCHITIS VIRUS. MOL CELL PROTEOMICS, 2010. **9**(9): P. 1920-36.
201. EMMOTT, E., ET AL., ELUCIDATION OF THE AVIAN NUCLEOLAR PROTEOME BY QUANTITATIVE PROTEOMICS USING SILAC AND CHANGES IN CELLS INFECTED WITH THE CORONAVIRUS INFECTIOUS BRONCHITIS VIRUS. PROTEOMICS, 2010. **10**(19): P. 3558-62.
202. MUNDAY, D.C., J.A. HISCOX, AND J.N. BARR, QUANTITATIVE PROTEOMIC ANALYSIS OF A549 CELLS INFECTED WITH HUMAN RESPIRATORY SYNCYTIAL VIRUS SUBGROUP B USING SILAC COUPLED TO LC-MS/MS. PROTEOMICS, 2010. **10**(23): P. 4320-34.
203. KORTE, T., ET AL., TRANSIENT CHANGES OF THE CONFORMATION OF HEMAGGLUTININ OF INFLUENZA VIRUS AT LOW PH DETECTED BY TIME-RESOLVED CIRCULAR DICHROISM SPECTROSCOPY. J BIOL CHEM, 1997. **272**(15): P. 9764-70.
204. ZUKER, M., J.A. JAEGER, AND D.H. TURNER, A COMPARISON OF OPTIMAL AND SUBOPTIMAL RNA SECONDARY STRUCTURES PREDICTED BY FREE ENERGY MINIMIZATION WITH STRUCTURES DETERMINED BY PHYLOGENETIC COMPARISON. NUCLEIC ACIDS RES, 1991. **19**(10): P. 2707-14.
205. WASHBURN, M.P., *DRIVING BIOCHEMICAL DISCOVERY WITH QUANTITATIVE PROTEOMICS.* TRENDS BIOCHEM SCI, 2011. **36**(3): P. 170-7.
206. FALCON S, G.R., USING GOSTATS TO TEST GENE LISTS FOR GO TERM ASSOCIATION. BIOINFORMATICS, 2007. **23**(2).
207. FUTSCHIK ME, C.B., *NOISE-ROBUST SOFT CLUSTERING OF GENE EXPRESSION TIME-COURSE DATA.* J BIOINFORM COMPUT BIOL, 2005. **3**(4): P. 965-88.
208. GENTLEMAN RC, C.V., BATES DM, BOLSTAD B, DETTLING M, DUDOIT S, ELLIS B, GAUTIER L, GE Y, GENTRY J, HORNIK K, HOTHORN T, HUBER W, IACUS S, IRIZARRY R, LEISCH F, LI C, MAECHLER M, ROSSINI AJ, SAWITZKI G, SMITH C, SMYTH G, TIERNEY L, YANG JY, ZHANG J, *BIOCONDUCTOR: OPEN SOFTWARE DEVELOPMENT FOR COMPUTATIONAL BIOLOGY AND BIOINFORMATICS.* GENOME BIOL, 2004. **5**(10): P. R80.
209. STRAY, S.J. AND G.M. AIR, APOPTOSIS BY INFLUENZA VIRUSES CORRELATES WITH EFFICIENCY OF VIRAL MRNA SYNTHESIS. VIRUS RES, 2001. **77**(1): P. 3-17.
210. ROTT, R., ET AL., STUDIES ON THE ADAPTATION OF INFLUENZA VIRUSES TO MDCK CELLS. EMBO J, 1984. **3**(13): P. 3329-32.
211. MARTIN, K.C. AND A. EPHRUSSI, *MRNA LOCALIZATION: GENE EXPRESSION IN THE SPATIAL DIMENSION.* CELL, 2009. **136**(4): P. 719-30.
212. SILVESTER, N.C., ET AL., EFFECT OF TERMINAL AMINO ACIDS ON THE STABILITY AND SPECIFICITY OF PNA-DNA HYBRIDISATION. ORG BIOMOL CHEM, 2007. **5**(6): P. 917-23.
213. ATKINS, G.J., B.J. SHEAHAN, AND N.J. DIMMOCK, SEMLIKI FOREST VIRUS INFECTION OF MICE: A MODEL FOR GENETIC AND MOLECULAR ANALYSIS OF VIRAL PATHOGENICITY. J GEN VIROL, 1985. **66 (PT 3)**: P. 395-408.
214. ROMAN, L.M. AND H. GAROFF, ALTERATION OF THE CYTOPLASMIC DOMAIN OF THE MEMBRANE-SPANNING GLYCOPROTEIN P62 OF SEMLIKI FOREST VIRUS DOES NOT AFFECT ITS POLAR DISTRIBUTION IN ESTABLISHED LINES OF MADIN-DARBY CANINE KIDNEY CELLS. J CELL BIOL, 1986. **103**(6 PT 2): P. 2607-18.
215. BLONDEL, D., G.G. HARMISON, AND M. SCHUBERT, *ROLE OF MATRIX PROTEIN IN CYTOPATHOGENESIS OF VESICULAR STOMATITIS VIRUS.* J VIROL, 1990. **64**(4): P. 1716-25.
216. ETCHISON, J.R., J.S. ROBERTSON, AND D.F. SUMMERS, *HOST CELL-DEPENDENT DIFFERENCES IN THE OLIGOSACCHARIDE MOIETIES OF THE VSV G PROTEIN.* J GEN VIROL, 1981. **57**(PT 1): P. 43-52.
217. RASMUSSEN, T.B., ET AL., QUANTITATIVE MULTIPLEX ASSAY FOR SIMULTANEOUS DETECTION AND IDENTIFICATION OF INDIANA AND NEW JERSEY SEROTYPES OF VESICULAR STOMATITIS VIRUS. J CLIN MICROBIOL, 2005. **43**(1): P. 356-62.

218. Rodriguez, L.L., Emergence and re-emergence of vesicular stomatitis in the United States. Virus Res, 2002. **85**(2): p. 211-9.
219. Takacs, A.M. and A.K. Banerjee, Inhibition of vesicular stomatitis virus in cells constitutively expressing an antisense RNA targeted against the virus RNA polymerase gene. J Gen Virol, 1997. **78 (Pt 1)**: p. 125-9.
220. Hwang, L.N., N. Englund, and A.K. Pattnaik, Polyadenylation of vesicular stomatitis virus mRNA dictates efficient transcription termination at the intercistronic gene junctions. J Virol, 1998. **72**(3): p. 1805-13.
221. Lemaitre, M., B. Bayard, and B. Lebleu, Specific antiviral activity of a poly(L-lysine)-conjugated oligodeoxyribonucleotide sequence complementary to vesicular stomatitis virus N protein mRNA initiation site. Proc Natl Acad Sci U S A, 1987. **84**(3): p. 648-52.
222. Li, T. and A.K. Pattnaik, Replication signals in the genome of vesicular stomatitis virus and its defective interfering particles: identification of a sequence element that enhances DI RNA replication. Virology, 1997. **232**(2): p. 248-59.
223. Garcia-Robles, I., et al., *Interaction of influenza virus proteins with nucleosomes.* Virology, 2005. **332**(1): p. 329-36.
224. Takizawa, N., et al., Association of functional influenza viral proteins and RNAs with nuclear chromatin and sub-chromatin structure. Microbes Infect, 2006. **8**(3): p. 823-33.
225. Hahn, Y., et al., Duplication of genes encoding non-clathrin coat protein gamma-COP in vertebrate, insect and plant evolution. FEBS Lett, 2000. **482**(1-2): p. 31-6.
226. Coughlin, P.B., T. Tetaz, and H.H. Salem, *Identification and purification of a novel serine proteinase inhibitor.* J Biol Chem, 1993. **268**(13): p. 9541-7.
227. Chen, K.C., et al., Mapping of the gene encoding the multifunctional protein carrying out the first three steps of pyrimidine biosynthesis to human chromosome 2. Hum Genet, 1989. **82**(1): p. 40-4.
228. Wang, X., et al., Phosphorylation of splicing factor SF1 on Ser20 by cGMP-dependent protein kinase regulates spliceosome assembly. EMBO J, 1999. **18**(16): p. 4549-59.
229. Vasudevan, S., N.G. Starostina, and E.T. Kipreos, The Caenorhabditis elegans cell-cycle regulator ZYG-11 defines a conserved family of CUL-2 complex components. EMBO Rep, 2007. **8**(3): p. 279-86.
230. Fang, H., Y. Shen, and J.S. Taylor, Native mRNA antisense-accessible sites library for the selection of antisense oligonucleotides, PNAs, and siRNAs. RNA, 2010. **16**(7): p. 1429-35.
231. Saiki, R.K., et al., Enzymatic amplification of beta-globin genomic sequences and restriction site analysis for diagnosis of sickle cell anemia. Science, 1985. **230**(4732): p. 1350-4.
232. Higuchi, R., et al., *Simultaneous amplification and detection of specific DNA sequences.* Biotechnology (N Y), 1992. **10**(4): p. 413-7.
233. Bustin, S.A., Real-time, fluorescence-based quantitative PCR: a snapshot of current procedures and preferences. Expert Rev Mol Diagn, 2005. **5**(4): p. 493-8.
234. Buh Gasparic, M., et al., Comparison of different real-time PCR chemistries and their suitability for detection and quantification of genetically modified organisms. BMC Biotechnol, 2008. **8**: p. 26.
235. Costa, J.M., et al., *Chimeric LNA/DNA probes as a detection system for real-time PCR.* Clin Biochem, 2004. **37**(10): p. 930-2.
236. Lamb, R.A.K., R. M. , *Orthomyxoviridae: The viruses and their replication.* Fields In Virology, 1996. **3**: p. 1353-1445

237. SVANVIK, N., ET AL., *FREE-PROBE FLUORESCENCE OF LIGHT-UP PROBES.* J AM CHEM SOC, 2001. **123**(5): P. 803-9.
238. MORRIS, S.J., ET AL., *ROLE OF NEURAMINIDASE IN INFLUENZA VIRUS-INDUCED APOPTOSIS.* J GEN VIROL, 1999. **80 (PT 1)**: P. 137-46.
239. LIU, B.R., ET AL., CELL-PENETRATING PEPTIDE-FUNCTIONALIZED QUANTUM DOTS FOR INTRACELLULAR DELIVERY. J NANOSCI NANOTECHNOL, 2010. **10**(12): P. 7897-905.
240. SHIM, M.S. AND Y.J. KWON, *EFFICIENT AND TARGETED DELIVERY OF SIRNA IN VIVO.* FEBS J, 2010. **277**(23): P. 4814-27.
241. FUTAKI, S., ET AL., ARGININE-RICH PEPTIDES. AN ABUNDANT SOURCE OF MEMBRANE-PERMEABLE PEPTIDES HAVING POTENTIAL AS CARRIERS FOR INTRACELLULAR PROTEIN DELIVERY. J BIOL CHEM, 2001. **276**(8): P. 5836-40.
242. HU, J.W., ET AL., PROTEIN TRANSPORT IN HUMAN CELLS MEDIATED BY COVALENTLY AND NONCOVALENTLY CONJUGATED ARGININE-RICH INTRACELLULAR DELIVERY PEPTIDES. PEPTIDES, 2009. **30**(9): P. 1669-78.
243. COOMBS, K.M., ET AL., QUANTITATIVE PROTEOMIC ANALYSES OF INFLUENZA VIRUS-INFECTED CULTURED HUMAN LUNG CELLS. J VIROL, 2010. **84**(20): P. 10888-906.
244. EMMOTT, E., ET AL., QUANTITATIVE PROTEOMICS USING SILAC COUPLED TO LC-MS/MS REVEALS CHANGES IN THE NUCLEOLAR PROTEOME IN INFLUENZA A VIRUS-INFECTED CELLS. J PROTEOME RES, 2010. **9**(10): P. 5335-45.
245. TILSNER, J. AND C. FLORS, FIT FOR PURPOSE: PNA-BASED PROBES ENABLE MRNA IMAGING IN LIVING CELLS. CHEMBIOCHEM, 2011. **12**(7): P. 1007-9.
246. SCHWANHAUSSER, B., ET AL., *GLOBAL ANALYSIS OF CELLULAR PROTEIN TRANSLATION BY PULSED SILAC.* PROTEOMICS, 2009. **9**(1): P. 205-9.

PUBLICATIONS

TALKS

"Imaging of viral mRNA using sequence specific fluorescent *Peptide Nucleic Acids* (PNAs)", *EMBO practical course (FRET, FLIM, FCS, FRAP, and 3D Imaging: Application to Cell and Developmental Biology),* Singapore (Singapore), 13th – 24th April 2009

"Detection of Influenza H1N1 mRNA in single living infected MDCK cells usingfluorescent *FIT-PNA*s as single labelled hybridisation probes", *4th European Congress of Virology,* Como (Italy), 7th – 11th April 2010

"Detection of Influenza H1N1 mRNA in single living infected MDCK cells usingfluorescent *FIT-PNA*s as single labelled hybridisation probes", *Max-Planck-Institute,* Magdeburg (Germany), 3rd May 2010

"Fluorescence Imaging of Influenza virus H1N1 mRNA in living infected cells using single-chromophore FIT-PNA", *55th Annual Meeting of the Biophysical Society,* Baltimore (U.S.A.), 5th – 9th March 2011

POSTERS

Kummer S., Knoll A., Seitz O., Herrmann A. "Imaging of viral mRNA using sequence-specific Peptide Nucleic Acids", *6th International Virus Assembly Symposium,* Crete (Greece), 3rd – 7th May 2009

Thaa B. and Kummer S. "Application of Confocal Laser Scanning Microscopy", *Young Scientist Workshop SFB 740,* Berlin (Germany), 4th September 2009

Kummer S., Knoll A., Seitz O., Herrmann A. "Detection of influenza H1N1 mRNA in living infected MDCK cells using FIT-PNAs as single labelled hybridisation probes", *International Symposium "Membranes and Modules"* , Berlin (Germany), 10th – 13th Dec 2009

"Detection of Influenza H1N1 mRNA in single living infected MDCK cells usingfluorescent *FIT-PNA*s as single labelled hybridisation probes", *4th European Congress of Virology,* Como (Italy), 7th – 11th April 2010

MANUSCRIPTS

Kummer S., Knoll A., Socher E., Bethge L., Hermann A., Seitz O. (2011). Fluorescence imaging of influenza H1N1 mRNA in living infected cells using single-chromophore FIT-PNA. Angew Chem Int Ed Engl. 50**,** 1931-4

Kummer S., Knoll A., Socher E., Bethge L., Hermann A., Seitz O. (2011). Fluoreszenzbildgebung der mRNA von Influenza-H1N1 in lebenden infizierten Zellen durch FIT-PNA mit einem einzigen Chromophor. Angew Chem. 123, 1972-1975

ACKNOWLEDGEMENT

First I would like to express my greatest thanks to my supervisor Prof. Dr. Andreas Herrmann. I appreciate his insistent fascination for science encouraging own concepts, creating a warm lab atmosphere and motivating during difficult times.

I am very grateful to PD Dr. Michael Veit who kindly provided the SFV and VSV stocks. I appreciate his untiringly kindness and patience while sharing his vast knowledge with me. I am much obligated to Prof. Dr. Edda Klipp for her interest in my work resulting in a precious collaboration. I am very thankful to Prof. Dr. Oliver Seitz for his continuous encouragement concerning the FIT-PNA project. I am much obligated to my collaborators Dr. Andrea Knoll who performed the FIT-PNA synthesis and RT-qPCR as well as Max Flöttmann and Björn Schwanhäußer who took me on a journey of fuzzy-c means and GO term analysis.

I am thankful to Dr. Thomas Korte for introducing me into the field of fluorescence microscopy and Dr. Martin Stöckl who helped me getting prepared for data analysis. I also would like to thank Gudrun Habermann and Sabine Schiller for keeping the lab-routine running. I am also thankful to Dr. Peter Müller for brightening up any rainy day with his wisdom.

I am greatly indebted to all my dear present and former lab members of the Molecular Biophysics group- thank you all for being friends rather than just colleagues. In particular, I would like to thank Aouefa for "frenching up" my life, Caro for her fantastic *Apfelstrudel* and Christian (C7) for kindly reviewing most parts of this work. It was a pleasure for me to meet you all!

I especially would like to thank Gabi and Roland from the bottom of my heart for their constant friendship, their sympathetic ear for every problem and the fantastic time we had. It was an honour to share the office with you both. I really will miss you!

ADDENDUM

I would like to thank my dear friends, Annett, Pia, Geraldine, Kerstin, Marie, Sarah and Theresa (and all the others I forgot), for their sincere friendship – science can be frustrating and a social backup is absolute mandatory. Many thanks for every moment I did not think about bothering experiments!

I am greatly indebted to Ines Thiere, PD Dr. Carsten Scheller and Kathrin Plochmann who had the deepest impact on my enthusiasm for molecular biology and virology.

I owe deepest thanks to my family for their unconditional love and confidence they have shown in me: My mother and the man in my life who deserves to be named my father for being the most wonderful parents I could ever expect. I am greatly indebted to my dear sisters, Alexandra, Andrea, Cathleen und Cathrin, and of course my lovely grandparents (here or somewhere else) who never stopped supporting me to reach my goals.

My most sincere thanks go to Karsten. Words are not enough to express my gratitude. I just want to thank you with all my heart for your everlasting love and faith you had in me. You know how to handle my sometimes effervescing nature and enthusiasm. What we share is simply wonderful. Thousand thanks!

And in the end I apologize for being so emotional:

For me a more than 15-year-old dream became true – and now it`s time for new ones!

EIDESSTATTLICHE ERKLÄRUNG

Hiermit erkläre ich, die vorliegende Arbeit selbständig ohne fremde Hilfe verfasst und nur die angegebene Literatur verwendet zu haben. Ein Teil der beschriebenen Ergebnisse wurden in Zusammenarbeit mit Frau Dr. Andrea Knoll, Herrn Dr. Björn Schwanhäußer und Herrn Max Flöttmann erzielt. Diese sind entsprechend gekennzeichnet.

Ich besitze keinen entsprechenden Doktorgrad und habe mich anderwärts nicht um einen Doktorgrad beworben.

Die dem Promotionsverfahren zugrunde liegende Promotionsordnung vom 01.09.2005 ist mir bekannt.

Susann Kummer